Tracking low temperature tectonism of the St. Lawrence Platform and Humber Zone, southern Quebec Appalachians through apatite and zircon (U-Th)/He thermochronology

Justin Emberley

Supervisor: David Schneider, University of Ottawa

A thesis submitted to the Faculty of Graduate and Postdoctoral Studies in partial fulfillment of the requirements for the degree of
Masters of Science
in Earth and Environmental Science

Table of contents

Acknowledgements

I would like to thank Dr. David Schneider, my thesis supervisor, for his invaluable professional direction given with respect to this project and for all of the experience that I gained from it. Thank you for giving me the opportunity to take part in this new and exciting research. A special thanks to the Schneider Research Group for thought provoking discussions on low temperature thermochronology. Thanks to everyone at the Colorado TRaIL for their laboratory expertise and helping provide a solid dataset. I would also like to thank my wife Diane, Rhubarb and the rest of my family, for the support and encouragement given throughout the duration of this project.

Tracking low temperature tectonism of the St. Lawrence Platform and Humber Zone, southern Quebec Appalachians through apatite and zircon (U-Th)/He thermochronology

J.M. Emberley
Department of Earth and Environmental Sciences, University of Ottawa, Canada

Abstract

The St. Lawrence Platform (SLP) and Humber Zone (HZ) of the southern Quebec Appalachians has historically been explored as a potential hydrocarbon reservoir. Extensive vitrinite reflectance studies on the basin resolved the degree of thermal maturation yet the timing of the thermal maximum is not well understood. Determining the timing of such low temperature events can allow for a better understanding of the shallow crustal processes that may have allowed for the generation and entrapment of oil and gas. We have employed apatite (AHe) and zircon (ZHe) (U-Th)/He thermochronmetry across a network of late Cambrian to late Ordovician siliciclastic and Grenvillian basement samples in order to resolve the thermal history within the 35-200°C window. Single crystal dates from individual samples show age dispersion by as much as 300 m.y. with a strong positive to negative correlation with increasing eU concentration. A similar positive correlation can be observed when significant intra-sample grain size variation is present. AHe and ZHe data in the southwestern portion of the basin, near Montreal, allow for thermal maxima of up to 200°C to occur either during the late Ordovician, as a result of the Taconic orogeny, or from the continued sedimentation into the Devonian as a result of the Acadian orogeny. Regional burial trends deduced from these thermal maxima along with local paleo-geothermal gradients indicate that if sedimentation continued after the late Ordovician there was no significant increase in burial in southwestern portion of the SLP as previously suggested. Maximum heating is followed by a protracted cooling through the ZHe partial retention zone (PRZ) into the late

Jurassic and early Cretaceous where the cooling rate increases by an order of magnitude through the AHe PRZ until ca. 100 Ma. The timing of this accelerated cooling is coeval with the passage of the Great Meteor Hot Spot across the area; the cooling may be a result of increased erosion from thermal uplift. Within the HZ, both the external and internal sections experienced rapid cooling through the Silurian after the Taconic thermal maximum. The timing of relatively rapid cooling coincides with documented normal faulting and back-thrusting in the orogen, which is the likely cause of exhumation. The HZ witnessed protracted cooling through the late Jurassic, when there is a one order of magnitude increase in cooling rate until surface conditions are attained. Increased recognition of these low temperature events has augmented our understanding of the evolution of accretionary orogens and consequently reduces the risks associated with oil and gas exploration.

1 Introduction

Advances in apatite and zircon (U-Th)/He thermochronology are allowing complex datasets to be resolved, helping unravel the low temperature thermal history of rocks in the upper 10 km of crust. These developments are made possible by quantifying the relationship between a crystal's radiation damage and He diffusivity (Flowers et al. 2009; Guenthner et al. 2013), along with a better understanding of the effects of inherited He on partially reset detrital grains (Guenthner et al. 2014). The pattern that emerges from the age dispersion within a sample illuminates a detailed cooling history as the sample passed through the He partial retention zone (PRZ), from ~140-210°C (zircon) and 35-90°C (apatite).

In this study we have employed apatite (AHe) and zircon (ZHe) (U-Th)/He thermochronometry across a network of late Cambrian to late Ordovician siliciclastic and Grenvillian basement samples in order to resolve the low temperature tectonic history of the St. Lawrence Platform and Humber Zone of the northwestern Appalachians. The St. Lawrence Platform (SLP) and Humber Zone (HZ) have historically been explored as potential hydrocarbon reservoirs. Previous vitrinite reflectance studies (Heroux and Bertrand 1991; Yang and Hesse 1993) have resolved the degree of thermal maturation yet the timing of the thermal maximum is not well understood. Two possible scenarios exist for the timing of the thermal maximum in the SLP (Lavoie et al. 2009): i) during the late Ordovician as a result of the Taconic Orogeny or ii) during the late Devonian as a result of the Acadian Orogeny. Determining the timing of burial and heating of this basin can allow for a better understanding of the shallow crustal processes that may have permitted the generation and entrapment of oil and gas. Application of ZHe and AHe thermochronology conducted on sedimentary rocks provides the possibility to determine the timing and magnitude of the thermal maximum. This information is particularly important in hydrocarbon exploration as by resolving the timing of hydrocarbon generation in source rocks and

by identifying reservoirs where the main phase of generation post-dates formation of potential structural traps, it will give greater confidence when selecting potential hydrocarbon sites.

Unraveling this Ordovician or Devonian history for the region may be complicated by more recent tectonism. The alkaline intrusions of the Monteregian Hills, dated at 124 Ma (Foland et al. 1986), are interpreted to be the surface expression of magmatism related to the passage of the early Cretaceous Great Meteor hotspot (Heaman and Kjarsgaard 2000). Previous studies suggest that significant uplift and extension occurred due to the passage of the hotspot under northeastern North America (Morgan 1981; White et al. 2000; Heaman and Kjarsgaard 2000; Bell 2001). Apatite fission track (AFT) and AHe thermochronological studies in the Adirondack Mountains and central New England (e.g. Roden-Tice and Tice 2005; Taylor and Fitzgerald 2011) have resolved cooling histories contemporaneous with the timing of the passage of the hotspot.

Results from this study yield significant, yet meaningful, ZHe date dispersion throughout the SLP on the order of hundreds of millions of years, from ca. 150-850 Ma over a range in effective uranium (eU) of ~1000 ppm. AHe date dispersion is considerably less scattered and ranges between ca. 100-200 Ma over 150 ppm eU. From this complex dataset it is determined that extended periods of protracted cooling took place after a common thermal maximum, which was interrupted by an interval of increased cooling in the early Cretaceous. Results in the HZ show a similar degree of dispersion in date and eU, for both zircon and apatite, and allowing for a greater range in the magnitude of thermal maxima.

2 Geological Setting and Sampling Strategy

2.1 Overview

The study area for this investigation is composed of two distinct lithotectonic units of the paleo-Laurentian continental margin (**Fig. 1**). These units consist of the autochthonous St. Lawrence Platform (SLP) and the allochthonous Humber Zone (HZ). The surface expression of the St. Lawrence platform is bound to the northwest by the Neoproterozoic metamorphic/ intrusive complex of the Grenville Province and to the southeast by Logan's Line. This line marks the structural front of the Appalachians and the boundary between the SLP and Humber zone, the western most tectonostratigraphic domain of the Appalachians.

The sampling strategy was based in part on previous thermal maturation studies (Heroux and Bertrand 1991; Yang and Hesse 1993, Bertrand and Lavoie 2006) whereby maximum burial temperatures were obtained through vitrinite reflectance analysis (%Ro; see surface thermal maturation map, **Appendix A1**). Thermal maturation data can provide a basic framework in which to conduct a strategic thermochronological study. In places of highest thermal maturation (>4.5 %Ro) both ZHe and AHe dates will likely be reset and can together uncover a portion of the post-depositional thermal history of the host rock through the entire temperature sensitivity range of both thermochronometers (35-210°C), without being affected by their pre-depositional history. In areas of lower thermal maturation (<1.5 %Ro), the zircon may not be reset and may therefore reveal information about pre-depositional events only. In such circumstances, apatite is the more effective thermochronometer to resolve the post-depositional thermal history. In total, fourteen samples were collected: seven from the SLP and seven from the HZ (**Fig. 2, Tables 1, 2**). Within the SLP, six samples contained suitable zircon and apatite whereas one sample contained zircon

only. Within the HZ, one sample contained suitable apatite and zircon, five samples contained zircon only and one sample contained apatite only.

2.2 St. Lawrence Platform

The St. Lawrence Platform consists of weakly deformed continental shelf and foreland basin sequences deposited between the late Cambrian to late Ordovician (**Fig. 2,3**). The basal sequence contains rift-derived siliciclastics of the Potsdam Group followed by passive margin shallow marine carbonates of the Beekmantown Group through to the deepening foreland basin units of the Chazy Group, Black River Group, Trenton Group limestone and calcareous sandstone, Utica Group black shales, Lorraine Group flysch and topped by siltstones of the Queenston Group. The basal rift-derived clastics of the Potsdam Group were deposited unconformably over the crystalline basement rocks of the Grenville Province during the break up of Rodinia. The provenance of the Potsdam Group units is primarily Grenvillian, with a small portion coming from the Superior Province (Gaudette et al. 1981; Montario and Garver 2009; D. Lowe pers. comm.). Approximately 90% of U-Pb detrital zircon ages from the Potsdam Group sandstone are between 950 and 1200 Ma (Montario and Garver 2009). No zircon is younger than 950 Ma with the oldest being slightly older than 2500 Ma, consistent with a Canadian Shield provenance. Except for a small exposure of Devonian carbonate breccia in the alkaline intrusions of the Montreal area (Clark 1972), there is no preserved record of post-Ordovician sedimentation on the SLP in southern Quebec. Vitrinite reflectance data from Yang and Hesse (1993) and Heroux and Bertrand (1991) along with fluid inclusion studies from Yang and Hesse (1991) indicates that southwest portions of the platform attained temperatures indicative of 7 km burial depth for the late Ordovician Trenton Group. This considerable amount of material deposited on top of these Ordovician strata is proposed to have

been a result of Devonian burial due to foreland deepening related to the Acadian orogeny (Yang and Hesse 1993).

During the Cretaceous, alkaline magmas intruded the region forming the Monteregian Hills of southern Quebec, dated at ca. 124 Ma (Foland et al. 1986). These intrusions are likely due to North America passing over the Great Meteor hotspot, and are aligned from northwest to southeast through the Montreal-Sherbrooke area and into the Humber Zone (**Fig 1,2**). The path of the hotspot can be traced to offshore Massachusetts from its present day location, into the Atlantic margin as a series of sea mounts (Duncan 1984; Sleep 1990). Heaman and Kjarsgaard (2000) extended the proposed track of the hotspot across the North American continent using a chronologic progression of kimberlitic dikes and intrusions in southern Quebec and New England (Foland and Faul 1977; McHone and Butler 1984; Foland et al. 1986). In accordance with this idea, Rondenay et al. (2000) found a well-resolved, low velocity mantle corridor that extends across the Superior and Grenville provinces of the Canadian Shield based on teleseismic experiments. They consider this low-velocity corridor to be an extension of the Monteregian/ New England seamount hotspot track that recorded the interaction of the Great Meteor plume and pre-existing zones of weakness within the craton.

Sampling was conducted to encompass the range in thermal maturity variation throughout the SLP as it increases from the northwest to southeast along the short axis of the basin, and from the northeast to the southwest along the long axis (**Appendix A1**). Thermal maturation in the SLP is likely related to the depth of burial due to sedimentation as this area was not affected by tectonic loading or regional metamorphism as a result of Appalachian tectonism. In the southwestern section of the SLP, the lowest most sedimentary unit (Potsdam Group) was sampled since it should reflect the most complete history of the region. These Potsdam Group samples in the southwest

have the highest degree of thermal maturation, with %Ro values >3.5 (Heroux and Bertrand 1991), and may record increased burial as a result of westward sedimentation from the Acadian orogeny as is debated in the literature (Yang and Hesse 1993; Lavoie et al. 2009). One sample from the Beekmantown/ Theresa formations was also sampled from this area. This unit was deposited unconformably over the Potsdam Group and is the mixed siliciclastic-carbonate basal unit in the Beekmantown Group passive margin carbonate sequence. These samples from the southwestern SLP are those collected closest to the alkaline intrusions related to the Great Meteor hotspot, with the closest at ~20 km from a surface exposure. The thermal effects probably extend only within a 5 km areole of the intrusions (Heroux and Tasse 1990; Yang and Hesse 1991; Yang and Hesse 1993).

The central and northeast portion of the basin experienced the least degree of thermal maturation with %Ro values as low as 1.4 (Heroux and Bertrand 1991). Two samples were collected from the Queenston Group, which is the uppermost sedimentary unit in the SLP. It was deposited after Taconic collision, as the SLP had evolved into a successor basin, and is composed of red shales and siltstones. Two samples were also collected in the northern portions of the basin where there is an intermediate to low degree of thermal maturation (1.5-2.0 %Ro). Due to a paucity of zircon and apatite in sedimentary samples collected from these parts of the basin, adjacent Grenville basement rocks near the unconformity were also collected. These basement rocks were collected with the premise that they most likely record the same post-depositional history as the sediment that was deposited directly above. Benefits of sampling the crystalline rock are that all grains likely have a uniform crystallization age and pre-depositional history. The Grenville samples are unconformably overlain by sediments of the Black River Group, deposited at the onset of the Taconic foreland basin, and thus likely share a similar history after this time.

2.3 Humber zone

The Humber zone formed as the result of the destruction of the Laurention continental margin during Taconic accretion of the Dunnage zone arc complexes (Williams 1979). The Humber zone can be subdivided into the internal Humber Zone (IHZ) and the external Humber Zone (EHZ) based on differences in deformation styles, tectonic fabrics and metamorphic grades (St-Julien and Herbert 1975; Tremblay and Pinet 1994; Tremblay and Castonguay 2002; Tremblay and Pinet 2016). The external Humber zone consists of continental slope and rise sediments deposited from the late Cambrian to late Ordovician. These rock packages were thrust imbricated, from southeast to northwest, as a series of nappes with older packages overlying younger packages (St-Julien and Hubert 1975). The timing of emplacement of these nappes is thought to be between 460-450 Ma based on faunal constraints (St-Julien and Hubert 1975). The northwestern most package of nappes are affected by inverted diagenesis indicating a pre-orogenic, burial diagenesis whereas toward the southeast this was followed by syn-orogenic metamorphism (Ogunyomi et al. 1980; Yang and Hesse 1993). The EHZ is defined by a diagenetic to sub-greenschist metamorphic grade (Ogunyomi et al. 1980; Yang and Hesse 1993; Glasmacher et al. 2003; Sasseville et al. 2008) and is bound to the southeast by the Bennett-Brome back-thrust fault (Pinet et al. 1996; Castonguay and Tremblay 2003). To the southeast of this fault lies the IHZ, which has been affected by greenschist to amphibolite-facies regional metamorphism. These polydeformed metamorphic rocks represent distal facies of the Laurentian margin succession (St-Julien and Hubert 1975). The timing of Taconic crustal thickening occurred between 480-445 Ma with a dominant metamorphic event at ca. 469-445 Ma (Pinet and Tremblay 1995; Castonguay et al. 2001, 2007). Exhumation of the IHZ, through normal faulting and back-thrusting, is thought to have taken place during the Silurian to early Devonian as evinced by $^{40}Ar/^{39}Ar$ ages (Castonguay et al. 2001).

Samples were collected along two parallel transects across the Humber Zone, perpendicular and southeast of the Logan's Line towards the Dunnage Zone where there is a marked increase in thermal maturation (**Appendix A1**). Five samples were collected along the northeastern traverse, which extends along the Chaudiere River, originating from Quebec City, whereas the southwestern transect, originating from Drummondville, extends towards Sherbrooke. Of the northeastern traverse, three of these samples are from the EHZ and two are from the IHZ, whereas from the southwestern traverse one is from the EHZ and one from the IHZ. Northwestern sections of the EHZ, in the Quebec City region, have experienced thermal maxima due to diagenetic processes (Ogunyomi et al. 1980; Yang and Hesse 1991) and have not been upgraded during nappe stacking and regional metamorphism of the Taconic orogeny. These sections should have the oldest thermal maxima and not record Taconic/ Acadian events. In contrast, southeastern sections of the EHZ and IHZ have experienced regional metamorphism due to the Taconic and Devonian or younger signature can be resolved. Possible Silurian cooling (Castonguay et al. 2001) may have also been recorded in the rocks of the IHZ.

3 (U-Th)/He Thermochronology and Methodology

Apatite and zircon (U-Th)/He thermochronology is based on the production of radiogenic ^{4}He, through the α-decay of ^{238}U, ^{235}U and ^{232}Th with a small contribution from ^{147}Sm (Farley 2002; Harrison and Zeitler 2005), and the factors which control its rate of diffusion through the crystal. The closure temperature (T_c) of a crystal (Dodson 1973) is dependent on the cooling rate through the PRZ (partial retention zone; Stockli et al. 2000; Reiners 2005; Flowers et al. 2009; Guenthner et al. 2013), grain size (Farley 2000) and effective uranium concentration (eU; Shuster et al. 2006; Flowers et al. 2009, Guenthner et al. 2013). Zircon has a T_c of ~180°C and a PRZ of

140-210°C (Reiners 2002; Reiners et al. 2004; Stockli 2005; Wolf and Stockli 2010; Guenthner et al. 2013) where as apatite has a T_c of ~70°C and a PRZ of 35-90°C (Farley 2000; Stockli 2000; Schuster et al. 2006; Flowers et al. 2009). The finite T_c may only be applied to crystals that have cooled rapidly through the PRZ. At temperatures above the T_c (or PRZ) the crystal behaves as open system and allows the diffusion of ^{4}He. Once the crystal starts to cool into the PRZ does it begin to accumulate ^{4}He and acquire a non-zero date. Flowers et al. (2009) determined that older dates are obtained from grains with increased radiation damage, using effective uranium (eU) concentration as a proxy for damage, when the grains witness protracted cooling through the AHe PRZ. Guenthner et al. (2013) found a similar positive correlation in the zircon system with the exception that at elevated levels of radiation damage (high eU), the trend reverses and thus younger dates are recorded. This inflection from a positive to negative correlation with respect to ZHe date-eU values is the "roll over" point, and occurs at ~200 eU. Fractional loss of He is controlled by grain size, as well, such that larger grains will retain an increased fraction of radiogenic He, whereby an increase in grain size will yield older dates (Dodson 1973; Reiners and Farley 2001). This effect is also amplified by increased time spent in the PRZ.

Careful analysis is required to understand such complexities as individual crystal dates do not hold the same meaning as that of dates from more classic geochronometers. Studies using partially reset detrital grains, such as in this investigation, have other challenges. These challenges arise from the fact that the grains are derived from a varied provenance, each having a different pre-depositional history, whereby each population has differing amounts of inherited He and radiation damage. (U-Th)/He dates for a sample therefore will not plot on a simple date-eU curve and instead be defined within a region of date-eU space referred to as an "inheritance envelope" (Guenthner et al. 2014). The use of "inheritance envelopes" helps quantify the effects of inherited

He on partially reset detrital grains and allows for the unraveling of a thermal history with increased confidence.

Conventional procedures were used to extract and select the most appropriate zircon and apatite from rock samples in preparation for (U-Th)/He dating. Each sample was cleaned with a wire brush and water to remove any surface contamination. The sample was allowed to air dry and was then crushed to a size fraction of ≤1 cm with the use of a standard jaw crusher. The material was then passed through a series of sieves to obtain grain size fractions >250 µm, 63-250 µm and <63 µm. The 63-250 µm fraction was then rinsed through a decantation process to remove any remaining fine powder adhering to the grains and dried for 24 h at a temperature of 30°C using a heat lamp. Heavy mineral separation was then conducted using methylene iodide (SG: 3.3 g/cm^3 and 2.9 g/cm^3) in order to obtain a more concentrated fraction of zircon and apatite. The heavy mineral separates were then individually passed through a Frantz magnetic mineral separator to further isolate apatite and zircon.

The analytical portion of the experiments was conducted at the TRaIL (Thermochronology Research and Instrumentation Laboratory) (U-Th)/He facility at the University of Colorado at Boulder (USA). Individual mineral grains are handpicked using a Leica M165 binocular microscope equipped with a calibrated digital camera and capable of both reflected and transmitted, polarized light. The grains are screened for quality, including crystal shape and the presence of inclusions. The dimensions of the crystals are measured and converted to equivalent spherical radius (ESR) as this value is more readily incorporated into the equations that govern the diffusion of He throughout the grain; from this point forward in the paper references to grain size are actually measurements of ESR. After characterization, grains are placed into small Nb tubes that are then crimped on both ends. This Nb packet is then loaded into an ASI Alphachron He

extraction and measurement line. The packet is placed in the UHV extraction line (~$3x10^{-8}$ torr) and heated with a diode laser to ~800-1100°C for 5 to 10 m to extract the radiogenic ^{4}He. The degassed ^{4}He is then spiked with approximately 13 ncc of pure ^{3}He, cleaned via interaction with two SAES getters, and analyzed on a Balzers PrismaPlus QME 220 quadrupole mass spectrometer. Degassed grains are then removed from the line, and taken to a Class 10 clean lab for dissolution. Apatite grains, still enclosed in the Nb tubes, are placed in 1.5 mL Cetac vials, spiked with a ^{235}U-^{230}Th tracer in HNO_3, capped, and baked in a lab oven at 80°C for 2 h. Zircon are dissolved using Parr large-capacity dissolution vessels in a multi-step acid-vapor dissolution process. Grains (including the Nb tube) are placed in Ludwig-style Savillex vials, spiked with a ^{235}U-^{230}Th tracer, and mixed with 200 µl of Optima grade HF. The vials are then capped, stacked in a 125 mL Teflon liner, placed in a Parr dissolution vessel, and baked at 220°C for 72 h. After cooling, the vials are uncapped and dried down on a 90°C hot plate until dry. The vials then undergo a second round of acid-vapor dissolution, this time with 200 µl of Optima grade HCl in each vial that is baked at 200°C for 24 h. Vials are then dried down a second time on a hot plate. Once dry, 200 µl of a 7:1 HNO_3:HF mixture is added to each vial, the vial is capped, and cooked on the hot plate at 90°C for 4 h. Once the minerals are dissolved, regardless of the dissolution process, they are diluted with 1 to 3 mL of doubly-deionized water, and taken to the ICP-MS lab for analysis. Mineral standards of Durango Apatite (31.5 Ma) and Fish Canyon Tuff Zircon (28.2 Ma) are routinely analyzed (degassed and dissolved) in conjunction with the samples with each run to ensure data integrity. Sample solutions, along with standards and blanks, are analyzed for U, Th, and Sm content using a Thermo Element 2 magnetic sector mass spectrometer. Once the U, Th, and Sm contents have been measured, He dates and all associated data are calculated on a custom spreadsheet made by TRaIL staff.

4 Zircon and apatite (U-Th)/He results

The following section explores the (U-Th)/He data acquired from the analysis of single crystal zircon and apatite (**Tables 1, 2**) collected from rocks throughout the SLP and HZ. By exploring the dataset with respect to date, eU and grain size relationships it is possible to extract information about maximum temperatures, relative cooling rates and the low temperature history experienced by each sample. Such steps are also necessary prior to numerical modeling in order to more fully understand the dataset thereby allowing for more informed decisions when choosing parameters for the models.

The two regions SLP and HZ will be discussed separately. Different thermal events may have also effected the regions as well, therefore the SLP will be divided into the southwest, central and north (Grenville) subgroups and the Humber Zone into the Internal and External subgroups. Subgroups of the SLP are based on the degree of thermal maturation and geographic location. The southwest has possibly undergone significant burial after the Taconic orogeny as a result of the Acadian orogeny and also has the highest degree of thermal maturation according to vitrinite reflectance data. The central and northern locations likely have not seen this amount of burial after the Taconic as the central location has the lowest level of thermal maturation. The samples of the Humber zone are grouped into the Internal and External zones based on their structural location and metamorphic grade.

4.1 St. Lawrence Platform

All apatite and zircon He dates from the SLP are illustrated with histograms in **Figure 4a**. A common trend exists between all three subgroups whereby the AHe dates are consistently younger than ZHe dates (with a range between ca. 100-200 Ma), they have a much narrower range in date dispersion and they are all younger than their depositional age. The southwest and northern groups

have a similar dispersion in ZHe date, with the majority ranging from ca. 150-550 Ma, and most dates are younger than or similar to their depositional age. ZHe dates in the central location are on average older than the other two locations, with the majority of dates between ca. 575-825 Ma, and are older than the timing of deposition. Unsurprisingly, these dates that are older than that of their depositional ages correspond to the areas of lowest thermal maxima (<1.5 %Ro) in the SLP. The southwest and northern location, which have ZHe dates that are younger than their depositional age, correspond to areas of the SLP that have been affected by higher thermal maxima (2.0 to >4.0 %Ro).

Three distinct groups within our data can be observed in ZHe date-eU space (**Fig. 5a**), which correlate to the three subcategories (southwest, north and central), based largely on the degree of thermal maturation. Samples from the southwest, with the highest levels of thermal maturation, have the lowest eU values (<200 ppm) and with dates younger than that of their depositional age (<500 Ma). The central location experienced the lowest maximum temperatures, which corresponds to the oldest dates (<600 Ma) and no apparent trend with regard to eU, all at levels <300 ppm. Samples of the northern group have a strong negative correlation with eU values ranging from ~350-900 ppm over dates from ca. 200-500 Ma. The dates are mostly younger than that of their depositional age with a small portion being within ±50 Ma of this age.

The AHe date-eU relationship (**Fig. 5b**) does not exhibit the same distinct pattern. The southwest and central samples cluster with the majority of the eU values below 25 ppm with AHe date between ca. 100-200 Ma. The values of the north group are separate from the southwest and central locations, with a larger dispersion in eU (50-150 ppm) and an AHe date range from ca. 175-250 Ma. A slight positive trend can be observed in the data for the north group, but the error range for each grain overlaps on a single date of ca. 200 Ma.

To further explore correlations between and within individual samples where it could not be recognized when they are grouped together, the following sections discuss the samples with respect to date-eU and date-grain size relationships.

4.1.1 Southwest SLP

Three samples from the southwest SLP were collected and analyzed whereby two contain both zircon and apatite. From each dataset there are similar trends between samples therefore one will be discussed at length as a representative example. Sample SLP A-12, deposited in the middle to late Cambrian as a part of the Potsdam Group/ Covey Hill Formation, was chosen as it contains both zircon and apatite and has the largest range in eU and grain size. Also, as will be illustrated in the following sections, the dataset follows semi-quantifiable trends with respect to date-eU as defined by RDAAM (radiation damage accumulation and annealing model) (Flowers et al. 2009) and ZRDAAM (zircon radiation damage and accumulation and annealing model) (Guenthner et al. 2013). A combination of these factors allows this sample to reveal a reliable temperature-time history.

There is considerable ZHe date dispersion ranging from 236-522 Ma with a moderate range in eU from 19-158 ppm, and no obvious date-eU correlation for this sample (**Fig. 6a**). The sample possesses a bimodal grain size distribution with large grains from 82-121 μm and small grains from 33-50 μm. It should be noted that the larger grains have consistently older dates than younger grains with similar eU values. Although no date-eU correlations were initially observed, within each grain size population there is a positive correlation between date and eU (see **Appendix A2**). Concentrations of eU in the larger group range from 19-104 ppm over a range in date of 285-522 Ma whereas the small group ranges in eU from 65-158 ppm over a range in date of 236-408 Ma.

There is also AHe date dispersion that ranges from 90-321 Ma over eU concentrations of 1-41 ppm; within this dispersion are two outliers (204 Ma, 321 Ma) which are significantly older than the dominant population (**Fig. 6b**). The grain with the oldest age of 321 Ma also has the lowest eU value of 1.2 ppm which may indicate there are possibly other variables affecting its age such as helium implantation (Spencer et al. 2004; Spiegel et al. 2009) or mineralogical zonation (Meesters et al. 2002). When these two outliers are ignored a slight positive correlation exist between date-eU and between date-grain size.

4.1.2 Central SLP

Two samples from the central SLP were collected and analyzed with both samples containing zircon and apatite. From this group nearly identical trends in the dataset exist between samples therefore only one sample from the dataset will be discussed at length. Sample SLP_B-1, deposited in the late Ordovician as a part of the Queenston Group/ Becancour Formation, yielded zircon dates that range from 607-760 Ma, all of which are much older than the rock's depositional ages. There is no correlation between date and eU as almost all ages ± errors overlap at a single date of ca. 700 Ma over a span of 40-275 ppm eU (**Fig. 6a**). ZHe dates also remain relatively consistent with respect to a grain size over a range of 41-92 μm.

All AHe dates from this sample are much younger than that of the timing of deposition, ranging from 90-155 Ma with no correlation with respect eU or grain size (**Fig. 6b**). This being the case, there is a small range in eU (3-7 ppm) which may not be enough to generate a trend in date-eU space.

4.1.3 North SLP (Grenville)

Two samples from the north SLP (Grenville) were collected and analyzed with both samples containing zircon and apatite. From this group, nearly identical trends in the dataset exist between

samples therefore only one sample from the dataset will be discussed. Sample SLP_D-5 is a sample Grenville crystalline basement, unconformably overlain by the Black River Group/ La Gabelle Formation in the middle to late Ordovician.

A ZHe date dispersion spans 182-502 Ma with an eU content ranging from 434-837 ppm. There is a strong negative date-eU correlation in this sample as the eU concentrations are likely past that of the "roll over" point (~250 ppm; **Fig. 6a**). There is no significant range in grain size (<25 μm) for this sample and there does not appear to be any notable trend between date-grain size.

All apatite grains are younger than the timing of deposition of the Black River Group, and have a date dispersion ranging from 195-239 Ma. There is no correlation between date and eU as almost all ages ± errors overlap at a single date of ca. 210 Ma over eU concentrations of 53-134 ppm (**Fig. 6b**). There is also no significant variation in grain size and thus no notable trend in date-grain size. It is also noted that some of the zircon and apatite dates overlap and that the youngest zircon is slightly younger than the youngest apatite.

4.2 Humber Zone

Two histograms incorporating all the zircon and apatite dates for the HZ are shown in **Figure 4b**. Apatite dates for the two subcategories (EHZ and IHZ) are younger than the majority of zircon dates and have a narrower range of date dispersion. The majority of AHe dates are between ca. 150-200 Ma, which is considerably younger than their depositional ages. There is a relatively large dispersion in ZHe dates within the EHZ ranging from ca. 300-850 Ma and roughly half of the dates are older than the depositional ages. The ZHe dates in the IHZ are considerably less, ranging from ca. 100-325 Ma and younger on average. It can be noted that ZHe dates from the EHZ are essentially older than ca. 300 Ma where as ZHe dates from the IHZ are younger than ca. 300 Ma.

This distinction between these two groups can also be readily observed in the ZHe data-eU plot (**Fig. 5c**). The eU range in the EHZ is relatively low, between 10-300 ppm, and its maximum value is at the crest of the "roll over" point. No correlation is noted between date and eU in the EHZ due to a relative cluster of data points. The range in eU for the IHZ is high compared to that of the EHZ and has a range between ~20-1000 ppm. Within the IHZ there is a strong negative date-eU correlation at >300 ppm eU and the dates range from ca. 100-300 Ma.

Figure 5d illustrates the relationship between date-eU concentration for apatite in the EHZ and IHZ. AHe dates for the IHZ cluster between ~10-15 ppm eU and ca. 100-140 Ma with no obvious correlation between date-eU as there is little variation in the eU concentration. All the ages ± errors overlap at a single date of ca. 125 Ma. Within the EHZ there is relatively significant scatter in the dataset as there is no correlation between date-eU over a range of ca. 175-350 Ma and ~15-160 ppm, respectively.

It is possible that trends exist, such as correlations between date and eU within individual samples which were not visible when the samples are grouped together as in **Figure 5**. In order to illuminate these trends all sample have been individually assessed with respect to date-eU and date-grain size in the following section.

4.2.1 External Humber Zone

Four samples from the EHZ were collected and analyzed with one sample containing both zircon and apatite. Two samples from the EHZ will be discussed at length, one from the NE and one from the SW, as these samples have the most promising datasets (for reasons discussed in the previous sections) and are considered to most accurately record the thermal history of the area.

All ZHe dates for the southwestern sample EHZ_B-5 range from 277-388 Ma and are much younger than that of the timing of deposition. The dates follow a slight positive trend with respect

to eU concentration over a range from 112-237 ppm (**Fig. 6c**). The range in grain size is from ~40-80 µm and there is no notable correlation between date-grain size. All ZHe dates for the northeastern sample EHZ_C-13, which range from 574-842 Ma and eU concentrations of 38-332 ppm, are older than that of their depositional ages. There is no discernible correlation between date and eU and no notable trend between date and grain size.

Sample EHZ_C-13 was the only sample in the EHZ to contain enough suitable apatite for analysis. AHe dates span from 185-353 Ma over eU from 14-61 ppm. There is no correlation in the data with respect to date-eU or with date-grain size as the data appears dispersed (**Fig. 6d**).

4.2.2 Internal Humber Zone

Three samples were collected from the internal Humber Zone. Sample IHZ_B-9 will be discussed as it has the largest range in eU and follows date-eU trends as predicted by ZRDAAM. Sample IHZ_D-8, which is a sliver of the Grenville crystalline basement contained within the IHZ (Lebel and Hubert 1995), is the only sample to include apatite (but contains no zircon) and will be discussed as well.

ZHe dates and eU concentrations for sample IHZ_B-9 range from 79-332 Ma and 157-1026 ppm, respectively, demonstrating a strong negative date-eU correlation (**Fig. 6c**). Grain size, ranging from 48-94 µm, has no obvious correlation with ZHe date. AHe dates for sample IHZ_D-8 range from 103-141 Ma with eU values of 9-13 ppm. There is no noticeable correlation with respect to date and eU in this sample, nor date and grain size (**Fig. 6d**). All grains do however overlap at a single date of ca. 120 Ma when considering their age range.

5 Zircon and apatite (U-Th)/He data interpretation

A cursory examination of the data suggests that there was relatively slow cooling through the ZHe PRZ for the north and southwest areas of the SLP. This can be inferred from the relatively large ZHe date dispersion for those samples, particularly samples that contain a strong negative date-eU trend over >1000 ppm eU. Thermal maxima in these areas likely never exceeded the ZHe PRZ temperatures as some of the grains are only partially reset and have dates very close to, or slightly older than, their depositional ages. In the central region, temperatures never warmed significantly into the ZHe PRZ as all dates in this area are 100-350 m.y. older than their depositional age and thus still preserve a portion of their pre-depositional history. These trends in thermal maxima are roughly in accord with those determined from vitrinite reflectance studies. AHe data for all samples of the SLP have similar trends and therefore likely experienced similar thermal histories as they cooled through AHe PRZ temperatures. All dates are 300 m.y. younger than their depositional ages, clustering between c. 100-200 Ma, and therefore experienced thermal maxima high enough to reset the grains. This narrower dispersion in dates for apatite compared to zircon may also indicate that the samples cooled somewhat faster through the AHe PRZ window. Date-eU relationships for AHe data of the northern section show a slight positive correlation but when their error ranges are considered all dates overlap at a common age. The relatively concordant dates with respect to a ~100 ppm variance in eU also suggests a relatively faster cooling occurred through AHe PRZ.

The Humber Zone also appears to have witnessed slow cooling through ZHe PRZ temperatures. The relatively large date dispersion is noted particularly within the EHZ that spans over 550 m.y. Strong negative date-eU correlations in the IHZ (over a range of ~400-1000 ppm eU) and positive correlations in the EHZ (over a range of ~100-250 ppm eU) further supports slow

cooling through the ZHe PRZ. Thermal maxima in the IHZ exceeded that needed to reset the zircon as ZHe dates are all younger than their depositional ages by at least 175 m.y. In the EHZ ZHe dates encompass a range that are both older and younger than that of their depositional ages (**Fig. 4b**) implying that temperatures never significantly exceeded that of the ZHe PRZ which is needed to completely reset the most He retentive grains. Date-eU plots of individual samples in **Figure 6c** reveals more specifically that different locations within the EHZ may have experienced varying thermal maxima. The northeastern most section, as represented by sample EHZ_C_13, have ZHe dates that are all between 100-350 m.y. older than their depositional history. Directly to the south are samples EHZ_C-10 and EHZ_C-4, having the majority of their ZHe dates within ±50 m.y. of their depositional ages. It is likely that this region to the south was slightly hotter with temperatures well into or exceeding the ZHe PRZ to partially reset the grains. This trend is in accord with increasing thermal maturation deduced from vitrinite reflectance data from the northwest to the southeast, perpendicular to the Logan's Line. AHe dates in the IHZ depict similar trends to that of the SLP, which are fairly clustered between ca. 100-150 Ma. **Figure 6d** indicates that regardless of eU concentration or grain size, all dates are within error at ca. 125 Ma. Such a trend points to relatively fast cooling through the 90-35°C PRZ of apatite. AHe dates in the EHZ exhibit more scatter and have no obvious correlation with respect to eU or grain size. An older population of dates from ca. 190-350 Ma likely indicates that this region experienced thermal maxima that were not hot enough to fully reset these grains (and they therefore contain some inherited ^{4}He), such that it has been determined that this region of the EHZ experienced the lowest thermal maxima.

6 Numerical modeling

In order to extract more information from a complex dataset, where single crystal dates within a rock sample can vary by hundreds of millions of years, numeric modeling utilizing the program HeFTy (Ketcham 2005) was carried out on all samples. The application of this program allowed both forward and inverse models to be generated. The end result of inverse modeling is a series of temperature-time paths, generated through a Monte Carlo random search method, which illustrate the plausible thermal histories experienced by the sample. Parameters specific to zircon and apatite which control the range in date for a given grain, such as eU concentration and grain size along with user-specified independent temperature-time constraints, such as vitrinite reflectance data (%Ro), are input into the program and help define candidate temperature time paths. Modeled thermal paths, generated by HeFTy, are compared against the analytical dates. These dates are considered either "good" or "acceptable" dependent on a calculated goodness of fit, indicating the probability of failing the null hypothesis that the model and data are different. A value of 0.05 or higher reflects an "acceptable" fit between model and data. A value of 0.5 or higher reflects a "good" fit between model and data. Forward modeling was employed to create a series of inheritance curves for each sample, which cumulatively form an "inheritance envelope." The concept of inheritance envelopes (Guenthner et al. 2014) allows for post-depositional histories to be modeled within the ZHe data and utilize crystals with variable pre-depositional histories. The use of forward modeling can allow for a more in depth understanding of the dataset and how to better exploit the data.

Four independent temperature-time constraints were applied to each model. Firstly, each model has a pre-depositional constraint encompassing a temperature range between 200-220°C to reflect the grain's cooling history prior to deposition. Above this temperature range all ^{4}He is lost

such that modeling pre-depositional histories above these values does not yield meaningful temperature-time paths and has no affect on the consequent post-depositional temperature-time histories. At a subsequent time, the grains cool below 210°C whereby they begin to accumulate ^{4}He and acquire a non-zero date. Due to the possible variation in provenance between samples (i.e. Grenville or Superior), the time and duration of this constraint will be unique to each model. A second constraint defining the deposition of the sediment of each sample is determined from their stratigraphic position (**Fig. 2**) with each sample achieving a surface temperature of ~20°C at that time. The temperature range of the third constraint, encompassing the timing of the thermal maximum, was chosen to be broad enough so as not to limit the possible candidate temperature-time paths. The timing for the third constraint in the SLP is between 325-475 Ma allowing the thermal maximum to occur during the Taconic or Acadian orogenies. In the HZ the timing of the third constraint is unique to each sample and will be discussed in the following sections. A final constraint represents the present day surface temperature as the rocks are again exposed at the surface. The details of each group of samples are discussed in the following section.

6.1 Understanding data spread and grain selection

AHe and ZHe dates can have dispersion that span hundreds of millions of years over eU concentrations of >1000 ppm. Choosing multiple grains that have a range in eU, date and grain size is desirable as these grains will likely reflect a more complete thermal history of the sample since each grain will in essence be a unique thermochronometer. Using sample A-12 as an example in the section below, we discuss the modeling methodological approach to understand and illuminate trends in the dispersion and to subsequently aid in the selection of the most appropriate grains for modeling.

Two different inverse models were created for sample SLP_A-12 (**Fig. 7**) based on select zircon analyses. Both models use a pre-depositional constraint at 750-650 Ma and 200-220°C based on published Grenvillian cooling paths (Heizler and Harrison 1991; Mezger et al. 1991; Montario and Garver 2009) and a depositional constraint defined for the Potsdam Group sandstone (**Fig. 2**). Zircon U-Pb data of Montario and Garver (2009) reveal that the Potsdam near the Adirondack Mountains has a Grenville provenance so it is presumed that the zircon would have Grenvillian cooling as a pre-depositional condition. The grains chosen for model A range from ca. 500 Ma (the timing of deposition) to ca. 250 Ma where as model B only uses grains with dates at ca. 250 Ma. Given that these grains likely experienced a similar pre-depositional cooling history between 750-650 Ma and the same depositional age of ca. 500 Ma, the grains younger than the depositional age are likely more fully reset than the older grains. The contrast in magnitude of thermal maxima between model A and B, with model B allowing for hotter thermal maxima (>90°C difference), illustrates how grain selection can affect the possible outcome. Models generated with older, less reset grains, restrict thermal maxima to stay cooler than the upper limit of the PRZ whereas models generated with more fully reset grains (those significantly younger than the depositional age) allow for thermal maxima to be hotter than the upper limits of the PRZ.

To help assess the viability of the inverse models and to more fully understand the dispersion in the dataset, forward modeling was also utilized to create inheritance curves that account for the range of grain size (ESR: 34-130 μm) in this same sample. Three forward models (**Fig. 8a**) were created that have thermal maxima of 160, 180, and 200°C, respectively, which likely represents the possible variation in thermal maxima as resolved through inverse modeling (**Fig. 6**). From each forward model, a unique inheritance curve is created that considers grain size (**Fig. 8b**). The data for sample SLP_A-12 are placed into three categories based on grains sizes, which range from 30-

60 µm, 60-90 µm and 90-120 µm and are superimposed onto each of the three inheritance curves. The inheritance curve created using a 200°C thermal maximum (**Fig. 8b**) does not capture the dispersion in data very well. The smallest grain sizes, and large grains with very low eU, fall within its corresponding envelope and therefore is supported by this possible thermal history but larger grains are not satisfied by this scenario. At this higher temperature all zircon should be mostly reset. The inheritance curve created using a 180°C thermal maximum (**Fig. 8b**) allows for a broader grain size envelope and encompasses more of the data. The relative broader envelope is due to the fact that this cooler thermal maximum does not fully reset all the grains whereby it has a greater effect on resetting the smaller grains and a lesser effect on resetting the larger grains. The smaller zircons are satisfied by this history but many of the larger grains do not fall within the envelope. The inheritance curve created using a 160°C thermal maximum (**Fig. 8b**) allows for the entire dataset to be captured with this thermal history; at this maximum temperature the smallest grains appear to be more or less reset while the largest grains will retain a large portion of their pre-depositional history. According to this forward modeling process that utilizes grain size, a thermal history that has a thermal maximum of ~160°C is the most likely scenario as it is supported by most of the zircons in the dataset. Consequently, when considering the two possible inverse models in **Figure 7**, the most likely scenario is that of model A.

This process illustrates how grain selection is an important factor when inverse modeling. If only the smallest grains (30-60 µm) were chosen when inverse modeling, a large range in thermal maxima, from 140°C to >200°C, could be supported. By also incorporating the larger grains into each model (90-120 µm), the model is limited to a ~160°C thermal maximum. The series of date-eU grain size curves remain unchanged and narrowly defined at less than ~40 ppm eU, regardless of the thermal maximum. As a result, choosing grains in this field, even if they are large, will not

constrain the history as it will support a wide range of thermal maxima. Also, with the narrow spacing of the curves at this lower eU concentration, grains are more likely to overlap into adjacent grain size curves, due to their uncertainty, and incorrectly support a wider range of possible outcomes. The grain used in the thermal models discussed below are chosen with these considerations in mind when there is a significant range in grain size.

6.2 Inverse/forward modeling of the SLP and HZ

One model from each subcategory in the SLP and HZ is displayed in **Figure 9** and is discussed in detail below. The models satisfy most of the data and were created by using the grain selection method and forward modeling processes described in the previous section. The remainder of the models, along with information on which grains were utilized in each model, are available in the **Appendix**. Inheritance envelopes, discussed below for each sample, were created using the mean grain size. Subsequent inheritance envelopes, utilizing the entire range in grain size, were created for each sample to illustrate if it had a significant effect on the candidate thermal paths. These forward models are also available in the **Appendix**.

6.2.1 Southwest SLP (sample SLP_A-12)

Modeling of the ZHe data (**Fig. 9a**) demonstrate that the range of possible thermal histories upon heating during burial is not well constrained between the timing of deposition to the thermal maximum, with a broad window between 475-325 Ma as a result of either Taconic or Acadian tectonism. The thermal maxima is tightly defined between 155-170°C and does not exceed what is required to reset all of the grains, suggesting that some grains retained their pre-depositional history. From 325-200 Ma the history is a restricted cooling path that follows a relatively slow cooling rate of ~0.2°C/m.y. whereby it cools to the lower limits of the ZHe PRZ (~130°C). From roughly 200-150 Ma the history become slightly less constrained and cools to the upper limit of

the AHe PRZ (~80°C) at a rate of ~1°C/m.y. The cooling history becomes more constrained as it cools through the AHe PRZ, where the cooling rate increases to 2°C/m.y. until 100 Ma. From 100 Ma to present day the sample cools from the lower end of the AHe PRZ to surface temperatures at the rate of ~0.1°C/m.y.

6.2.2 Central SLP (Sample SLP_B-1)

The pre-depositional cooling history for this sample is not well know, thus a larger constraint was defined in order to accurately allow for all possible histories. The initial constraint is therefore placed between 1200-550 Ma. The maximum age of 1200 Ma was chosen as this was the oldest starting point for thermal paths generated in preliminary inverse modeling experiments, where the initial constraint was extended back to 2100 Ma.

The model supports the timing of thermal maxima between the post-Taconic thermal peak to the Acadian orogeny (**Fig. 9a**). Maximum possible temperatures range from 60-140°C which place it between the AHe and ZHe PRZs. After the maximum temperature is reached the thermal paths allow for relatively slow cooling at a rate of ~0.1°C/m.y. to occur from 325-150 Ma. At this point the rate of cooling is allowed to increase by roughly an order of magnitude, to a rate of 2.0°C/m.y., through the remainder of the AHe PRZ until ~100 Ma. From ~100 Ma to the present, the rate of cooling decreases by one order of magnitude until the present day surface temperature is reached.

Three different pre-depositional histories used in the creation for this sample's forward models and inheritance envelopes (**Fig. 10a**) are 750 Ma, 1200 Ma and 2100 Ma. These dates cover possible times that allow for the grains to be derived from either the Grenville (most likely candidate based on Montario and Garver 2009), the Superior Province or other sources such as the approaching arc system that has a similar age. The inheritance curves generated are essentially

horizontal, indicating that there is a nonaligned correlation between date and eU. A series of horizontal inheritance curves for each pre-depositional history indicate that the temperatures should have not reached values high enough to even partially reset the grains, regardless of eU value, and that the grains should have dates that completely reflect their pre-depositional cooling date. In this case all grains plot along a relatively horizontal line between 750-1200 Ma whereby all their dates overlap near a ca. 800 Ma inheritance curve. This pre-depositional cooling date is consistent with that of sediment sourced from the Grenville and helps validate the pre-depositional constraint used for inverse modeling. This thermal history accounts for the entire data set as there are no outlying grains.

6.2.3 North (Grenville) SLP (Sample SLP_D-5)

Two inverse models, both using the same pre-depositional constraint based on published Grenvillian cooling paths (Heizler and Harrison 1991; Mezger et al. 1989, 1991; Montario and Garver 2009) were created for this sample. One model used both zircon and apatite whereas the other model used zircon-only (**Fig. 9a**), each of which revealed somewhat dissimilar results. Two models were created as zircon grains that have dates younger than 250 Ma with higher eU values do not yield "good fit" thermal paths when modeled in conjunction with any of the apatite grains. As mentioned above, the zircon dataset appears promising, likely having the ability to record the thermal history over a wide temperature range (as it has a strong negative correlation over a significant spread in date and eU), such that it was determined that the entire dataset needed to be utilized. Ideally, models would be created using zircons that span the entire range of date and eU while incorporating apatite as well, but such models yielded no acceptable thermal paths. Of the two different models created, one used apatite and zircon (zircon that were older than 400 Ma with

eU values between 400-500 ppm) whereas the other model used zircon-only (zircon that spanned the entire range in date and eU). Both models, and their plausibility, are discussed below.

For both models the range of possible thermal histories upon heating is not well constrained from the timing of deposition to the timing of the possible thermal maxima. The timing of thermal maxima can occur anywhere between the Taconic and Acadian orogenies. The temperature ranges of the thermal maxima are similar between both models, occurring between 160-180°C for the model executed with both zircon and apatite, and between 140-170°C for the model with zircon-only. The main differences between the two thermal histories arise after 325 Ma. For the model with both zircon and apatite, cooling (~1°C/m.y.) commences at ca. 325 Ma where it cools from 160°C, through the remainder of the ZHe PRZ and all of the AHe PRZ by 200 Ma. In contrast the model executed with zircon-only indicates that relatively slow cooling takes place after 325 Ma whereby the sample remains in the ZHe PRZ until at least 150 Ma. During this time it cools from roughly 150°C to 130°C (~0.15°C/m.y.), at which point the cooling rate then increases relatively dramatically as the sample cools from 130-20°C (~1°C/m.y.) over the remaining 150 Ma. The history created from the model with zircon-only is more consistent with the histories created from the other zircon and apatite bearing samples in the St. Lawrence Platform.

Forward models were used to created inheritance envelopes in order to help assess the inverse models. All the zircon for this sample, belonging to a Grenville source, should have the same pre-depositional history and therefore all grains should plot on the same inheritance curve that corresponds to a Grenville source. To test this, two series of inheritance envelopes were generated, both of which include pre-depositional histories between 650-2100 Ma, from both zircon-only and apatite and zircon forward models (**Fig. 10b, c**). For the inheritance curves created with zircon-only, all zircons fall within an envelope that suggests a Grenville source. These grains

plot between 650-1200 Ma with the majority of the grains closely aligned with the 950 Ma envelope. The fact that all the zircon grains follow a similar predictable trend, with no anomalous grains plotting elsewhere, helps to strengthen the zircon-only model.

The next series of inheritance curves were generated from the forward model using both apatite and zircon. From this analysis, there are three apparent populations of zircons, one that closely aligns on the 950 Ma curve, one between the 1200 and 2100 Ma curve (at ~1750 Ma) and another on the 2100 Ma curve. The likelihood of zircons having these very old pre-depositional histories of 2100 Ma and 1750 Ma is very low as these dates are older than the age of the Grenville Province, from which the sample is collected. It is established that this is not a result of an anomaly, such as would occur from parentless He for example, as these zircons would also plot spuriously on the zircon-only inheritance envelope plot. As a result of the above sensitivity tests, the thermal histories generated from the zircon-only models are more plausible and are also more consistent with thermal histories determined for other parts of the St. Lawrence Platform. It is possible that the apatite grains are yielding dates that are erroneously old due to various factors that can contribute to parentless He (Farley et al. 1996; Meesters et al. 2002; Spencer et al. 2004; Spiegel et al. 2009).

6.2.4 External Humber Zone, South West (Sample EHZ_B-5)

As the pre-depositional history is not well defined for this sample a large constraint was placed from 2600-650 Ma. This time frame allows for sediments to be derived from the Grenville and the Superior provinces. Preliminary models executed with this pre-depositional history did not support thermal histories that were older than Grenville ages (**Appendix**) so subsequent models were run using a pre-depositional constraint of 1200-650 Ma. For each model the thermal histories generated from 475 Ma to present day are almost identical and, therefore, the different pre-

depositional constraints does not affect the thermal history. The constraint encompassing the thermal maximum is placed between 475-400 Ma to allow for a thermal maximum to occur during the Taconic Orogeny and to test whether cooling could have commenced during the Silurian as determined by Castonguay et al. (2001) for the IHZ. All thermal maxima occur between 475-425 Ma whereby they are not confined by the younger, 400 Ma boundary of the constraint. This therefore indicates that the thermal maximum occurs syn-Taconic orogeny, with maximum temperatures of ~240-300°C. All histories indicate a cooling rate of ~2.0°C/m.y. from the thermal maximum to the end of the Silurian, at which point the cooling rate decreases by an order of magnitude. This slower cooling (~0.15°C/Ma) continues through the ZHe PRZ until c. 150 Ma. After which the majority of the thermal paths cool below the ZHe PRZ but the history is not well defined past this point due to the lack of AHe data. Most paths do however support an order of magnitude increase in cooling rate after c. 150 Ma.

Pre-depositional histories of 750 Ma, 1200 Ma and 2100 Ma were used to create the inheritance envelopes for this sample. (**Fig. 11b**). Half of the zircon grains plot within the zero to 1200 Ma inheritance envelope. The remaining grains fall in date-eU space above the inheritance curves but are within error of the 1200 Ma inheritance curve. This history therefore broadly accounts for most of the grains in this dataset as they have a date similar to that of Grenville derived sediment.

6.2.5 External Humber Zone, North East (Sample EHZ_C-13)

As the pre-depositional history is not well defined for this sample a large constraint was placed from 2600-650 Ma. This time frame allows for sediments to be derived from the Grenville and the Superior provinces. Preliminary models executed with this pre-depositional history did not support thermal histories that were older than Grenville ages (**Appendix**) so subsequent models

were run using a pre-depositional constraint of 1200-650 Ma. A constraint encompassing the thermal maximum has a range from 500-450 Ma which encompasses the timing of nappe emplacement (St-Julien and Hubert 1975) and inferred thermal maximum.

Thermal maxima plot between a temperature range of 80-170°C, with the majority of "good fits" above 120°C, and have a uniform distribution between 500-450 Ma (**Fig. 9b**). After the thermal maximum, cooling commences at a rate of ~0.5°C/m.y. until it enters the upper portion of the AHe PRZ. Once all the cooling paths enter the AHe PRZ by c. 325 Ma, the history becomes well constrained and cools at a slower rate of 0.15°C/m.y. until 150 Ma. After 150 Ma thermal paths support an increase in cooling rate to ~1°C/m.y. while others continue to cool at the previous rate until present day.

Inheritance envelopes were created with pre-depositional histories of 750 Ma, 1200 Ma and 2100 Ma (**Fig. 11a**). All grains plot in an envelope between 750-1200 Ma, again confirming a Grenville source with no outliers.

6.2.6 Internal Humber Zone, South West (Sample IHZ_B-9)

The pre-depositional history for this sample is not well defined, but the temperatures likely experienced by rocks of the IHZ were significant enough to fully reset the grains to a point where the pre-depositional history does not affect the low temperature history. However, a pre-depositional history constraint was still placed between 1200-650 Ma to be consistent with other models. The constraint encompassing the thermal maximum was placed between 475-450 Ma to allow for a thermal maximum as a result of the Taconic orogeny, consistent with $^{40}Ar/^{39}Ar$ data for the IHZ (Castonguay et al. 2001).

Thermal maxima range from 230-290°C for this sample indicating that the grains are likely fully reset (**Fig. 9b**). Extra models were executed with pre-depositional histories extending as far

back as 2600 Ma but little change was noted in the post-depositional thermal history (**Appendix**). Cooling at a rate of 1°C/m.y. ensues after the timing of the thermal maxima until 325 Ma where the temperature falls to within the middle of the ZHe PRZ. From 325-150 Ma the cooling rate decreases by an order of magnitude, to 0.15°C/m.y., as it proceeds through the remainder of the ZHe PRZ. After 150 Ma the cooling rate increases by an order of magnitude to ~1°C/Ma, but the history from this point onward is not well constrained as there are no AHe data.

6.3 Modeling summary

Numerical modeling reveals that a number of common trends exist throughout the SLP and the HZ. Within the SLP all models support thermal maxima that develop during the time of the Taconic or Acadian collisional events, even those samples closest to the track of the hot spot. All samples also indicate that following the thermal maximum relatively slow cooling (0.1-0.2°C/m.y.) occurred for the next c. 125 m.y., at which point the cooling rate increased by an order of magnitude (1.0-2.0°C/m.y.). Most thermal histories allow for this increase in cooling rate until 100 Ma at which point it slows by an order of magnitude until the present day. Regional differences between the magnitude of maximum temperatures are apparent: the southwest and the north experienced the hottest thermal maxima whereas the central region experienced the coolest thermal maxima. The same general trend occurs in the HZ whereby after c. 325 Ma there is relatively slow cooling (0.1-0.2°C/m.y.) until c. 125 Ma and after which the cooling rate increases by an order of magnitude (1.0-2.0°C/m.y.). One of the main differences between the two regions is that cooling (at a rate of 1.0-2.0°C/m.y.) commences after c. 450 Ma and continues until 325 Ma for the HZ whereas cooling only begins at c. 325 Ma in the SLP. In general, the maximum temperatures in the HZ attained hotter conditions than those in the SLP.

7 Discussion

7.1 Burial trends and timing of the thermal maximum in the St. Lawrence Platform

An increase in burial depth of the SLP from the northeast to the southwest along strike of the Logan's Line has been proposed (Yang and Hesse 1993). The investigators of that study applied Barker et al.'s (1986) method of calculating maximum temperatures from vitrinite reflectance values to Heroux and Bertrand's (1991) well data for core samples in the SLP. They obtained a regional geothermal gradient of 33-37°C/km (for areas east of Montreal), and determined a burial depth of ~5 km for the surface rock in a central region of the basin, close to the location of sample SLP_B-1. This corresponds to a maximum burial temperature of 165-185°C. Further to the west, in the Granby area east of Montreal, they estimated a maximum burial depth of ~8 km for the Trenton Group sandstone. Moreover, estimates made from this study using Castonguay et al.'s (2006; 2010) seismic profile interpretations, place the Potsdam Group ~1 km below the Trenton Group, at ~9 km total burial depth. This significant amount of burial in the Granby area indicates that there must have been continued burial after the Taconic orogeny and is likely a result sedimentation due to the Acadian orogeny (Yang and Hesse 1993).

Non-reset zircons from this study for sample SLP_B-1 of the Queenston Group indicate maximum temperatures did not exceed 140°C. Thermal maxima determined through inverse modeling allows for a 60-140°C range with the most probable scenario placing it closer to 120°C. Considering a maximum temperature of 120°C and a geothermal gradient of 33°C/km, there would have been ~3.6 km of sedimentation deposited above this unit, slightly less than the estimated ~5 km of sedimentation in that area (Yang and Hesse 1993). Considering the lower acceptable temperature possibilities at 60°C, along with the higher 37°C/km thermal gradient, the amount of sediment deposited on the lower limit would have been much less, at 1.6 km.

Applying the geothermal gradient of 33-37°C/km to the inferred ~9 km burial depth for the Potsdam Group yields a maximum burial temperature of 294-325°C. However, partially reset ZHe dates obtained for the Potsdam Group samples from this study indicate that the paleotemperatures could not have exceeded a maximum of ~220°C, which is needed to reset the grains. Furthermore, thermal modeling for the Potsdam Group sample SLP_A-12 places the maximum temperature between ~160-180°C. Considering a 33-37°C/km geothermal gradient with this revised temperature estimate, the Potsdam Group sample SLP_A-12 would have been buried to a depth of ~4.3-5.5 km. Thermal modeling for Potsdam Group samples collected further to the south, along the Quebec / US boarder, allow for thermal maxima of up to 220°C which permit slightly deeper burial depths of up to 6.7 km with the same geothermal gradients (**Appendix**).

Although the sampling network is not especially dense, results from this study do not show a significant increase of burial depth from the northeast toward the southwest as previously suggested. The difference in thermal maximum between the central and southwest locations can primarily be accounted for by the ~3.0 km depth the Potsdam Group is buried below the Queenston Group and not due to significant amounts of missing strata deposited after the Late Ordovician. Inverse modeling confirms thermal maxima encompassing the timing of both the Taconic and Acadian events, but continued burial after the Taconic was likely not as significant as previously proposed (**Fig. 12**).

Potsdam Group samples collected further to the south, close to the US border, do allow for slightly higher thermal maxima but this likely reflects the trend of increased burial depth, across the short axis of the basin, towards the Logan's Line due to greater subsidence of the underlying continental margin as a result of tectonic loading. Moreover, immediately to the south in the Adirondack Mountains of New York, Taylor and Fitzgerald (2011) calculated an elevated

geothermal gradient of 38-60°C/km which they attribute to the presence of the Great Meteor hotspot. If the southwest SLP study area experienced these higher geothermal gradients, resolved within the thermal maxima produced from ZHe data, the total burial depth would be even less. Other thermal maturation studies utilizing conodont alteration indices (Legal et al. 1981; Nowlan and Barnes 1987) attribute the increase in maturation in the southwest SLP from the hotspot related intrusions of the Monteregian Hills.

7.2 Taconic thermal maximum and Silurian exhumation in the Humber zone

Middle Ordovician $^{40}Ar/^{39}Ar$ ages (Castonguay et al. 2001) along with olistostromal deposits at the base of the nappes of the External Humber zone (St-Julian and Hubert 1975) and flysch sedimentation as a result of a deepening foreland basin during Taconian convergence (Lavoie 1994) are coeval with crustal thickening and nappe emplacement throughout the Humber zone (Castonguay et al. 2001). The timing of this thermal peak is supported by all inverse models for the Humber zone and is the only possible outcome for the thermal maximum for the model of sample EHZ_B-5 of the External Humber Zone. Silurian-early Devonian back-thrusting and normal faulting in the Internal Humber zone was an important factor in the exhumation of the region (Castonguay et al. 2001). Inverse modeling results for all Humber zone samples (particularly those of the southwest External and Internal Humber zones) indicate that cooling (~1.0-2.0°C/Ma) commenced after a middle Ordovician thermal maximum, from the Silurian into the middle to late Devonian (**Fig. 12**). This is consistent with previous $^{40}Ar/^{39}Ar$ studies (Castonguay et al. 2001).

7.3 Tectonic inactivity from the Late Devonian to Early/Late Jurassic

All inverse thermal models for the St. Lawrence Platform and Humber zone allow for the relatively slow cooling of ~0.05-0.2°C/m.y. from the late Devonian to the early/late Jurassic.

Considering an average paleogeothermal gradient of 35°C/km (Yang and Hesse 1991), exhumation rates would range from 1.4-5.7 m/m.y. Such exhumation rates are indicative of mechanical erosion (cf. Ring et al. 1999); it is likely that no significant uplift had occurred. The timing of this protracted cooling is contemporaneous with events of the Alleghenian Orogeny indicating that it likely had little to no effect on this portion of the study area.

7.4 Hotspot related cooling from the Jurassic/Early Cretaceous to the Late Cretaceous

Several types of mafic magmatism, including the lamprophyre dykes throughout southern Quebec and New England Appalachians (McHone 1992) and the alkaline intrusions of the Monteregian Hills, occurred throughout northeastern North America during the Mesozoic. The timing of this magmatism is confined to two periods between Jurassic (200-165 Ma) and Cretaceous (124 Ma; Foland et al. 1986) in accord with the AHe dates obtained in this study.

The passage of the Great Meteor hotspot through southern Quebec is a possibly driver for the onset of sudden cooling as determined from the AHe data. Yang and Hesse (1993) established that heating of the country rock by extrusive sequences is restricted to an area of <1 km as demonstrated by vitrinite reflectance data. However, hotspots can commonly produce surface uplift of >1 km and related exhumation over a broad region with a radius of hundreds of kilometers as a result of dynamic uplift (Sengor 2001). For example, delamination of the lithosphere under the Yellowstone hotspot (Foster 2008) is thought to produce dynamic uplift over a broad region as asthenosphere replaces mantle lithosphere. It is possible that if uplift occurred from these events it could allow for slightly accelerated exhumation, resulting in regional cooling. Furthermore, to the south in the Adirondacks, Taylor and Fitzgerald (2011) determined that there was an elevated geothermal gradient between 40-60°C/km at ca. 130-120 Ma, and subsequent relaxation of isotherms as the region moved away from the hotspot, which could allow for an increased cooling

rate. AFT and AHe studies by Roden-Tice and Tice (2005) in the Adirondacks and central New England, which yielded dates ranging from late Jurassic to late Cretaceous, suggest extensional thinning of the lithosphere may have caused reactivation of regional-scale normal faults in the southeastern Adirondacks and in the Connecticut River valley and thus accommodated regional unroofing during the middle Jurassic through to the late Cretaceous. Alternatively, increased recognition of late Cretaceous cooling along the North Atlantic margin may suggest a period activity in what is an otherwise passive margin setting (Amidon et al. 2016).

AHe dates from this study range from ca. 200-100 Ma and inverse thermal models allow for the onset of relatively rapid cooling occurring during middle Jurassic-early Cretaceous (**Fig. 12**). The timing of this cooling is broadly coeval with the passage of the Great Meteor hot spot, as well as cooling recorded from a regional perspective. Cooling rates markedly increase, by one order of magnitude, after a period of tectonic inactively from the Carboniferous to the early Jurassic. The slightly older AHe dates in the northeast EHZ are likely a result of a thermal maximum in this region that was not hot enough to fully reset all of the grains. Inverse modeling for the northwest EHZ does, however, allow for the onset of cooling to occur during the early Cretaceous.

8 Summary

Through the understanding of the relationship between radiation damage and He diffusion, along with the effects of inherited He on partially reset AHe and ZHe detrital grains, it is possible to gain significant insight into the low temperature evolution the SLP and HZ. Such an understanding can reveal trends in complex datasets that exhibit dispersion. A few highlighted summary points from this study are as follows (**Fig. 12**):

1. The thermal maximum in the SLP could have occurred either in the late Ordovician as a result of the Taconic orogeny or in the late Devonian as a result of continued sedimentation from the Acadian Orogeny. Regional burial trends deduced from maximum temperatures obtained through numerical modeling along with local paleo-geothermal gradients indicate that if sedimentation continued after the late Ordovician, there was no significant increase in burial in southwestern portion of the SLP as previously suggested.
2. ZHe data indicate that thermal maxima for the EHZ and IHZ occurred in the middle Ordovician as a result of the Taconic orogeny. Cooling occurred in the Silurian at an average rate of ~2°C/m.y. and continued into the middle/late Devonian.
3. Relatively constant thermal conditions existed throughout the SLP and HZ from the late Devonian to the early/late Jurassic, as defined by a cooling rate of ~0.2°C/m.y. Such a cooling rate indicates that this area was relatively tectonically stable.
4. Abruptly following this period of slow cooling and tectonic stability is a one-fold increase in cooling rate that continued until the late Cretaceous. This acceleration in cooling throughout the SLP and HZ is may be due to the passage of region over the Great Meteor hotspot, which produced increased erosional rates as a result of uplift and the subsequent relaxation of isotherms as the region moved away.

An increased recognition and resolution of these low temperature events can augment our understanding of the tectonic evolution of accretionary orogenies and, consequently, may help to reduce the risks associated with oil and gas exploration in the SLP.

References

Amidon, W. H., Roden-Tice, M., Anderson, A. J., McKeon, R., and Shuster, D., 2016. Late Cretaceous unroofing of the White Mountains, New Hampshire, USA: An episode of passive margin rejuvenation? Geology, **44**: 415-418.

Barker, C. E., Crysdale, B. L., and Pawlewicz, M. J. 1986. The relationship between vitrinite reflectance, metamorphic grade and temperature in the Cerro Prieto, Salton Sea and East Mesa geothermal systems, Salton Trough, United States and Mexico. Studies in Diagenesis. United States Geologic Survey Bulletin, **1578**: 83-95.

Bell, K. 2001. Carbonatites: relationships to mantle-plume activity. *In* Ernst, R. E., and Buchan, K. L., eds. Mantle plumes: their identification through time. Geological Society of America Special Paper, **352**: 267–290.

Bertrand, R., and Lavoie, V. 2006. Hydrocarbon source rocks and organic matter maturation of lower Paleozoic successions in the St. Lawrence Platform and in the external domain of the Quebec Appalachians. Geological Association of Canada-Mineralogical Association of Canada annual meeting, Montreal 2006, Program with abstracts.

Castonguay, S., Dietrich, J., Shinduke, R., and Laliberté, J.-Y. 2006. Nouveau regard sur l'architecture de la plate-forme du Saint-Laurent et des Appalaches du sud du Québec par le retraitement des profils de sismique réflexion M-2001, M-2002 et M-2003. Geological Survey of Canada, Open File 5328.

Castonguay, S., Ruffet, G., Tremblay, A., and Féraud, G. 2001. Tectonometamorphic evolution of the southern Quebec Appalachians: $^{40}Ar/^{39}Ar$ evidence for Ordovician crustal thickening and Silurian exhumation of the internal Humber Zone. Geological Society of America Bulletin, **113**: 144-160.

Castonguay, S., Ruffet, G., and Tremblay, A. 2007. Dating polyphase deformation across low-grade metamorphic belts: an example based on $^{40}Ar/^{39}Ar$ muscovite age constraints from the southern Quebec Appalachians, Canada. Geological society of America Bulletin, **119**: 978-992.

Castonguay, S., Dietrich, J., Lavoie, D., and Laliberte, J.-Y. 2010. Structure and petroleum plays of the St. Lawrence Platform and Appalachians in southern Quebec: insights from interpretation of MRNQ seismic reflection data. Bulletin of Canadian Petroleum Geology, **58**: 219-234.

Castonguay, S., and Tremblay, A. 2003. Tectonic evolution and significance of Silurian-Early Devonian hinterland-directed deformation in the internal Humber zone of the southern Quebec Appalachians. Canadian Journal of Earth Science, **40**: 255-268

Clark, T.H. 1972. Region de Montreal. Ministere des Richesses Naturelles du Quebec, Service de l'exploration geologique, Rapport Geologique 152.

Dodson, M. H. 1973. Closure temperature in cooling geochronological and petrological systems. Contributions to Mineralogy and Petrology, **40**: 259-274.

Duncan, R.A. 1984. Age progressive volcanism in the New England Seamounts and the opening of the central Atlantic Ocean. Journal of Geophysical Research, **89**: 9980-9990.

Farley K. A. 2000. Helium diffusion from apatite: general behavior as illustrated by Durango fluorapatite. Journal of Geophysical Research, **105**: 2903-2914.

Farley, K. A. 2002. (U-Th)/He dating: techniques, calibrations, and applications. Reviews in Mineralogy and Geochemistry, **47**: 819-844.

Farley, K. A., Wolf, R. A., and Silver, L. T. 1996. The effects of long alpha-stopping distances on (U-Th)/He dates. Geochimica et Cosmochimica Acta, **60**: 4223-4230.

Flowers, R. M.; Ketcham, R. A., Shuster, D. L., and Farley, K. A. 2009. Apatite (U-Th)/He thermochronometry using a radiation damage accumulation and annealing model. Geochimica et Cosmochimica Acta, **73**: 2347-2365.

Foland, K.A., and Faul, H. 1977. Ages of the White Mountain intrusives-New Hampshire, Vermont, and Maine, USA. American Journal of Science, **277**: 888-904.

Foland, K. A., Gilbert, L. S., Sebring, C. A., and Jiang-Feng, C. 1986. $^{40}Ar/^{39}Ar$ ages for plutons of the Monteregian Hills, Quebec: Evidence for a single episode of Cretaceous magmatism. Geological Society of America Bulletin, **97**: 966-974.

Foster, D. A. 2008. Delamination of the subcontinental lithosphere of the Wyoming craton related to the Yellowstone hot spot. Geological Society of America Abstracts with Programs, **40**: 327.

Gaudette, H. E., Vitrac-Michard, A., and Allegre, C. J. 1981. North American Precambrian history recorded in a single sample: high-resolution U-Pb systematics of the Potsdam sandstone detrital zircons, New York State. Earth and Planetary Science Letters, **54**: 248-260.

Glasmacher, U. A., Tremblay, A., and Clauer, N. 2003. K-Ar dating constraints on the tectonothermal evolution of the external Humber Zone, southern Quebec Appalachians. Canadian Journal of Earth Science, **40**: 285-300.

Guenthner, W. R., Reiners, P. W., DeCelles, P. G., and Kendall, J. 2014. Sevier belt exhumation in central Utah constrained from complex zircon (U-Th)/He data sets: Radiation damage and He inheritance effects on partially reset detrital zircons. Geological Society of America Bulletin, **127**: 323-348.

Guenthner, W. R., Reiners, P. W., Ketcham, R. A., Nasdala, L., and Geister, G. 2013. Helium diffusion in natural zircon: radiation damage, anisotropy, and the interpretation of zircon (U-Th)/He thermochronology. American Journal of Science, **313**: 145-198.

Harrison, M. T., and Zeitler, P. K. 2005. Fundamentals of noble gas thermochronometry. Reviews in Mineralogy and Geochemistry, **58**: 123-149.

Heaman, L. M., and Kjarsgaard, B. A. 2000. Timing of eastern North American kimberlite magmatism: continental extension of the Great Meteor hotspot track? Earth and Planetary Science Letters, **178**: 253-268.

Heizler, M. T., and Harrison, M. 1998. The thermal history of New York basement determined from the $^{40}Ar/^{39}Ar$ K-feldspar studies. Journal of Geophysical Research, **103**: 29,795-29,814.

Heroux, Y., and Bertrand, R. 1991. Maturation thermique de la matiere organique dans un bassin du Paleozoique inferieur, basses-terres du Saint-Laurent, Quebec, Canada. Canadian Journal of Earth Science, **28**: 1019-1030

Heroux, Y., and Tasse, N. 1990. Organic matter alteration in an early Paleozoic basin: zonation around mineral showings compared to that around intrusion, St. Lawrence Lowlands, Quebec, Canada. Geological Society of America Bulletin, **102**: 877-888.

Ketcham, R. A. 2005. Forward and inverse modeling of low-temperature thermochronometry data. Reviews in Mineralogy and Geochemistry, **58**: 275-314.

Lavoie, D. 1994. Diachronic collapse of the Ordovician continental margin, eastern Canada: comparison between the Quebec Reentrant and the St. Lawrence Promontory. Canadian Journal of Earth Science, **31**: 1309-1319.

Lavoie, D., Pinet, N., Dietrich, J., Hannigan, P., Castonguay, S., Hamblin, A., and Giles, P. 2009. Petroleum resources assessment, Paleozoic successions of the St. Lawrence Platform and Appalachians of eastern Canada. Geological Survey of Canada, Open File 6174.

Lebel, D., and Hubert, C. 1995. Geologie de la region de Saint-Malachie (Chaudiere Appalaches), Quebec. Ministere Des Resources Naturelles, ET (93-03, 63 pp.).

Legall, F. D., Barnes, C. R., and Macqueen, R. W. 1981. Thermal maturation, burial history and hotspot development, Palaeozoic strata of southern Ontario-Quebec, from conodont and acritarch colour alteration studies. American Association of Petroleum Geologists Bulletin, **75**: 139-155.

McHone, J. G. 1992. Mafic dike suites within Mesozoic igneous provinces of New England and Atlantic Canada. *In* Puffer, J. H., and Ragland, P. C., eds, Eastern North American Mesozoic magmatism. Geologic Society of America Special Paper, **268**: 1-12.

McHone, J. G., and Butler, J. R. 1984. Mesozoic igneous provinces of New England and the opening of the North Atlantic Ocean. Geological Society of America Bulletin, **95**: 757-765.

Meesters, A. G. C. A., and Dunai, T. J. 2002. Solving the production-diffusion equation for finite diffusion domains of various shapes: Part 2. Application to cases with α-ejection and nonhomogeneous distribution of the source. Chemical Geology, **186**: 57-73.

Mezger, K., Rawnsley, C. M., Bohlen, S. R., and Hanson, G. N. 1991. U-Pb garnet, sphene, monazite, and rutile ages: implications for the duration of high-grade metamorphism and cooling histories, Adirondack Mts., New York. Journal of Geology, **99**: 415-428.

Montario, M. J., and Garver, J. I. 2009. The thermal evolution of the Grenville Terrane revealed through U-Pb and fission-track analysis of detrital zircon from Cambro- Ordovician

quartz arenites of the Potsdam and Galway Formations. Journal of Geology, **117**: 595-614.

Morgan, W. J. 1981. Hot spot tracks and the early rifting of the Atlantic. Tectonophysics, **94**: 123-139.

Nowlan, G.S., and Barnes, C.R. 1987. Thermal maturation of Palaezoic strata in eastern Canada from conodont colour alteration index (CAI) data, with implications for burial history, tectonic evolution, hotspot tracks and hydrocarbon exploration. Geological Survey of Canada Bulletin, **367**: 7-11.

Ogunyomi, O., Hesse R., and Heroux Y. 1980. Pre-orogenic and synorogenic diagenesis and anchimetamorhism in the Lower Palaeozoic continental margin sequences of the Northern Appalachians in and around Quebec City, Canada. Bulletin of Canadian Petroleum Geology, **28**: 559-557.

Pinet, N., and Tremblay, A. 1995. Tectonic evolution of the Quebec-Maine Appalachians: from oceanic opening to obduction and collision in northern Appalachians. American Journal of Science, **295**: 173-200.

Pinet, N., Castonguay, S., Tremblay, A. 1996. Thrusting and back thrusting in the Taconian internal zone, southern Quebec Appalachians. Canadian Journal of Earth Science, **33**: 1283-1293.

Reiners, P. W. 2002. (U-Th)/He chronometry experiences a renaissance. Earth and Space News, **83**: 21-27.

Reiners, P. W. 2005. Zircon (U-Th)/He thermochronometry. Reviews in Mineralogy and Geochemistry, **58**: 151-179.

Reiners, P. W., and Farley, K. A. 2001. Influence of crystal size on apatite (U-Th)/He

thermochronology: an example from the Bighorn Mountains, Wyoming. Earth and Planetary Science letters. **188**: 413-420.

Reiners, P. W., Spell, T. L., Nicolescu, S., and Zanetti, K. A. 2004. Zircon (U-Th)/He thermochronometry: He diffusion and comparisons with $^{40}Ar/^{39}Ar$ dating. Geochimica et Cosmochimica Acta, **68**: 1857-1887.

Ring, U., Brandon, M., Willett, S., and Lister, G. 1999. Exhumation processes. Geological Society, London, Special publications, **154**: 1-27.

Roden-Tice, M. K., and Tice, S. J. 2005. Regional-scale Mid-Jurassic to Late Cretaceous unroofing from the Adirondack Mountains through Central New England based on apatite fission-track and (U-Th)/He thermochronology. Journal of Geology, **112**: 535-552.

Rondenay, S., Bostock, M. G., Hearn, T. M., White, D. J., and Ellis, R. M. 2000. Lithospheric assembly and modification of the SE Canadian Shield: Abitibi-Grenville teleseismic experiment. Journal of Geophysical Research, **105**: 13,735-13,754.

Sasseville, C., Tremblay, A., Clauer, N., and Liewig, N. 2008. K-Ar constraints on the evolution of polydeformed fold-thrust belt: the case of the Northern Appalachians (southern Quebec). Journal of Geodynamics, **45**: 99-119.

Sengor, A.M.C. 2001. Elevation as indicator of mantle plume activity, *in* Ernst, R.E., and Buchan, K.L., eds., Mantle Plumes: Their Identification through Time. Geological Society of America Special Paper, **352**: 183-225.

Shuster, D. L., Flowers, R. M., and Farley, K. A. 2006. The influence of natural radiation damage on helium kinetics in apatite. Earth and Planetary Science Letters, **249**: 148-161.

Sleep, N. H. 1990. Monteregian hotspot track: A long-lived mantle plume. Journal of Geophysical Research, **95**: 983-21.

Spencer, S. Kohn, B., Gleadow, A., Norman, M., Belton, D., and Carter, T. 2004. The importance of residing in a good neighbourhood: rechecking the rules of the game for apatite (U-Th)/He thermochronometry. Abstract Volume of the 10th International Conference on Fission Track Dating and Thermochronology, Amsterdam, p. 20.

Spiegel, C., Kohn, B., Belton, D., Berner, Z., and Gleadow, A. 2009. Apatite (U-Th-Sm)/He thermochronology of rapidly cooled samples: The effect of He implantation. Earth and Planetary Science Letters, **285**: 105-114.

Stockli, D. 2005. Application of Low-Temperature Thermochronometry to Extensional Tectonic Settings. Reviews in Mineralogy and Geochemistry, **58**: 411-448.

Stockli, D., Farley, K. A., and Dumitru, T. 2000. Calibrations of the apatite (U-Th)/He thermochronometer on an exhumed fault clock, White Mountains California. Geology, **28**: 983-986.

St. Julien, P., and Hubert, C. 1975. Evolution of the Taconian Orogeny in the Quebec Appalachians. American Journal of Science, **275-A**: 337-362.

Taylor, J., and Fitzgerald, P. 2011. Low-temperature thermal history and landscape development of the eastern Adirondack Mountains, New York: Constraints from apatite fission-track thermochronology and apatite (U-Th)/He dating. Geological Society of America Bulletin, **123**: 412-426.

Theriault, R. 2012 Caracterisation du shale d'Utica et du Groupe de Lorraine, Basses-Terres du Saint-Laurent Partie 2: Interpretation geologique. Geologie Quebec, DV 2012-04.

Tremblay, A., and Pinet, N. 1994. Distribution and characteristics of the Taconian and Acadian deformation, southern Quebec Appalachians. Geological Society of American Bulletin, **106**: 1172-1181.

Tremblay, A., and Pinet, N. 2016. Late Neoproterozoic to Permian tectonic evolution of the Quebec Appalachians, Canada. Earth-Science Reviews, **160**: 131-170.

Tremblay, A., and Castonguay, S. 2002. Structural evolution of the Laurention margin revisited (southern Quebec Appalachians): implications for the Salinic orogeny and successor basins. Geology, **30**: 79-82.

White, T. S., Witzke, B. J., and Ludvigson, G. A. 2000. Evidence for an Albian Hudson arm connection between the Cretaceous Western Interior Seaway of North America and the Labrador Sea. Geological Society of America Bulletin, **112**: 1342-1355.

Wolfe, M. R., and Stockli, D. F. 2010. Zircon (U-Th)/He thermochronometry in the KTB drill hole, Germany, and its implications for bulk He diffusion kinetics in zircon. Earth and Planetary Science Letters, **295**: 69-82.

Williams, H. 1979. Appalachian Orogen in Canada. Canadian Journal of Earth Sciences, **16**: 792-807.

Yang, C., and Hesse, R., 1991. Clay minerals as indicators of diagenetic and anchimetamorphic grade in an overthrust belt, external domain of the southern Canadian Appalachians. Clay Minerals. **26**: 211-231.

Yang, C., and Hesse, R., 1993. Diagenesis and anchimetamorphism in an overthrust belt, external domain of the Taconian Orogen, southern Canadian Applachians-II. Paleogeothermal gradients derived from maturation of different types of organic matter. Organic Geochemistry, **20**: 381-403.

Table 1. (U-Th)/He analysis for zircon from the St. Lawrence Platform and Humber zone of Southern Quebec.

Grain #	Corrected Date (Ma)	±2σ (Ma)	Raw Date (Ma)	eU (ppm)	rs* (μm)	^{4}He (nmol/g)	U (ppm)	Th (ppm)	Th/U	Ft**
St. Lawrence Platform										
SLP_A-12 *(45.322°N/73.950°W) Late Cambrian, Potsdam Group, Covey Hill Formation*										
Zr-1	318.75	56.40	231.59	158.6	41.36	202.033	142.69	67.73	0.475	0.727
Zr-3	353.86	50.70	266.35	125.1	46.28	183.867	110.43	62.61	0.567	0.753
Zr-4	506.10	36.60	445.46	104.2	101.17	259.369	80.16	102.18	1.275	0.880
Zr-5	408.85	32.59	312.11	146.8	48.47	253.766	131.98	62.90	0.477	0.763
Zr-6	368.68	26.85	323.99	76.3	99.64	136.960	60.91	65.58	1.077	0.879
Zr-8	522.85	39.51	448.02	80.0	82.82	200.865	72.03	33.80	0.469	0.857
Zr-9	267.14	20.53	205.43	65.6	50.00	74.299	56.21	39.90	0.710	0.769
Zr-11	236.66	28.43	158.86	84.3	33.77	73.181	73.19	47.20	0.645	0.671
Zr-12	285.45	21.03	258.54	19.4	129.93	27.638	14.55	20.67	1.421	0.906
SLP_A-2 *(44.253°N/73.802°W) Early Ordovician, Beakmantown Group, Theresa Formation*										
Zr-1	278.97	49.09	199.46	67.7	40.08	74.030	52.43	64.94	1.239	0.715
Zr-2	276.72	19.37	217.56	73.1	53.09	87.397	58.61	61.85	1.055	0.782
Zr-3	483.38	67.39	357.57	39.2	43.73	77.849	34.79	18.58	0.534	0.740
Zr-4	226.21	17.63	194.20	44.2	84.55	47.039	36.30	33.59	0.925	0.858
Zr-5	198.90	33.79	147.36	63.8	42.47	51.320	53.62	43.24	0.806	0.741
Zr-6	249.84	18.45	203.85	144.2	64.30	161.202	113.77	129.38	1.137	0.816
Zr-7	386.19	57.42	283.40	80.2	42.98	125.445	66.12	59.76	0.904	0.734
Zr-8	739.64	57.41	613.92	210.8	68.75	737.193	199.36	48.69	0.244	0.830
SLP_A-5 *(45.044°N/73.685°W) Late Cambrian, Potsdm Group, Cairnside Formation*										
Zr-1	230.00	17.87	192.68	22.9	72.85	24.202	19.89	12.81	0.644	0.838
Zr-2	213.66	20.41	148.81	265.7	36.62	215.971	250.61	64.20	0.256	0.696
Zr-3	155.74	11.92	123.49	37.3	56.27	25.090	31.88	22.92	0.719	0.793
Zr-4	164.77	12.01	122.87	94.6	44.77	63.347	85.68	38.10	0.445	0.746
Zr-5	192.45	14.31	162.89	43.5	76.61	38.759	40.63	12.26	0.302	0.846
Zr-6	244.44	32.78	179.79	117.9	42.81	116.030	108.29	40.73	0.376	0.736
Zr-7	272.47	20.17	225.13	141.9	67.44	175.661	129.15	54.39	0.421	0.826
Zr-8	194.15	17.86	149.93	201.1	50.37	164.666	186.04	64.12	0.345	0.772
SLP_B-1 *(46.026°N/72.707°W) Late Ordovician, Queenston Group, Becancour Formation*										
Zr-1	676.15	51.42	588.46	44.1	92.16	147.274	38.29	24.92	0.651	0.870
Zr-2	607.07	48.14	489.63	40.5	60.57	111.407	34.39	25.97	0.755	0.807
Zr-3	681.82	49.46	572.17	274.6	72.84	891.775	261.20	57.09	0.219	0.839
Zr-4	722.63	68.21	565.84	118.4	53.56	378.728	100.47	76.11	0.758	0.783
Zr-5	688.04	54.24	583.93	43.9	78.65	145.013	36.89	29.65	0.804	0.849
Zr-6	759.54	64.88	596.32	107.5	54.19	363.345	90.00	74.47	0.827	0.785
Zr-7	706.34	54.74	601.41	161.4	79.55	551.734	147.13	60.75	0.413	0.851
Zr-8	757.06	123.34	550.53	57.5	41.67	178.696	49.25	34.90	0.709	0.727
SLP_D-10 *(46.155°N/72.537°W) Late Ordovician, Queenston Group, Becancour Formation*										
Zr-1	693.15	48.52	580.11	77.6	67.14	255.632	68.32	39.56	0.579	0.828
Zr-2	776.16	54.33	626.91	139.0	56.81	496.038	115.25	101.06	0.877	0.797
Zr-3	779.00	54.53	638.03	36.2	60.19	131.846	30.88	22.73	0.736	0.808
Zr-4	134.24	9.40	99.00	10.5	46.08	5.690	4.30	26.46	6.154	0.735
Zr-5	371.99	26.04	300.11	237.3	57.73	394.215	209.37	118.99	0.568	0.801
Zr-6	817.57	57.23	639.06	196.8	48.56	719.238	184.05	54.18	0.294	0.768
Zr-7	570.88	39.96	441.40	68.6	48.11	169.688	60.45	34.64	0.573	0.764
Zr-8	612.50	42.87	438.65	106.4	38.00	261.446	91.95	61.32	0.667	0.705
SLP_D-5 *(46.445°N/72.738°W) Grenville Province*										
Zr-1	501.85	35.13	408.19	433.7	58.66	990.410	405.28	121.09	0.299	0.806
Zr-2	181.59	12.71	153.15	708.1	71.77	592.531	681.49	113.27	0.166	0.841
Zr-3	426.50	29.85	353.94	469.4	64.78	924.889	444.79	104.95	0.236	0.824
Zr-4	427.38	29.92	354.42	474.3	64.69	935.692	444.14	128.38	0.289	0.824
Zr-5	434.09	30.39	341.39	496.9	50.86	943.483	482.53	61.07	0.127	0.779
Zr-6	234.77	16.43	182.10	628.4	49.13	626.961	602.98	108.28	0.180	0.772
Zr-7	222.80	15.60	171.17	837.2	47.71	784.199	790.19	199.93	0.253	0.764
Zr-8	470.62	32.94	362.10	446.5	47.14	900.401	416.90	125.86	0.302	0.762
SLP_D-6 *(46.736°N/71.562°W) Grenville Province*										
Zr-2	348.40	24.39	285.02	452.2	60.91	712.824	424.63	117.50	0.277	0.813
Zr-3	424.17	29.69	342.75	423.3	57.27	806.722	396.19	115.50	0.292	0.802
Zr-4	420.20	29.41	328.85	386.6	50.41	705.899	361.88	105.20	0.291	0.776
Zr-5	450.23	31.52	372.42	383.1	63.58	795.566	363.19	84.70	0.233	0.821
Zr-6	288.26	20.18	229.96	730.8	54.84	924.646	680.76	213.02	0.313	0.793
Zr-7	233.40	16.34	184.44	872.7	52.98	881.957	815.61	242.92	0.298	0.787
Zr-8	335.04	23.45	264.48	470.4	52.24	686.831	444.59	109.89	0.247	0.784

Table 1. (continued)

Grain #	Corrected Date (Ma)	2σ (Ma)	Raw Date (Ma)	eU (ppm)	rs* (μm)	4He (nmol/g)	U (ppm)	Th (ppm)	Th/U	Ft**
External Humber Zone										
EHZ_B-5 *(45.862°N/72.450°W) Early Cambrian, Granby Formation, Granby nappe*										
Zr-1	363.36	26.01	308.63	237.2	77.91	405.701	229.57	32.55	0.142	0.849
Zr-2	327.07	24.80	271.77	170.6	68.97	255.981	164.61	25.31	0.154	0.831
Zr-3	321.17	22.89	260.71	112.2	61.72	161.387	105.49	28.70	0.272	0.812
Zr-4	359.59	25.97	296.44	143.0	66.50	234.477	133.41	40.59	0.304	0.824
Zr-5	372.97	26.42	318.95	201.8	77.38	356.937	189.68	51.68	0.272	0.855
Zr-6	277.66	23.44	217.69	125.1	53.29	149.684	116.80	35.54	0.304	0.784
Zr-7	384.37	36.62	297.57	141.8	51.09	233.440	125.45	69.68	0.555	0.774
Zr-8	388.27	46.93	293.68	161.5	46.82	262.417	149.17	52.64	0.353	0.756
EHZ_C-13 *(46.734°N/71.369°W) Cambrian/Lower Ordovician, Sillery Group, Lauzon Formation, Chaudiere nappe*										
Zr-1	818.01	61.50	737.47	78.9	112.61	334.308	64.95	59.26	0.912	0.895
Zr-2	645.96	49.72	558.66	38.0	83.26	119.860	30.01	33.86	1.128	0.858
Zr-3	574.86	45.71	474.13	53.9	63.74	143.360	43.98	42.05	0.956	0.817
Zr-4	628.77	50.74	510.57	45.8	59.04	131.814	37.39	35.98	0.962	0.804
Zr-5	694.69	53.66	596.14	159.5	76.80	541.294	146.20	56.66	0.388	0.850
Zr-6	842.46	65.26	721.92	87.7	77.56	362.401	67.63	85.25	1.261	0.848
Zr-7	743.79	58.04	619.41	113.3	66.91	398.121	84.88	121.01	1.426	0.824
Zr-8	774.27	60.49	643.13	332.5	65.80	1215.383	249.94	351.25	1.405	0.821
EHZ_C-10 *(46.749°N/71.301°W) Middle Cambrian, Sillery Group, Saint Nicolas Formation*										
Zr-1	443.33	32.74	370.05	53.5	71.43	110.250	46.55	29.75	0.639	0.835
Zr-2	534.82	58.71	415.46	58.4	51.92	135.522	49.84	36.46	0.732	0.777
Zr-3	520.27	59.27	401.29	88.1	50.40	197.272	77.67	44.33	0.571	0.771
Zr-4	480.48	35.72	408.51	60.0	79.87	136.597	47.89	51.40	1.073	0.850
Zr-5	495.78	36.04	414.39	66.2	72.24	153.132	55.19	46.85	0.849	0.836
Zr-6	529.34	52.38	410.56	77.6	51.49	177.927	67.85	41.53	0.612	0.776
Zr-7	530.65	44.42	441.99	49.4	70.78	122.156	41.98	31.48	0.750	0.833
Zr-8	434.01	46.88	330.71	207.1	48.30	379.799	181.17	110.17	0.608	0.762
EHZ_C-4 *(46.548°N/71.182°W) Middle Ordovician, Drummondville Group, Riviere Etchemin Formation*										
Zr-1	427.05	30.22	379.03	73.8	99.10	155.895	66.42	31.49	0.474	0.888
Zr-2	402.10	28.68	350.03	33.7	93.20	65.444	26.32	31.37	1.192	0.871
Zr-3	438.53	32.13	390.80	33.0	102.68	71.980	27.64	22.99	0.832	0.891
Zr-4	386.32	27.94	328.63	11.8	80.44	21.474	9.01	11.84	1.315	0.851
Zr-5	520.82	37.08	462.82	64.4	107.81	167.286	56.72	32.77	0.578	0.889
Zr-6	510.19	37.96	430.01	132.1	74.83	317.995	122.63	40.15	0.327	0.843
Zr-7	509.31	39.57	412.89	109.2	61.75	251.820	96.41	54.32	0.563	0.811
Zr-8	487.21	34.85	407.25	121.9	72.31	276.945	100.82	89.73	0.890	0.836
Internal Humber Zone/Dunnage Zone										
IHZ_B-9 *(45.668°N/72.261°W) Lower/Upper Cambrian, Oak Hill Group, Pinnacle 2 formation*										
Zr-1	82.37	6.04	72.06	1026.0	94.75	400.946	979.00	200.11	0.204	0.875
Zr-2	246.96	17.79	209.29	834.4	76.98	958.842	796.28	162.23	0.204	0.847
Zr-3	192.89	14.43	158.41	767.1	65.57	664.072	684.27	352.34	0.515	0.821
Zr-4	332.21	24.69	274.75	358.2	68.10	543.263	310.41	203.55	0.656	0.827
Zr-5	219.31	16.12	176.10	497.2	58.71	479.326	473.24	102.06	0.216	0.803
Zr-6	282.69	26.77	219.64	400.8	51.23	483.879	390.52	43.87	0.112	0.777
Zr-7	268.49	33.71	205.71	157.7	48.92	178.060	146.79	46.49	0.317	0.766
Zr-8	79.83	5.76	62.31	452.1	52.33	152.648	427.14	106.29	0.249	0.781
IHZ_C-8 *(46.318°N/70.865°W) Early/Middle Cambrian, Rosaire4 Group*										
Zr-1	330.31	24.16	285.30	39.2	88.04	61.762	31.87	31.19	0.979	0.864
Zr-2	289.86	21.06	249.49	33.5	86.21	45.985	26.73	28.71	1.074	0.861
Zr-3	231.68	19.57	192.54	25.8	71.06	27.218	18.35	31.70	1.727	0.831
Zr-4	297.90	24.00	241.25	137.6	61.18	182.816	127.00	45.28	0.357	0.810
Zr-5	286.48	37.88	216.44	217.3	47.31	258.288	174.26	183.31	1.052	0.756
Zr-6	325.18	25.74	254.74	203.3	53.50	285.347	177.43	109.99	0.620	0.783

rs*- spherical radius

Ft**- alpha ejection correction (Farley et al. 1996)

Table 2. (U-Th)/He analysis for apatite from the St. Lawrence Platform and Humber zone of Southern Quebec.

Grain #	Corrected Date (Ma)	±2σ (Ma)	Raw Date (Ma)	eU (ppm)	rs* (μm)	^{4}He (nmol/g)	U (ppm)	Th (ppm)	Sm (ppm)	Th/U	Ft**
St. Lawrence Platform											
SLP_A-12 *(45.322°N/73.950°W) Late Cambrian, Potsdam group, Covey Hill formation*											
Ap-1	132.34	10.27	104.72	12.2	73.89	7.092	12.02	0.92	25.97	0.076	0.791
Ap-2	129.21	9.38	109.74	6.8	105.06	4.117	5.88	3.74	15.94	0.635	0.849
Ap-3	139.12	9.97	108.48	41.8	77.83	24.854	28.00	58.89	27.80	2.103	0.780
Ap-4	123.93	9.23	90.19	7.9	62.42	4.044	4.42	14.88	39.83	3.367	0.728
Ap-5	90.84	17.91	57.68	2.3	42.47	0.731	2.14	0.74	3.09	0.346	0.635
Ap-6	321.12	53.30	232.28	1.2	56.34	1.606	0.65	2.55	1.55	3.948	0.723
Ap-7	204.76	16.26	138.02	11.6	48.58	8.765	10.54	4.47	6.14	0.424	0.674
SLP_A-5 *(45.044°N/73.685°W) Late Cambrian, Potsdam Group, Cairnside Formation*											
Ap-1	106.43	11.46	81.10	1.6	69.19	0.717	1.48	0.47	5.30	0.317	0.762
Ap-2	99.14	11.15	62.15	17.1	45.70	5.862	5.46	49.38	32.99	9.041	0.627
Ap-4	127.30	43.35	88.48	0.8	53.23	0.381	0.24	2.32	0.00	9.479	0.695
SLP_B-1 *(46.026°N/72.707°W) Late Ordovician, Queenston Group, Becancour Formation*											
Ap-1	126.02	16.25	80.05	5.1	42.25	2.317	1.60	15.05	21.23	9.381	0.635
Ap-2	154.52	22.13	99.88	3.3	45.87	1.849	0.74	10.69	16.80	14.362	0.646
Ap-4	89.48	7.58	61.86	7.3	51.88	2.507	2.02	22.38	20.39	11.071	0.691
Ap-5	102.36	8.33	69.29	5.3	53.45	2.067	1.79	14.96	22.08	8.375	0.677
Ap-6	127.14	21.81	75.66	5.5	39.63	2.357	1.13	18.75	22.74	16.651	0.595
SLP_D-10 *(46.155°N/72.537°W) Late Ordovician, Queenston Group, Becancour Formation*											
Ap-1	149.44	38.60	77.93	11.2	30.42	4.879	3.70	31.84	38.23	8.595	0.510
Ap-2	197.10	44.71	112.98	6.4	34.92	4.088	1.40	21.07	34.36	15.047	0.558
Ap-3	158.81	31.13	97.09	8.8	37.91	4.861	2.20	28.03	48.74	12.743	0.597
Ap-4	115.92	18.45	74.29	8.4	41.48	3.476	2.15	26.44	28.51	12.319	0.632
Ap-5	205.68	28.42	150.06	3.9	54.97	3.363	1.16	11.70	22.99	10.050	0.718
SLP_D-5 *(46.445°N/72.738°W) Grenville Province*											
Ap-1	208.40	27.93	133.39	68.7	37.59	50.274	65.76	12.71	45.22	0.193	0.634
Ap-2	238.84	16.14	161.66	134.4	41.37	119.117	127.84	27.79	49.82	0.217	0.671
Ap-3	201.44	21.63	133.64	88.0	40.20	64.571	84.63	14.32	74.31	0.169	0.658
Ap-4	226.30	38.09	133.83	128.3	32.54	94.064	123.73	19.44	71.69	0.157	0.585
Ap-5	194.76	13.98	153.58	53.6	64.77	45.338	52.38	5.35	48.92	0.102	0.784
SLP_D-6 *(46.736°N/71.562°W) Grenville Province*											
Ap-1	177.23	14.07	124.56	66.2	45.44	45.123	65.84	1.55	35.07	0.024	0.698
Ap-2	170.70	15.58	113.75	158.2	40.32	98.261	156.89	5.46	64.68	0.035	0.662
Ap-3	233.69	17.19	179.47	105.2	58.71	103.733	103.78	6.22	35.95	0.060	0.764
Ap-4	185.70	24.38	124.97	56.9	41.09	38.893	56.67	0.76	32.55	0.013	0.668
Ap-5	182.80	17.86	126.30	51.1	43.21	35.357	50.96	0.37	39.36	0.007	0.686
External Humber Zone											
EHZ_C-13 *(46.734°N/71.369°W) Cambrian/Lower Ordovician, Sillery Group, Lauzon Formation*											
Ap-1	185.97	13.23	130.95	46.6	46.37	33.711	37.51	38.65	74.61	1.030	0.698
Ap-2	187.00	19.53	123.03	14.2	40.06	9.587	11.51	11.27	16.83	0.979	0.652
Ap-3	222.73	15.82	176.45	61.6	65.50	59.581	60.46	4.82	10.02	0.080	0.789
Ap-4	292.52	30.58	188.52	52.7	37.20	55.226	50.26	10.33	92.98	0.206	0.635
Ap-5	353.19	25.35	279.29	34.4	65.17	53.697	30.79	15.29	51.91	0.497	0.784
Internal Humber Zone											
IHZ_D-8 *(46.532°N/70.913°W) Grenville Province (Sainte-Marguerite Complex)*											
Ap-1	137.52	12.54	91.98	12.4	43.62	6.249	6.61	24.62	10.40	3.725	0.665
Ap-2	103.54	11.62	65.49	13.0	37.17	4.752	10.38	11.24	42.84	1.083	0.624
Ap-3	124.19	11.58	86.51	13.0	44.98	6.296	11.53	6.25	48.18	0.542	0.688
Ap-4	117.43	10.43	85.82	9.0	49.67	4.363	8.50	2.27	40.39	0.267	0.722
Ap-5	141.98	24.37	82.39	13.5	33.37	6.078	8.56	20.80	14.22	2.429	0.575

rs* - spherical radius

Ft** - alpha ejection correction (Farley et al. 1996)

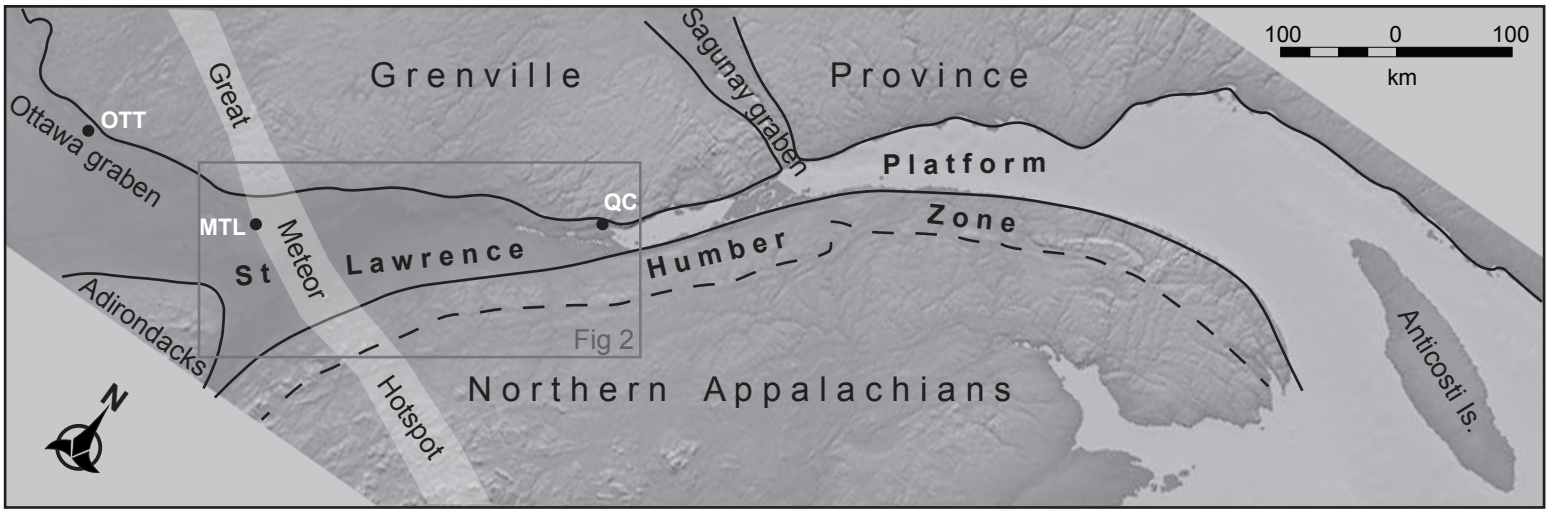

Figure 1. Simplified map of Quebec Appalachians and adjacent regions highlighting the St. Lawrence Platform and Humber Zone. The surface trace of the Mesozoic Great Meteor Hotspot is also shown. The area of interest is denoted with the grey box and shown in detail in Figure 2. OTT: Ottawa; MTL: Montreal; QC: Quebec City.

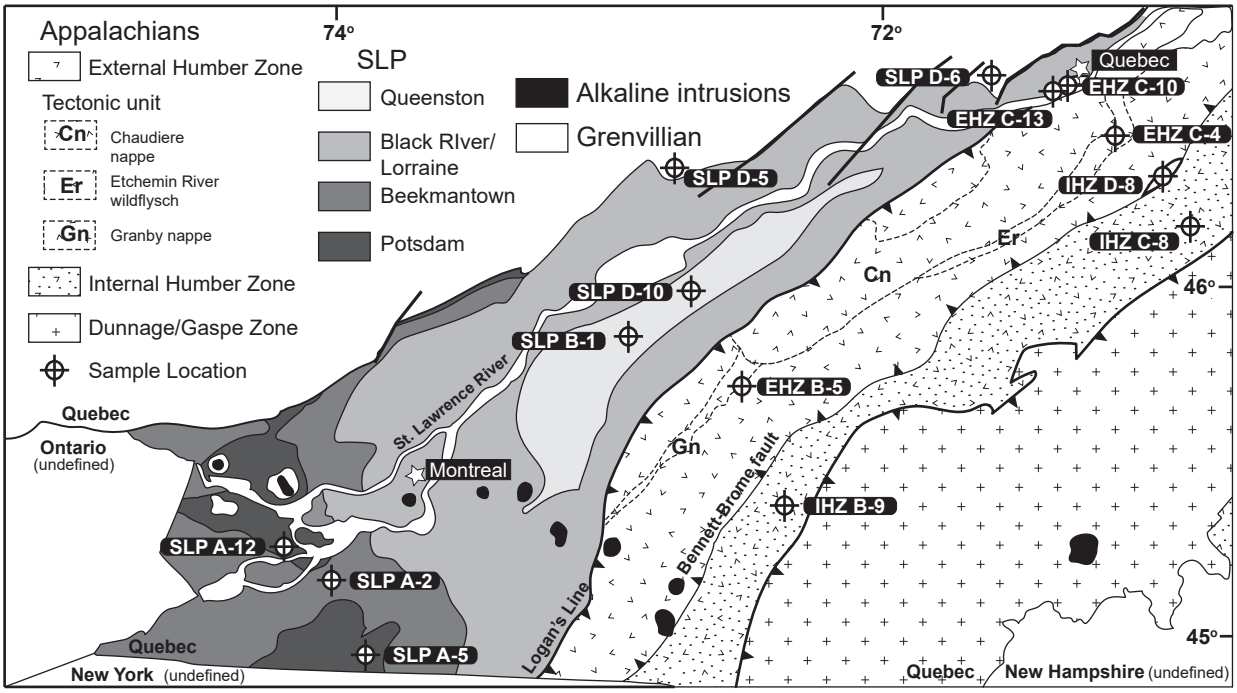

Figure 2. Simplified geological map of southestern Quebec illustrating the late Cambrian to late Ordovician sedimentary sequences of the St. Lawrence Platform (SLP), the tectonically displaced deep marine sedimentary units of the Appalachian structural front (Humber Zone), the underlying crystalline basement of the Grenvillian Province and the early Cretaceous alkaline intrusions of the Meteor Hotspot (modified from Theriault et al., (2012)). The locations of samples collected from surface outcrop for this study are also shown.

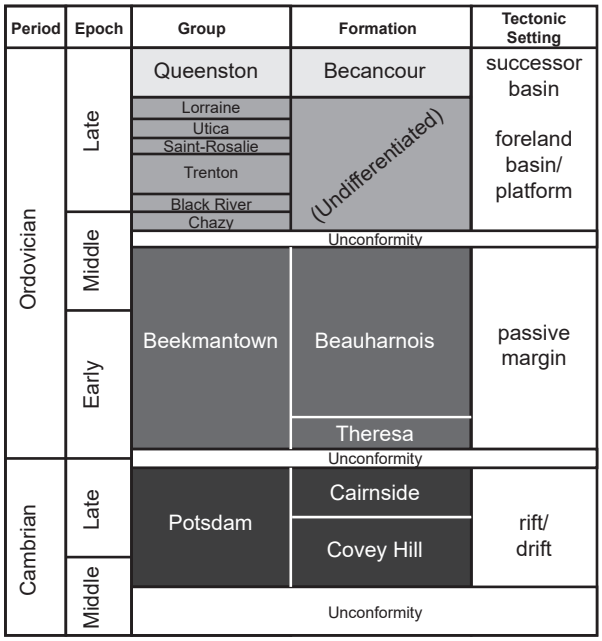

Figure 3. Stratigraphic section of the St. Lawrence Platform. Shading of the stratigraphic groups corresponds to the shading of the St. Lawrence Platform region in figure 1 (Modified from Theriault et al. 2012).

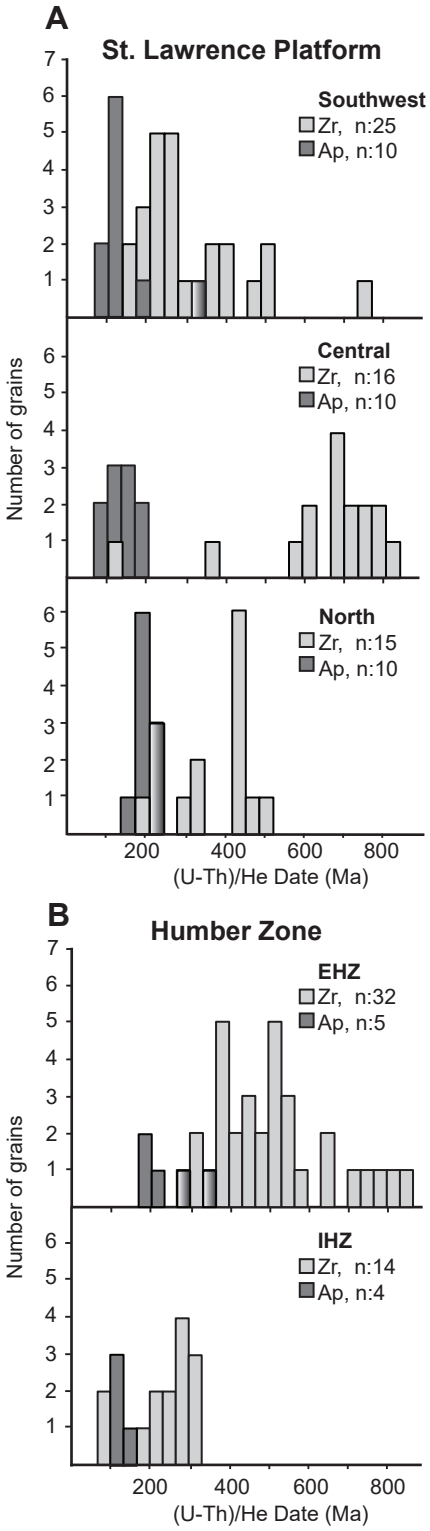

Figure 4. Histograms of ZHe and AHe dates from the St. Lawrence Platform (A) and the Humber Zone (B). Values for zircon are shaded in light grey; values for apatite are shaded in dark grey. Values where zircon and apatite overlap are shaded in a gradient from light to dark grey.

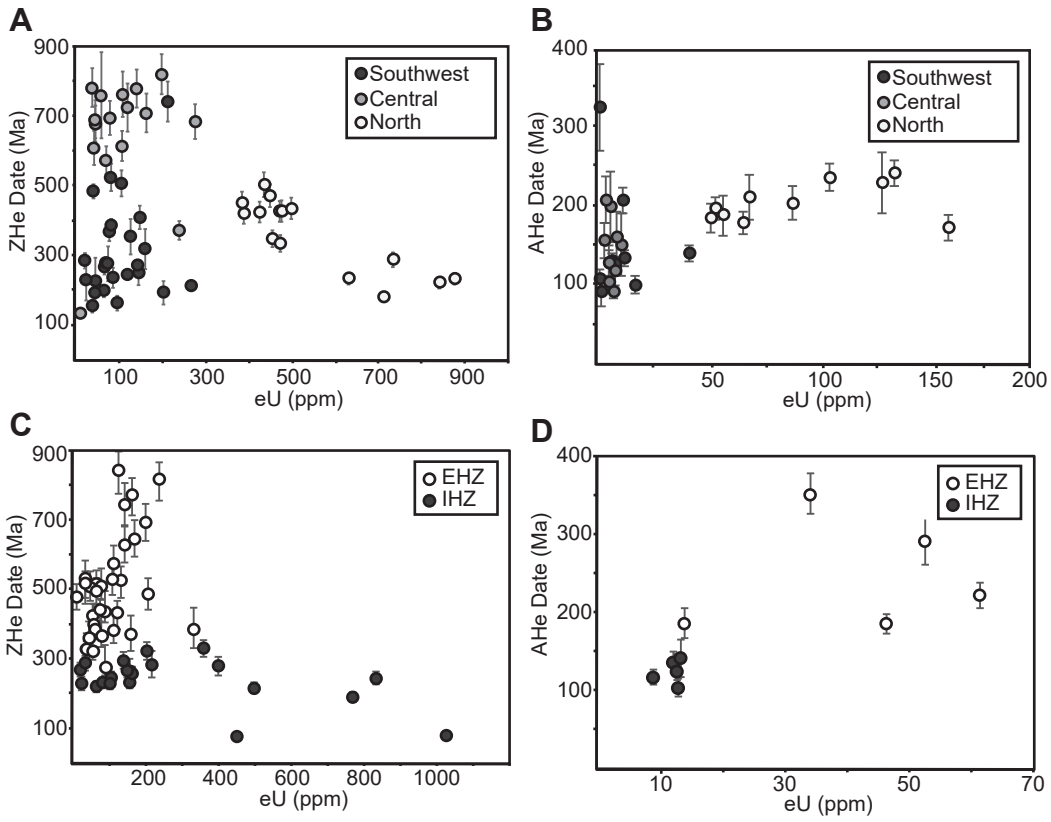

Figure 5. ZHe and AHe date/eU graphs for the St. Lawrence Platform (A,B) and the Humber Zone (D,C)

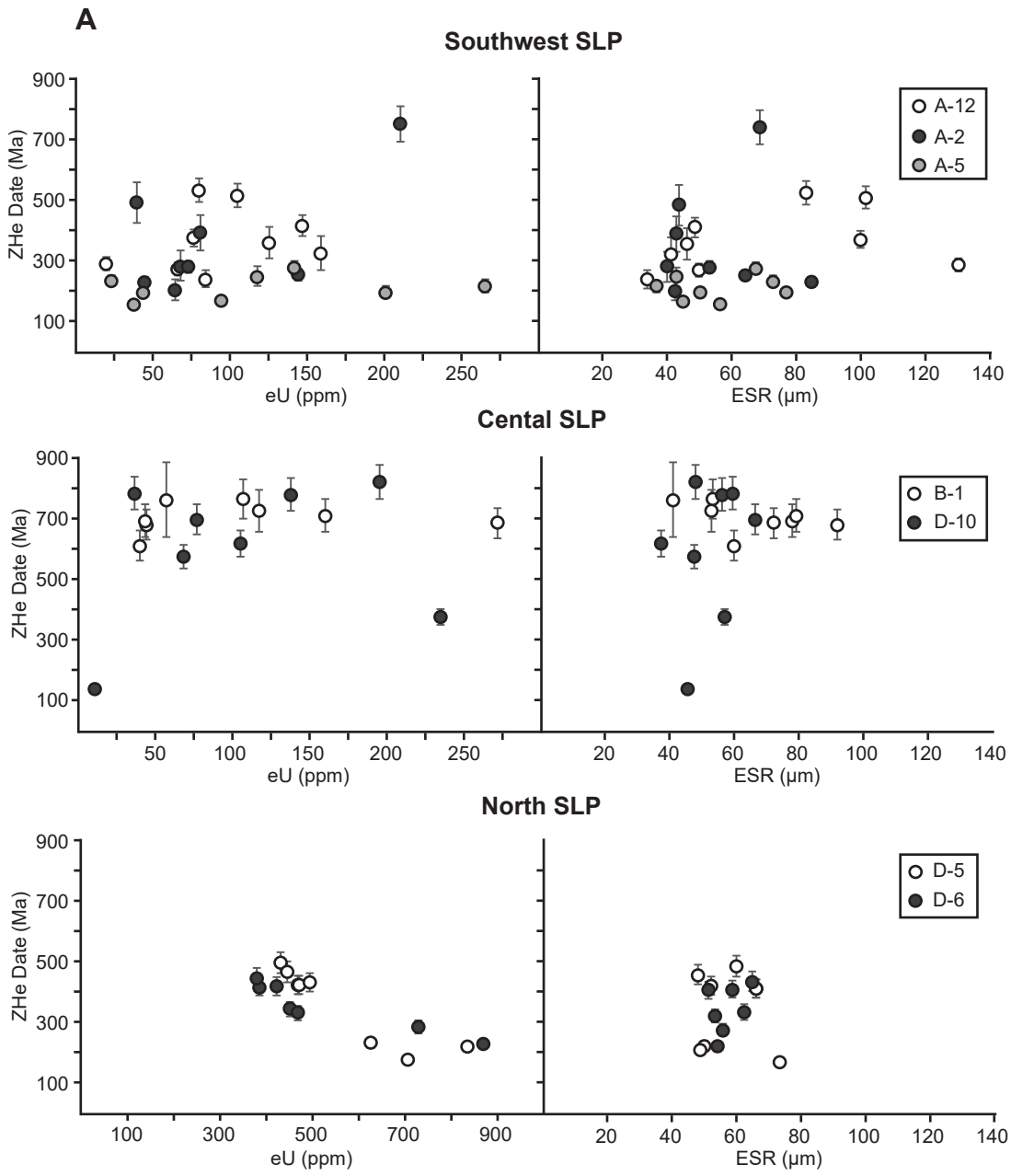

Figure 6a. ZHe date/eU and date/ESR graphs for the St. Lawrence Platform.

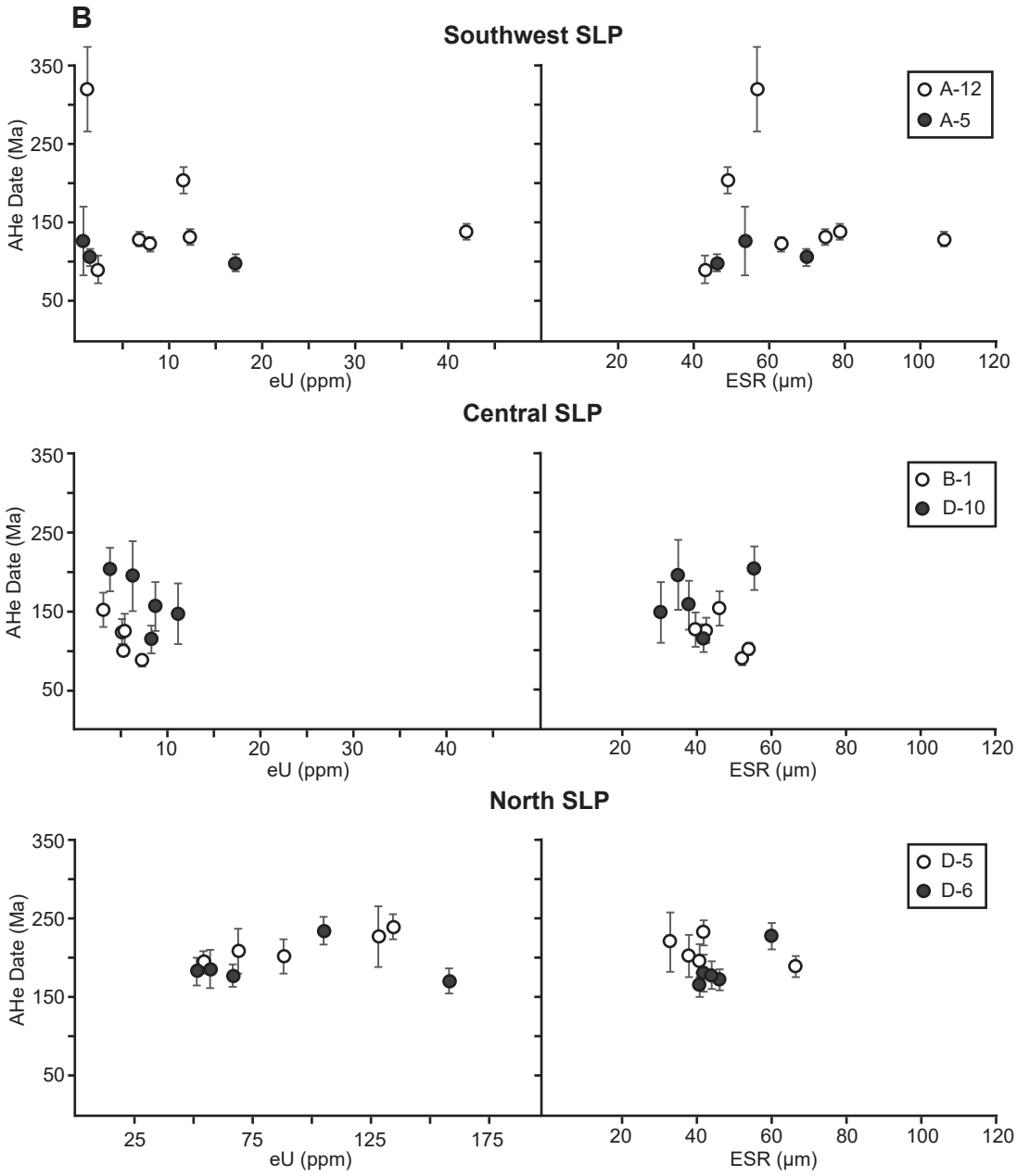

Figure 6b. AHe date/eU and date/ESR graphs for the St. Lawrence Platform.

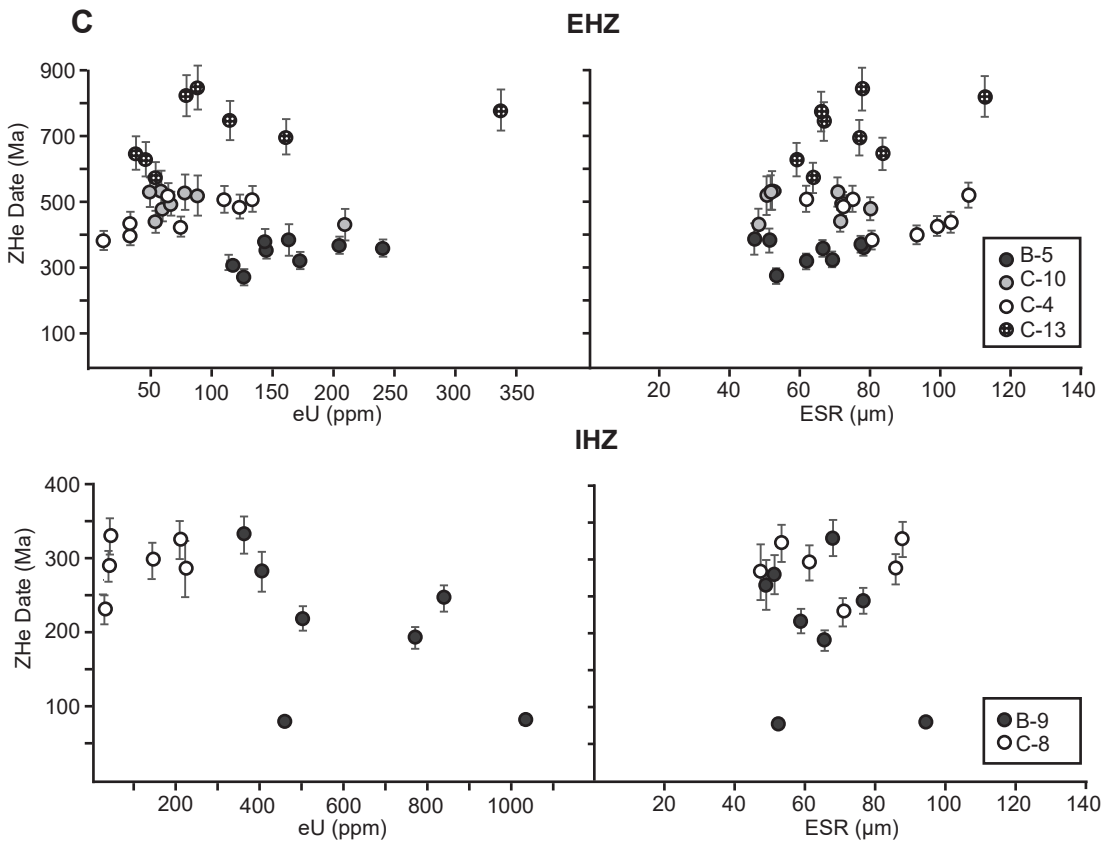

Figure 6c. ZHe date/eU and date/ESR graphs for the Humber Zone.

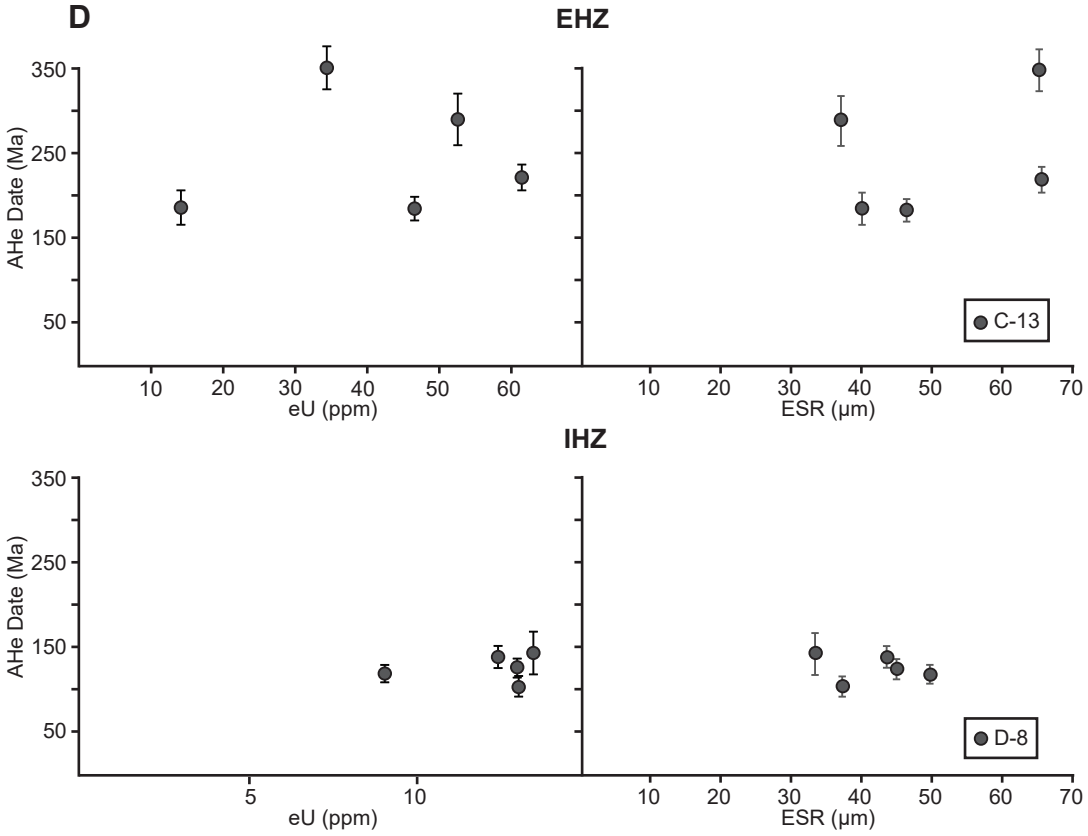

Figure 6d. AHe date/eU and date/ESR graphs for the Humber Zone.

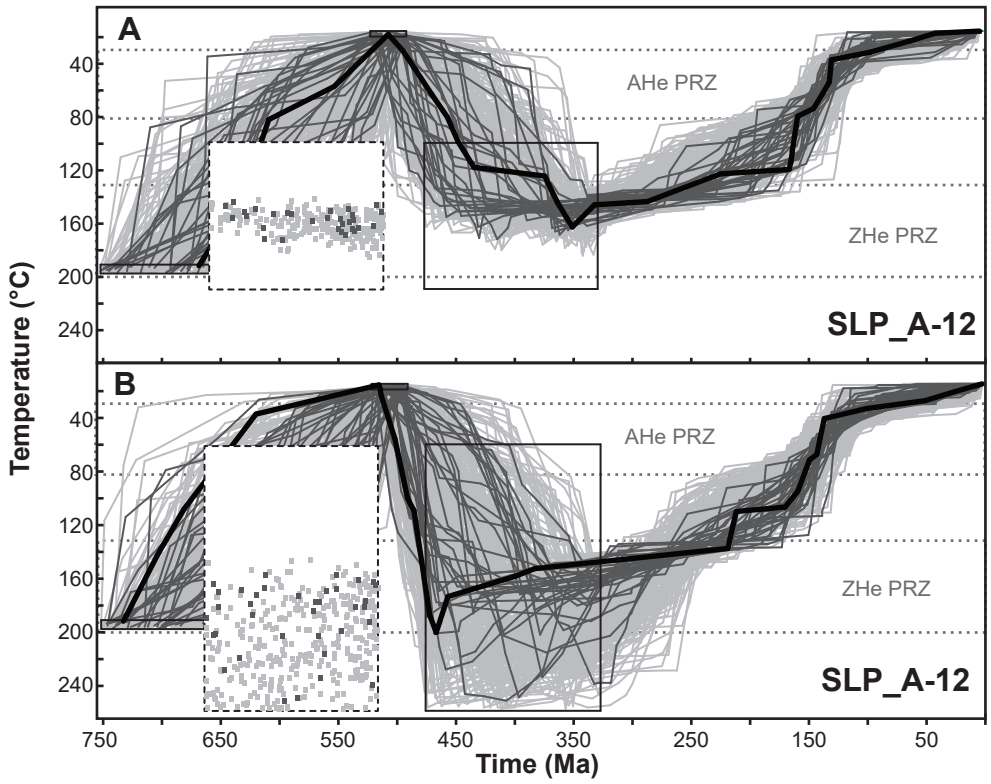

Figure 7. Inverse thermal history models from HeFTy for sample SLP_A-12. (A) Inverse model constructed using both partially and fully reset zircon with apatite. (B) Inverse model constructed using only fully reset zircon with apatite. The "best fit" solutions are represented by a solid black lines, "good fit" solutions by dark gray lines and "acceptable fit" solutions by light grey lines. Coloured points inclosed in the dotted box represent the magnitude of thermal maximum (inflection point) for each thermal path, whereby light grey points correspond to "acceptable fit" solutions and dark grey points correspond to "good fit" solutions.

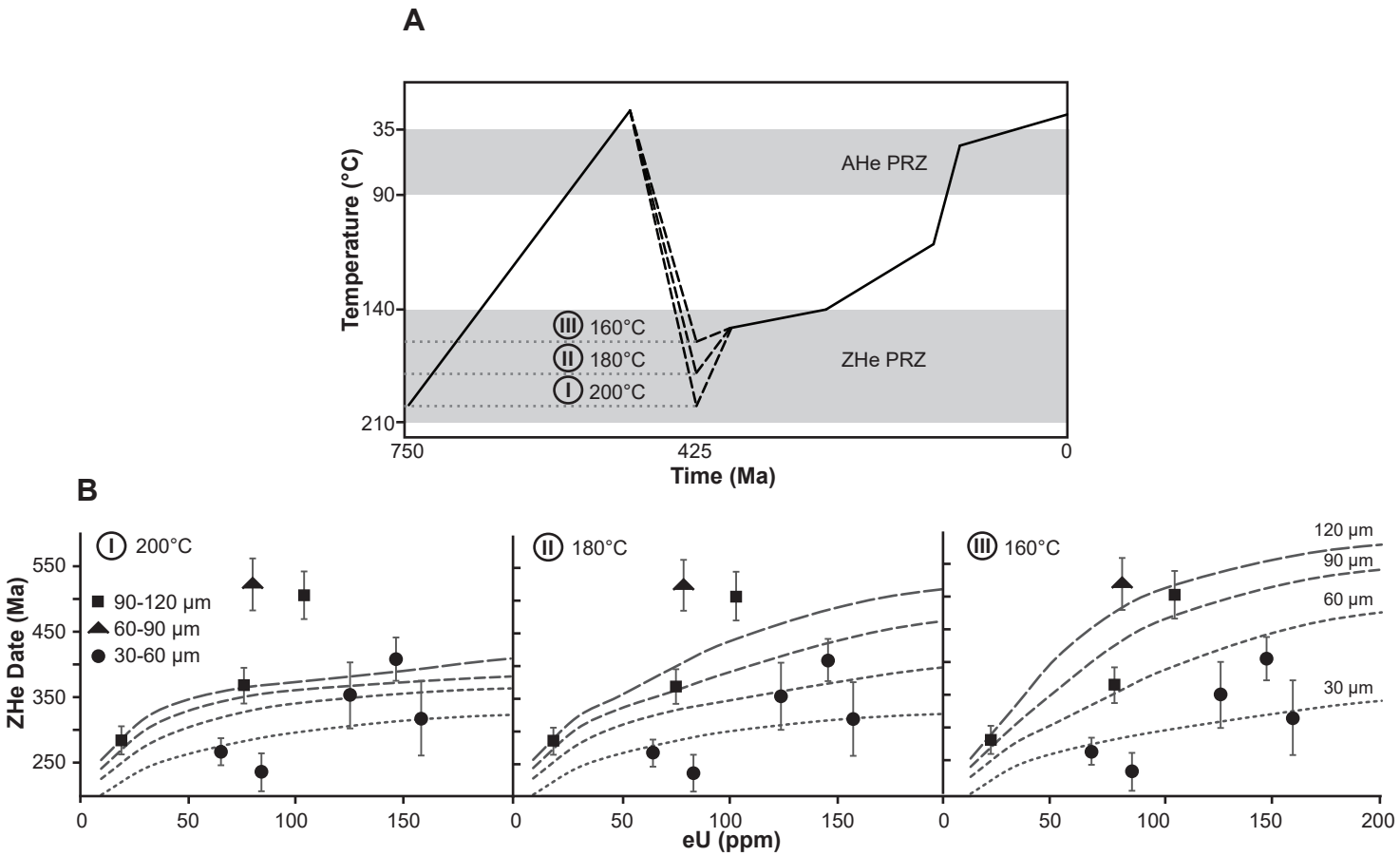

Figure 8. (A) Forward model from HeFTy for sample SLP_A-12 based on three different maximum temperature possibilities. (B) Inheritance curves based on figure 8a, each having a different thermal maximum (200°C, 180°C and 160°C) and all having a pre-depositional history of 750 Ma. Date/eU values for zircon are plotted onto each diagram whereby the symbols demonstrate different grain sizes.

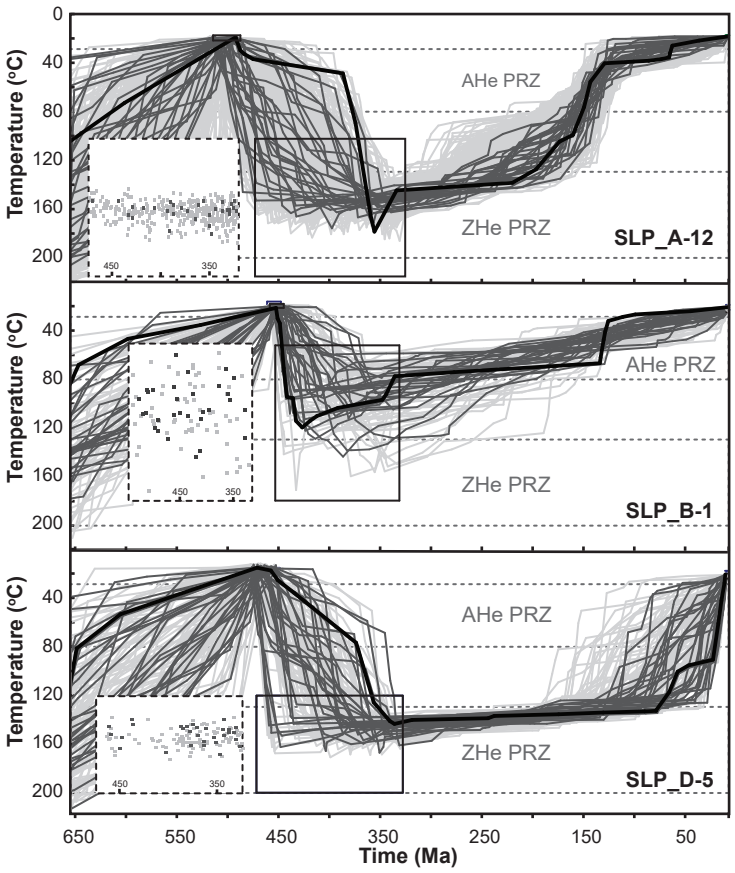

Figure 9a. Inverse thermal history models created using HeFTy for the St. Lawrence Platform (SLP) with one representative model from each of the subcategories. Boxes with solid black lines indicate temperature-time constraints where as boxes with dashed lines illustrate thermal maximums as single points. The "best fit" solutions are represented by a solid black lines, "good fit" solutions by dark gray lines and "acceptable fit" solutions by light grey lines. Coloured points inclosed in the dotted box represent the magnitude of thermal maximum (inflection point) for each thermal path, whereby light grey points correspond to "acceptable fit" solutions and dark grey points correspond to "good fit" solutions.

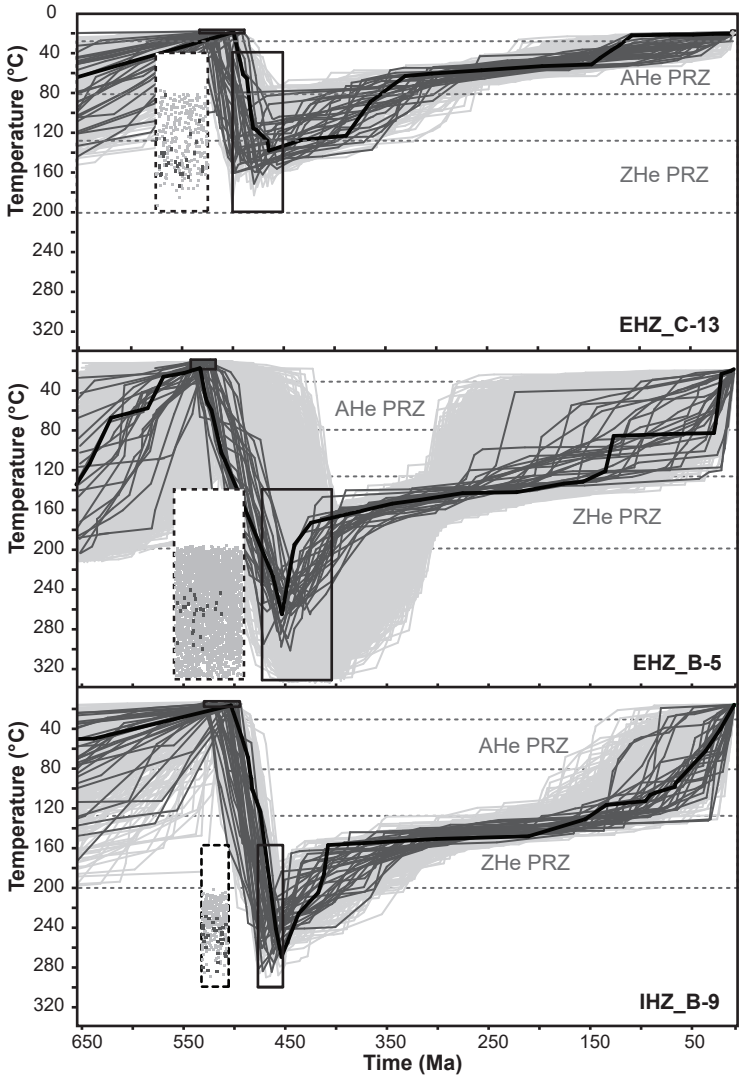

Figure 9b. Inverse thermal history models created using HeFTy for the Humber Zone (HZ) with representative models from each of the subcategories. Boxes with solid black lines indicate temperature-time constraints where as boxes with dashed lines illustrate thermal maximums as single points. The "best fit" solutions are represented by a solid black lines, "good fit" solutions by dark gray lines and "acceptable fit" solutions by light grey lines. Coloured points inclosed in the dotted box represent the magnitude of thermal maximum (inflection point) for each thermal path, whereby light grey points correspond to "acceptable fit" solutions and dark grey points correspond to "good fit" solutions.

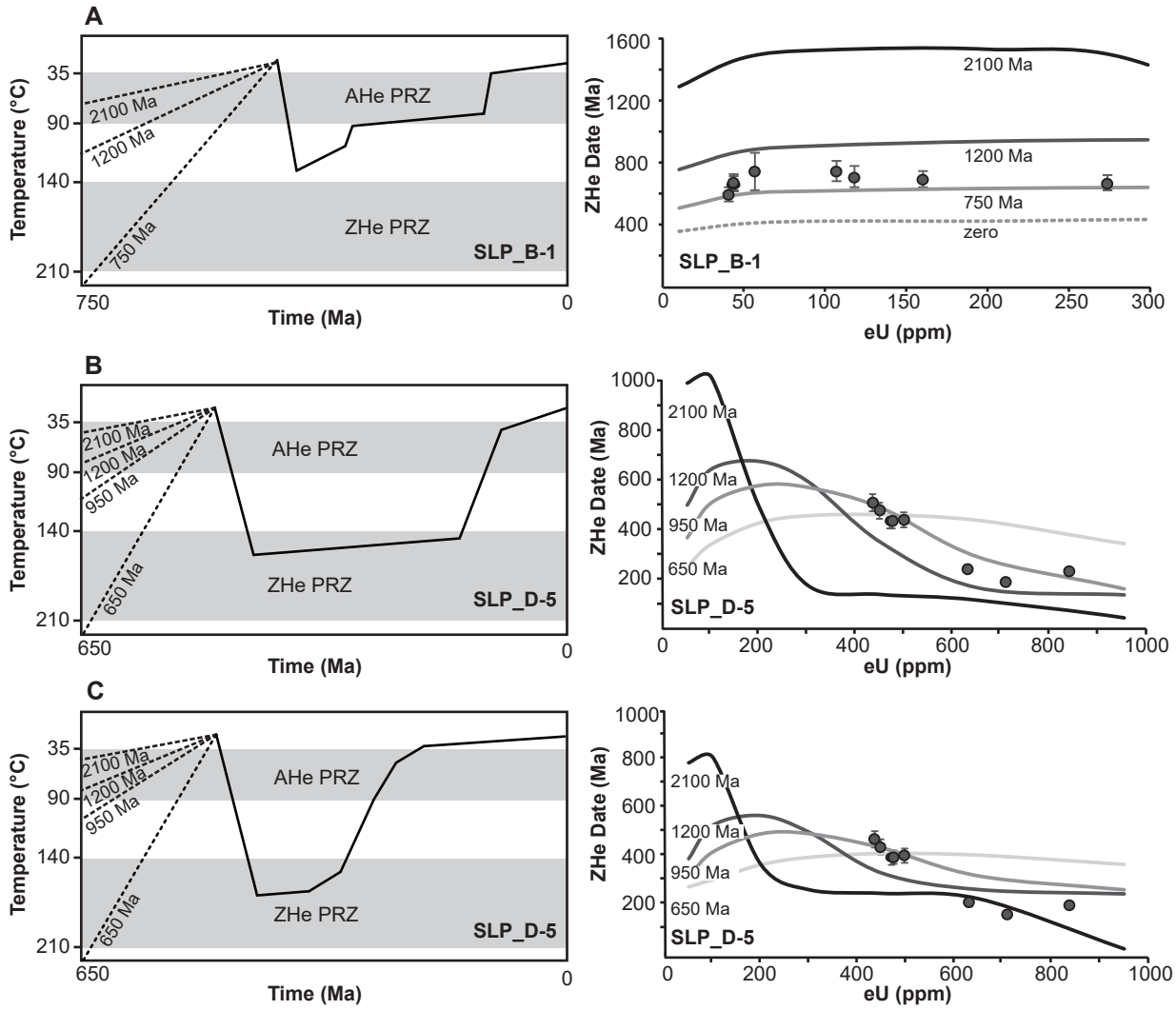

Figure 10. Forward models with corresponding zircon inheritance curves for samples of the St. Lawrence Platform. Each pre-depositional history in the forward models are represent by a dashed line whereby each dashed line extends to its assigned pre-depositional starting point at a temperature of 220°C. (A) Forward model and inheritance curves (using a mean grain size of 65 μm) for sample SLP_B-1. (B) Forward model (generated with zircon only) and inheritance curves (using a mean grain size of 60 μm) for sample SLP_D-5. (C) Forward model (generated with zircon and apatite) and inheritance plot (using a mean grain size of 60 μm) for sample SLP_D-5.

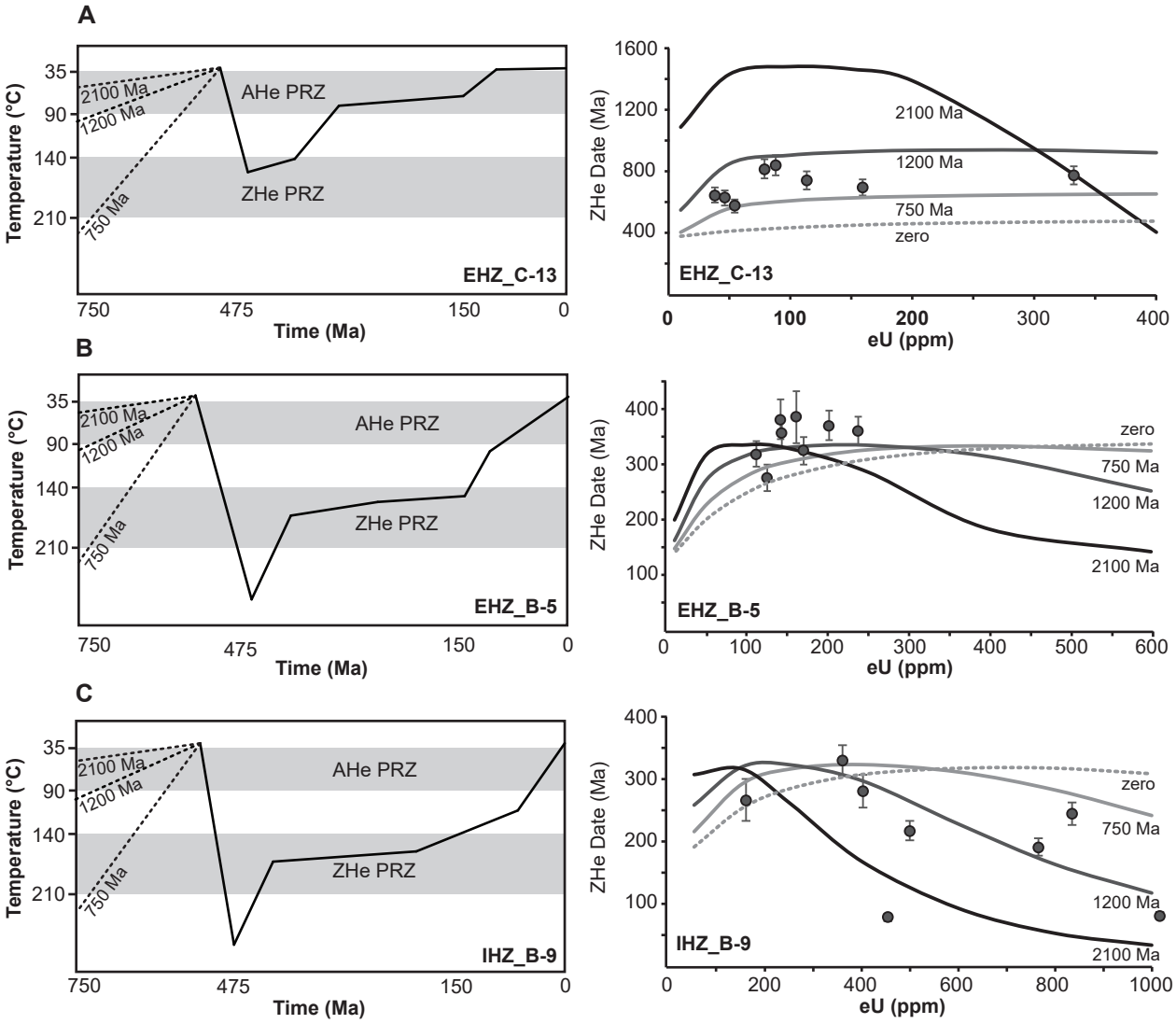

Figure 11. Forward models with corresponding zircon inheritance curves for samples of the Humber zone. Each pre-depositional history in the forward models are represent by a dashed line whereby each dashed line extends to its assigned pre-depositional starting point at a temperature of 220°C. (A) Forward model and inheritance curves (using a mean grain size of 70 μm) for sample EHZ_C-13. (B) Forward model and inheritance plot (using a mean grain size of 65 μm) for sample EHZ_B-5. (C) Forward model and inheritance plot (using a mean grain size of 65 μm) for sample IHZ_B-9.

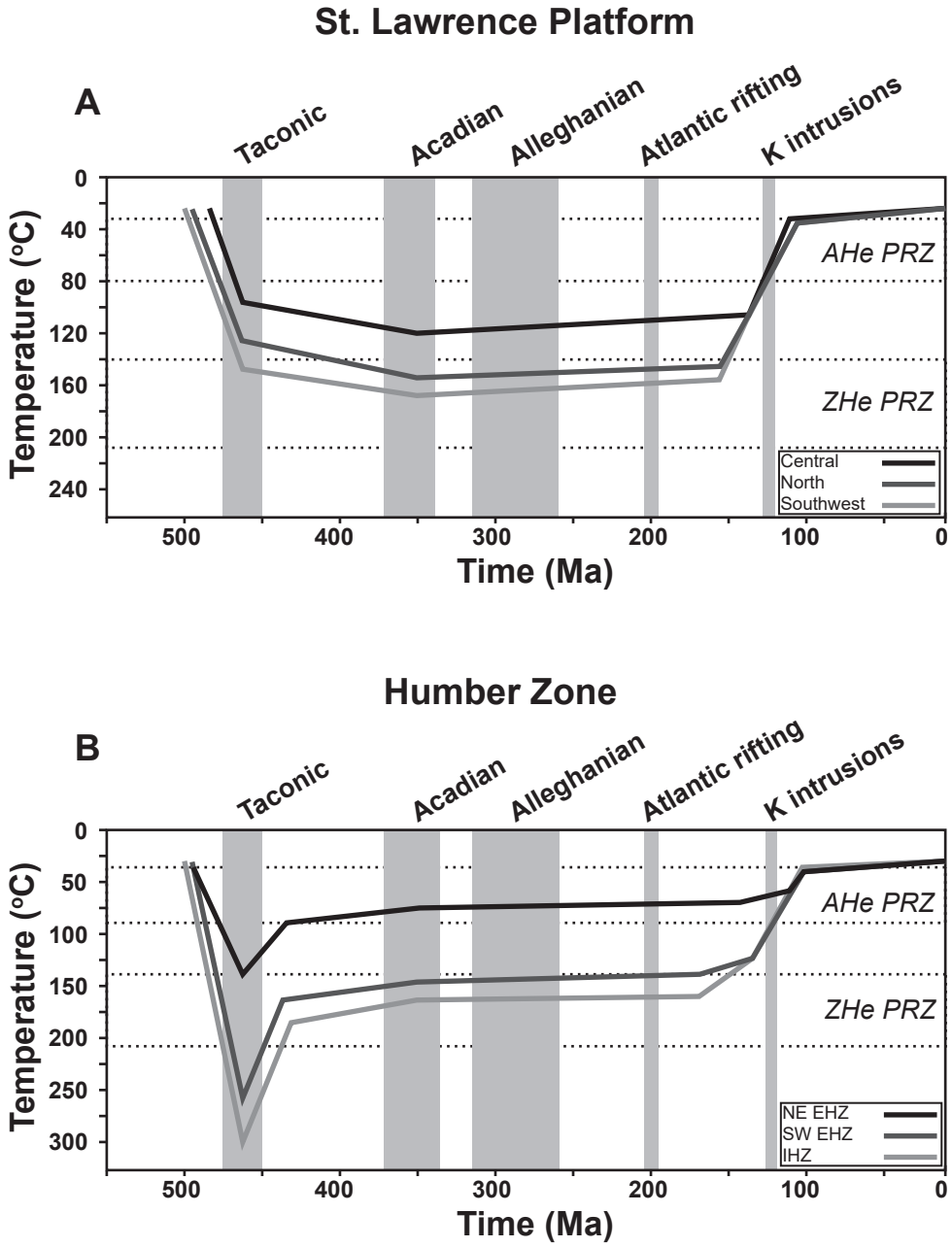

Figure 12. Summary of post-depositional thermal histories for the (A) St. Lawrence Platform and (B) Humber Zone. Three representative thermal histories derived from the HeFTY thermal models are illustrated in (A) which correspond to the southwest, central and northern regions of the SLP. Similar to (A), three thermal histories are illustrated in (B) which correspond to the northeast EHZ, the southwest EHZ and the IHZ. The timing of various geologic events that may have affected the region are superimposed as shaded columns in the diagrams.

APPENDIX TO:

Tracking low temperature tectonism of the St. Lawrence Platform and Humber Zone, southern Quebec Appalachians through apatite and zircon (U-Th)/He thermochronology

J.M. Emberley

Department of Earth and Environmental Sciences, University of Ottawa, Canada

TABLE OF CONTENTS

A1: Introduction

This supplementary document contains additional information on grains that were selected for modeling and sample descriptions. It also includes inverse models for all samples along with additional forward models and inheritance envelopes (created using the total range in grain size for each sample).

A2: Grain selection for numeric modeling

Sample SLP_A-12

Apatite grains Ap2 and Ap3 with date/eU values of 129 Ma / 6 ppm and 139 Ma / 41 ppm respectively were chosen for modeling as they cover the total range in date/eU values for the sample. Zircon grains Zr1, Zr4 and Zr12 with date /eU values of 318 Ma / 158 ppm, 506 Ma / 104 ppm and 285 Ma / 19 ppm respectively were chosen as they cover the total range in eU value for the sample, have a large spread in date and a significant variation grain size. No %Ro value was used for this model.

Sample SLP_A-5

Apatite grain Ap1 with a date/eU value of 106 Ma / 2 ppm was chosen for modeling. Zircon grains Zr7 and Zr2 with date/eU values of 272 M a/ 141 ppm and 213 Ma / 265 ppm respectively,

were chosen as they cover a significant range in eU and grain size. Ro% was not used for this model.

Sample SLP_B-1

Zircon grains Zr1 and Zr7 with date/eU values of 676 Ma / 44 ppm and 706 Ma / 161 ppm respectively were chosen as they span a considerable range in eU. Apatite grains Ap1 and Ap6 with date/eU values of 126 Ma / 5 ppm and 127 Ma / 5ppm respectively were also chosen. Choosing apatite grains that spanned a wider range in date would not allow for good fits. Grains size was not a major consideration in grain selection (for both apatite and zircon) as there was an insignificant effect on the resulting models due to its relatively small range in value. A %Ro value of 0.8 ± 0.3 was chosen based on previous thermal maturation studies (Heroux and Bertrand 1991; Yang and Hesse 1993).

Sample SLP_D-10

Zircon grains Zr1 and Zr7 with date/eU values of 693 Ma / 77 ppm and 570 Ma / 68 ppm respectively were chosen for modeling along with apatite grain Ap3 with a date/eU value of 149 Ma / 11 ppm. Grains size was not a major consideration in grain selection (for both apatite and zircon) as there was an insignificant effect on the resulting models due to its relatively small range in value. A %Ro value of 0.8 ± 0.3 was chosen based on previous thermal maturation studies (Heroux and Bertrand 1991; Yang and Hesse 1993).

Sample SLP_D-5

One model used zircon grains Zr1 and Zr5 with date and eU values of 501 Ma / 433 ppm and 434 Ma / 496 ppm respectively in conjunction with Apatite grains Ap2 and Ap3 with date and eU values of 238 Ma / 134 ppm and 201 Ma / 88 ppm. The chosen zircon grains do not span the entire date/eU range as younger zircon grains would not yield good fits when modeled in

conjunction with the apatite grains. Apatite grains Ap2 and Ap3 were chosen as they span a considerable date/eU range. The other model, that incorporated only zircon, used grains Zr5 and Zr7 with date/eU values of 434 Ma / 496 ppm and 222 Ma / 837 ppm respectively which span the range of date and eU. Grains size was not a major consideration in grain selection (for both models) as there was an insignificant effect on the resulting models due to its relatively small range in value. A %Ro value of 1.5 ± 0.25 was also used, for both models, based off of previous thermal maturation studies (Heroux and Bertrand 1991; Yang and Hesse 1993).

Sample SLP_D-6

One model used zircon grain Zr5 with a date/eU value of 450 Ma / 383 ppm in conjunction with Apatite grains Ap2 and Ap4 with date and eU values of 170 Ma / 158 ppm and 185 Ma / 56 ppm. The apatite grains were chosen as they span a considerable date/eU range. The other model that incorporated zircon only used grains Zr5, Zr6 and Zr7 with date/eU values of 450 Ma/ 383 ppm, 288 Ma / 730 ppm and 233 Ma / 872 ppm respectively. These date and eU values where chosen as they span a considerable range. Grains size was not a major consideration in grain selection (for both models) as there was an insignificant effect on the resulting models due to its relatively small range in value. A %Ro value of 1.5 ± 0.25 was also used, for both models, based off of previous thermal maturation studies (Heroux and Bertrand 1991; Yang and Hesse 1993).

Sample EHZ_B-5

Zircon grains Zr1, Zr3 and Zr6 with date/eU values of 363 Ma / 237 ppm, 321 Ma / 112 ppm and 277 Ma / 125 ppm respectively were chosen for modeling. These grains span the entire range of eU over almost the complete spread in date. A %Ro value of 4.0 ± 0.75 was also used based off of previous thermal maturation studies (Heroux and Bertrand 1991; Yang and Hesse 1993).

Sample EHZ_C-13

Zircon grains Zr1, Zr4, and Zr8 with date/eU values of 818 Ma / 78 ppm, 628 Ma / 45 ppm and 774 Ma / 332 ppm respectively where chosen as they encompass almost the full range in eU and date. Apatite grains Ap2 and Ap4 with date/eU values of 187 Ma / 14 ppm and 292 Ma / 52 ppm where chosen as they encompass a significant date and eU range for the sample. A %Ro value of 1.0 ± 0.5 was used based off of previous thermal maturation studies (Heroux and Bertrand 1991; Yang and Hesse 1993).

Sample EHZ_C-10

Zircons grains Zr1, Zr3 and Zr8 with date/eU values of 443 Ma / 53 ppm, 520 Ma / 88 ppm and 434 Ma / 207 ppm were chosen for modeling as they span almost the entire range in date and eU. A %Ro value of 1.5 ± 0.5 was used based off of previous thermal maturation studies (Heroux and Bertrand 1991; Yang and Hesse 1993).

Sample EHZ_C-4

Zircon grains Zr3, Zr4, Zr5 and Zr6 with date/eU values of 438 Ma / 33 ppm, 386 Ma / 11 ppm, 520 Ma / 64 ppm and 510 Ma / 132 ppm were chosen for modeling as they encompass the entire range in date and eU. No %Ro value was used for this sample.

Sample IHZ_B-9

Zircon grains Zr3, Zr4 and Zr6 with date/eU values of 192 Ma / 767 ppm, 332 Ma / 358 ppm and 282 Ma / 400 ppm respectively were used for modeling as they follow a negative trend in date/eU and span a significant portion of the values. A %Ro value of 4.25 ± 0.75 was also used based off of previous thermal maturation studies (Heroux and Bertrand 1991; Yang and Hesse 1993).

Sample IHZ_D-8

Apatite grains Ap1, Ap3 and Ap4 with date/eU values of 137 Ma / 12 ppm, 124 Ma / 13 ppm and 117 Ma / 9 ppm were chosen for modeling as they cover a significant portion of the date/eU values for the sample. No %Ro value was used for this sample.

Sample IHZ_C-8

Zircon grains Zr1, Zr2, Zr4 and Zr5 with date/eU values of 330 Ma / 39 ppm, 289 Ma / 33 ppm, 297 Ma / 137 ppm and 286 Ma / 217 ppm were chosen as they cover a significant portion of the range in values for date and eU. No %Ro value was used for this sample.

A3: Grainsize considerations when utilizing inheritance envelopes

Using the average grains size while forward modeling with inheritance envelopes, when the dataset contains a large range in grainsize, may yield inaccurate and conflicting results. To illustrate this point two inheritance envelopes were created based off of forward models for sample SLP_A-12, which contains a large spread in grain size from 33-130 µm (**Fig. A9).** One inheritance envelope utilizes a 30 µm grain size where as the other uses a 90 µm grain size, both having pre-depositional histories of 750, 1200 and 2100 Ma (this date range encompasses possible sources such as the Grenville and the Superior). If one were only to consider the inheritance envelope created using the 30 µm grain size, the conclusion could be drawn that the dataset is well explained by the associated forward model that incorporates these different pre-depositional histories. This scenario is unlikely however as the proportion of grains with pre-depositional histories older than 750-1200 Ma is too great. According to U/Pb studies (Montario and Garver 2009) only a very small fraction of zircon from the Potsdam Group have been sourced from the Superior. Also, grains originally sourced from the Superior could have been

later incorporated into the Grenville, thus their ZHe dates would likely have been reset. This would therefore further decrease the number of grains that have a pre-depositional signature older than 1200 Ma. In contrast the inheritance envelope created with a 90 μm grain size more closely fits the idea that most grains have a Grenville pre-depositional history (but contains a number of outliers that fall below the zero inheritance curve). The significant difference between the two inheritance envelopes indicates the need for incorporating individual grainsize, when there is significant spread in grain size, when forward modeling while utilizing inheritance envelopes.

References

Heroux, Y., and Bertrand, R. 1991. Maturation thermique de la matiere organique dans un bassin du Paleozoique inferieur, basses-terres du Saint-Laurent, Quebec, Canada. Canadian Journal of Earth Science, **28**, 1019-1030.

Montario, M. J., and Garver, J. I. 2009. The thermal evolution of the Grenville Terrane revealed through U-Pb and Fission-Track analysis of detrital zircon from Cambro- Ordovician quartz arenites of the Potsdam and Galway Formations. Journal of Geology, **117**: 595-614.

Yang, C., and Hesse, R., 1993. Diagenesis and anchimetamorphism in an overthrust belt, external domain of the Taconian Orogen, southern Canadian Applachians-II. Paleogeothermal gradients derived from maturation of different types of organic matter. Organic Geochemistry, **20**: 381-403.

Appendix Supplementary Files

Tables

Table A1: Sample information

Figures

Figure A1: Surface thermal maturation

Figure A2: Sample SLP_A-12 eU, date and grains size relationship

Figures A3-A8: Inverse models

Figures A9-A14: Forward models with inheritance envelopes

Table A1. Sample location and rock descriptions

Sample #	Lat.	Long.	Province	Group	Formation	Age	Rock Name	Grain size	Mineralogy
SLP_B-1	46.026	72.707	SLP	Queenstone	Becancour	Upper Ordovician	Red quartz wacke	fine	50% clay matrix, 40%Qz, 4% Cal, 4 %lithic frag., 2% oxides
SLP_D-10	46.155	72.537	SLP	Queenstone	Becancour	Upper Ordovician	Red quartz wacke	fine	50% clay matrix, 40%Qz, 4% Cal, 4 %lithic frag., 2% oxides
SLP_D-6	46.736	71.562	Grenville	n/a	n/a	Mesoproterozoic	Granitic gneiss	medium-coarse	50% Qz, 25% Or, 10% Pl, 10% Bt, 5% Amp
SLP_D-5	46.445	72.738	Grenville	n/a	n/a	Mesoproterozoic	Granitic gneiss	medium-coarse	50% Qz, 25% Or, 10% Pl, 10% Bt, 5% Amp
SLP_A-2	44.253	73.802	SLP	Beakmantown	Theresa	Lower Ordovician	Calcareous sandstone	medium	80% Qz, 20% Cal cement
SLP_A-5	45.044	73.685	SLP	Potsdam	Cairnside	Upper Cambrian	Quartz arenite	coarse	99% Qz, 1% other
SLP_A-12	45.332	73.950	SLP	Potsdam	Covey Hill	Upper Cambrian	Quartz arenite	coarse	99% Qz, 1% other
EHZ_C-13	46.734	71.369	EHZ	Sillery	Lauzon	Cambrian/Lower Ordovician	Quartz arenite	coarse	97% Qz, 3% Cal cement
EHZ_C-10	46.749	71.301	EHZ	Sillery	Saint Nicolas	Middle Cambrian	Feldspathic wacke	coarse	70% Qz, 15% clay, 10% Or, 5% Pl, 3% Cal, 2% oxides
EHZ_C-4	46.548	71.182	EHZ	Drummondville	Riviere Etchemin	Middle Ordovician	Lithic wacke	coarse	65% Qz, 15% lithic, 10% Cal, 5% Or, 5% Pl
EHZ_B-5	45.861	72.450	EHZ	n/a	Granby	Early Cambrian	Feldspathic wacke	coarse	65% Qz, 10% Pl, 10% Or, 5% lithic 5% Bt, 5% oxides
IHZ_D-8	46.532	70.913	IHZ	St. Marguerite 1	n/a	Neoproterozoic	Amphibolite (retrograde)	coarse	40% Chl,20% clay minerals, 20% Amp, 10% Bt, 10% Grt
IHZ_B-9	45.668	72.216	IHZ	Oak Hill	Pinnacle 2	Lower/Upper Cambrian	Pebble conglomerate	coarse	70% Qz, 15% lithic, 10% feldspar, 5% oxides
IHZ_C-8	46.318	70.865	IHZ	Rosaire 4	n/a	Cambrian/Lower Ordovician	Quartzite	medium	90% Qz, 10% Cal

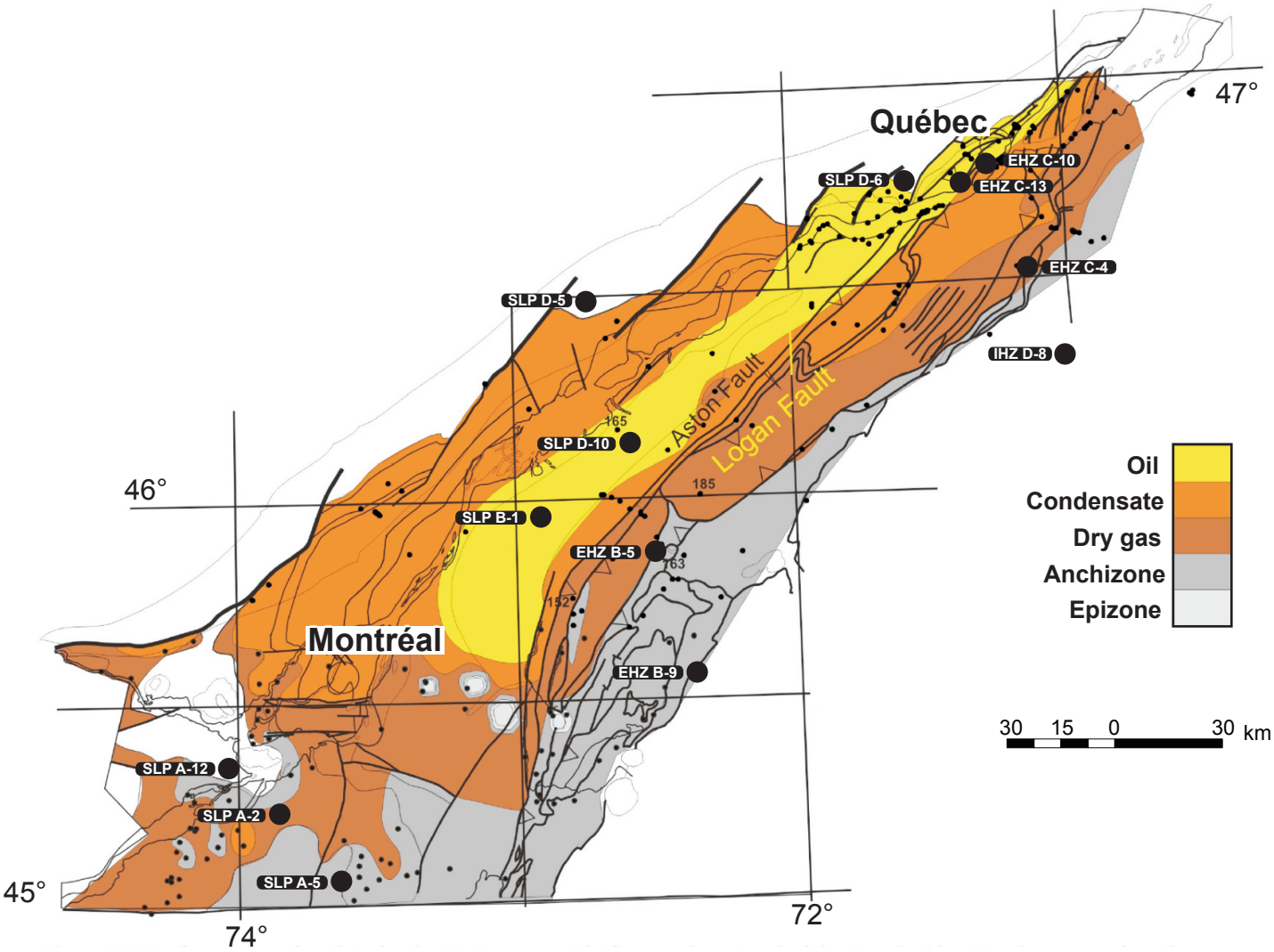

Figure A1. Surface thermal maturation for the St. Lawrence Platform and Humber Zone of southern Quebec, Canada, based on vitrinite reflectance (%Ro) data (Bertrand and Lavoie, 2006). Sampling was carried out based in part by regional trends in maturation.

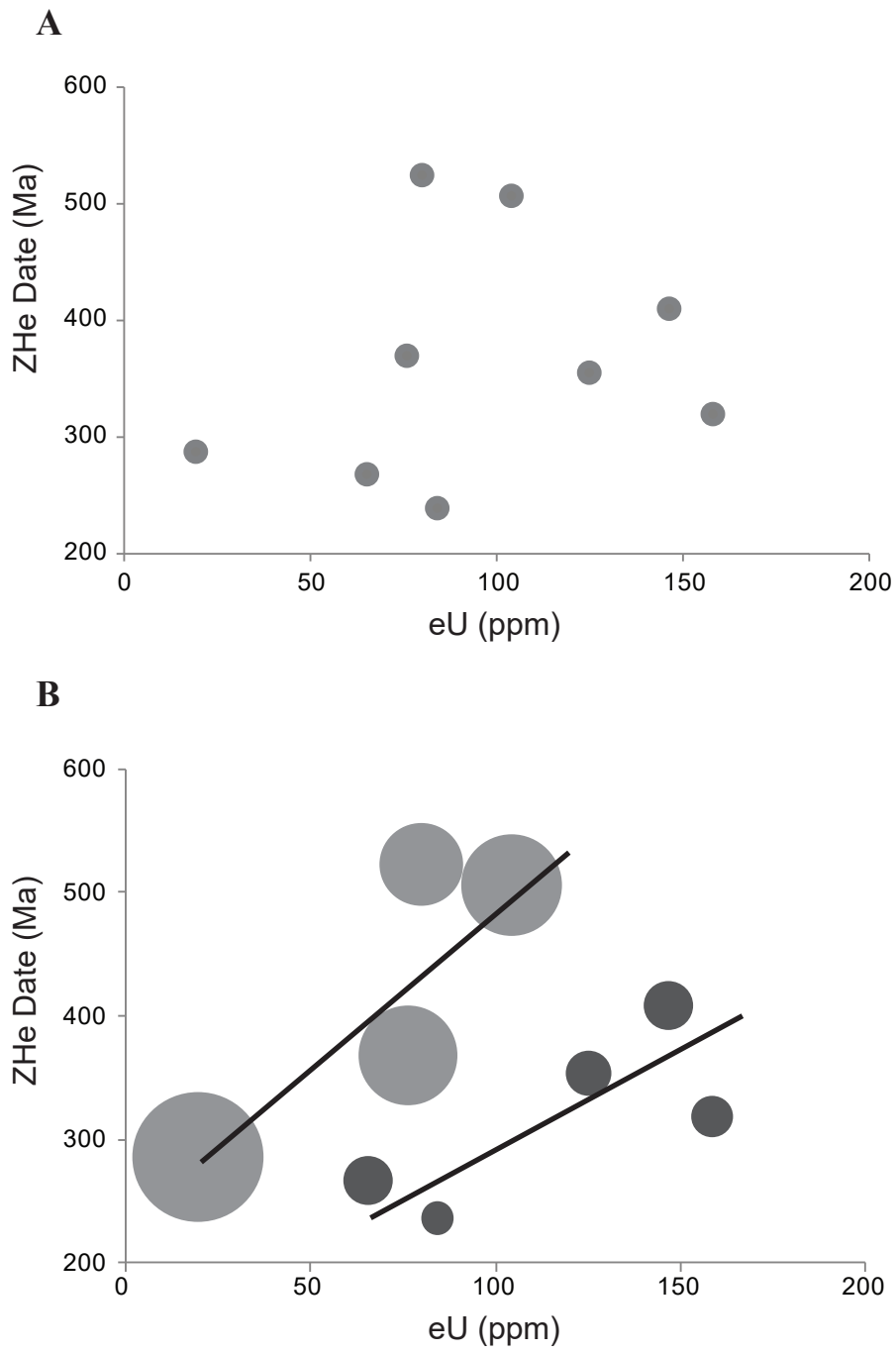

Figure A2. ZHe Date vs. eU plots for sample SLP_A-12. (**A**) No discernable trend between ZHe date and eU can be noted. (**B**) Each grain is represented by a shaded circle whereby the width of each circle is preportional to the ESR of each grain. The sample possesses a bimodal grain size distribution with large grains from 82-121 μm (represented by light grey circles) and small grains from 33-50 μm (represented by dark grey circles). Each population is given its own line of best fit (solid black line). Although no date-eU correlations were initially observed (**A**), within each grain size population there is a positive correlation between date and eU (**B**). Larger grains have consistently older dates than younger grains with similar eU values.

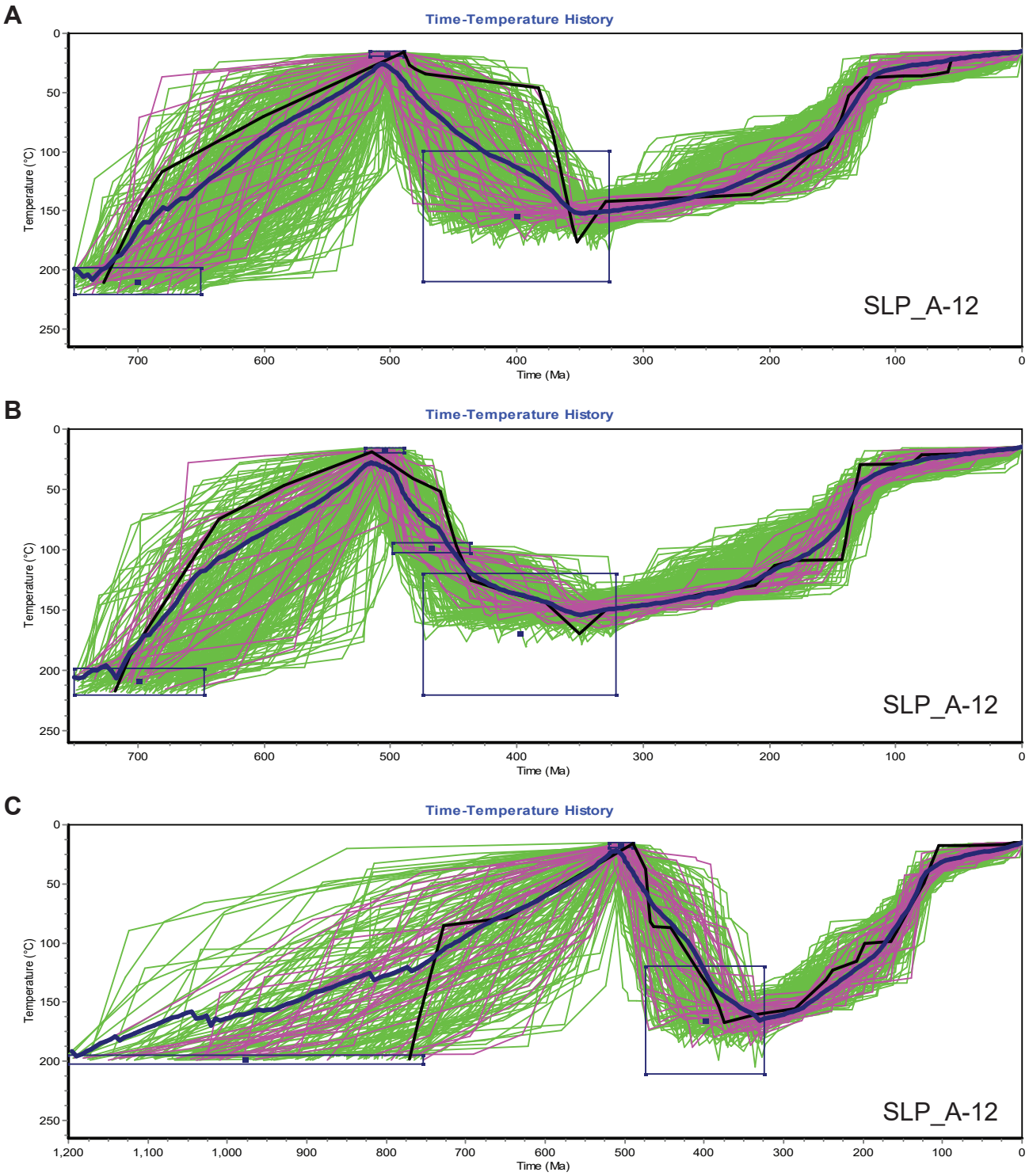

Figure A3. Variations of inverse thermal models for sample SLP_A-12. “Good fit” solutions are purple, “acceptable” solutions are green, the best fit solution is black and the weighted mean is blue. Model **A** is the same as that discussed in the main report except the full pre-depositional history is shown here. Model **B** uses the same grain selection, except that it has an extra constraint that eliminates improbabaly slow burial paths. Model **C** utilzes a larger pre-depositional constraint that extends further back in time to 1200 Ma. Regardless of the variation, thermal histories post 325 Ma remain consistant.

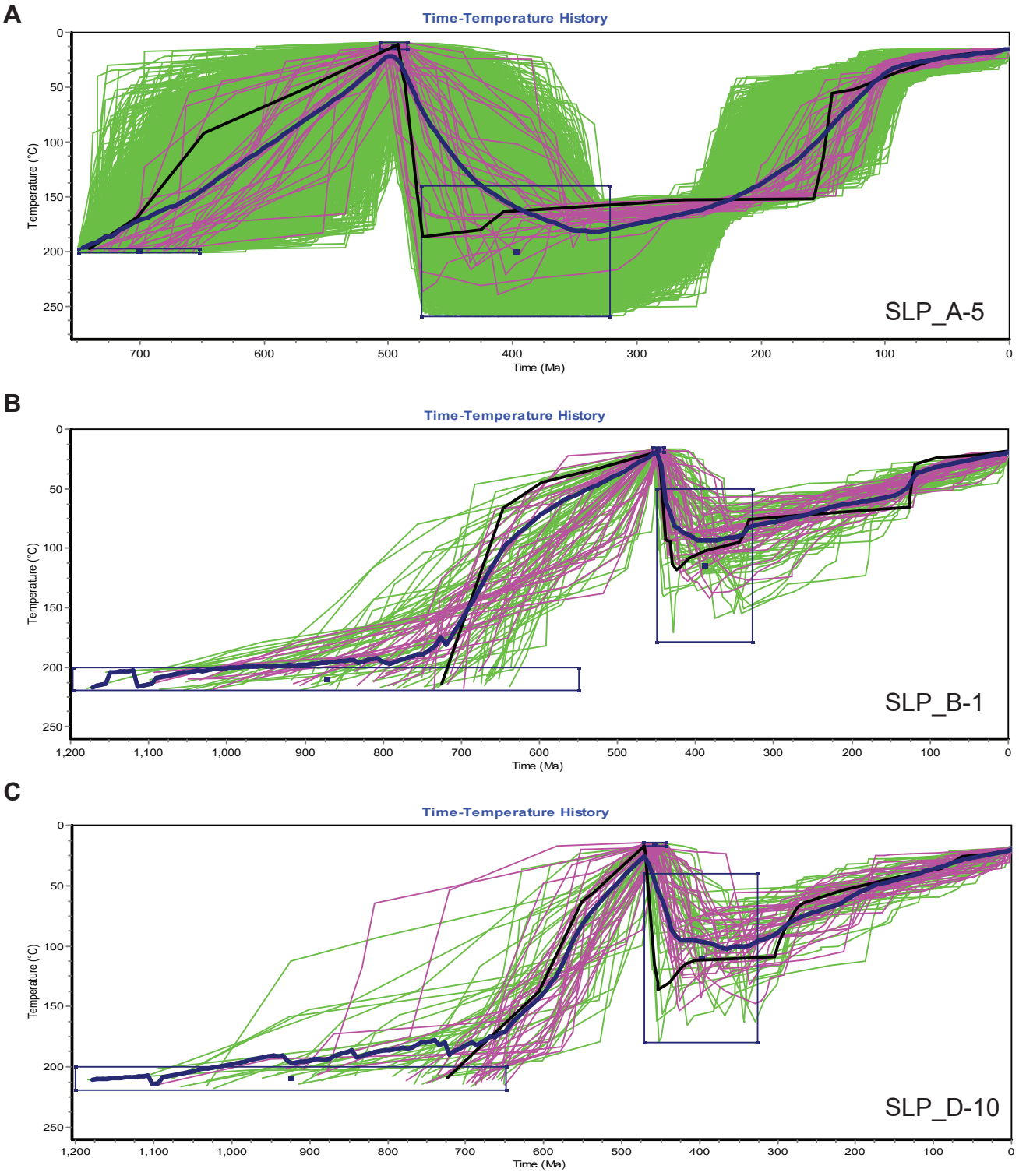

Figure A4. Inverse thermal models depicting "Good fit" solutions in purple, "acceptable" solutions in green, the best fit solution in black and the weighted mean in blue. Model **A** is for sample SLP_A-5, which was not included in the main report. Model **B** is the same as that discussed in the main report except that it illustrates the entire pre-depositional history. Model **C** is for sample SLP_D-10, which was not included in the main report.

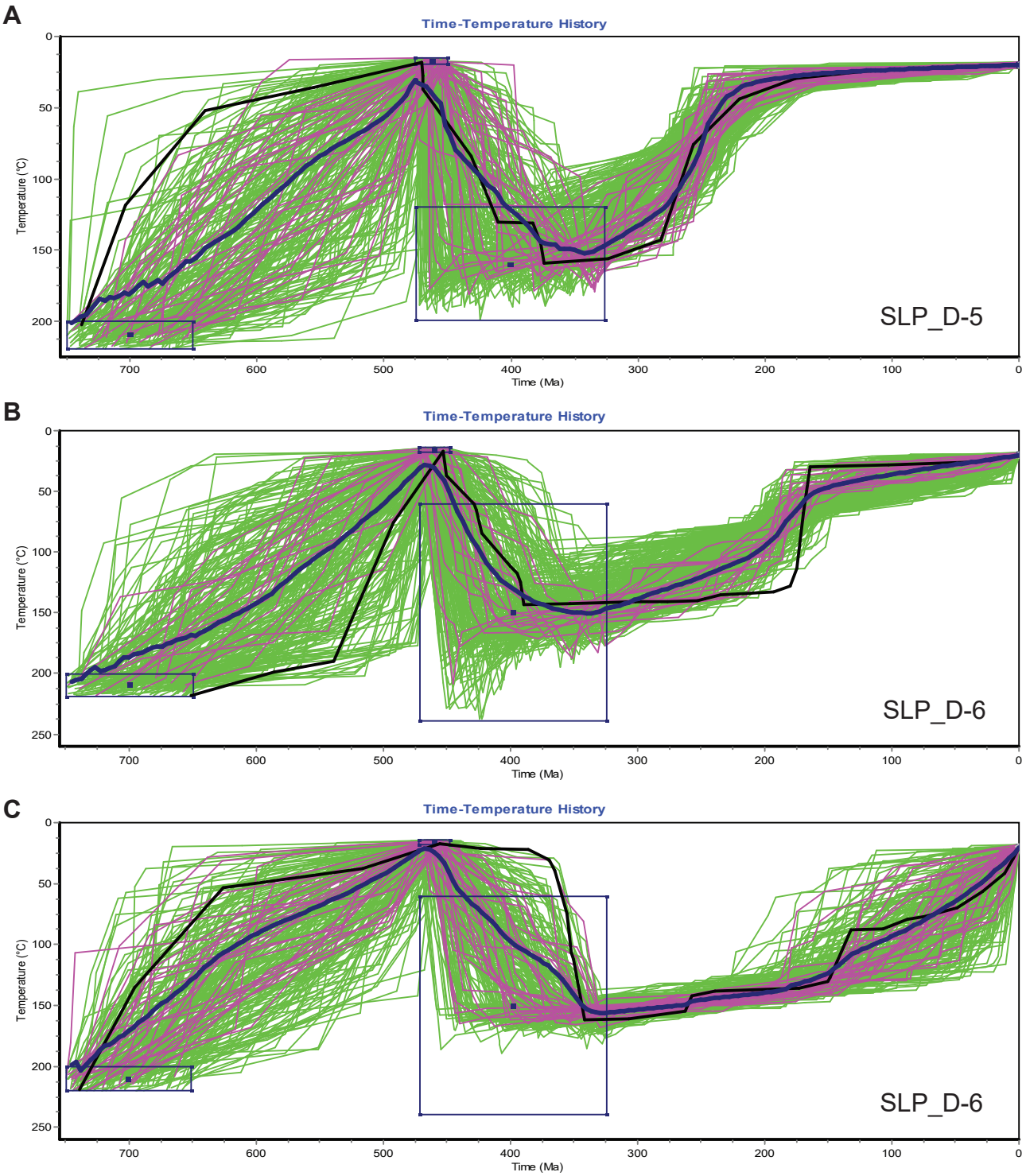

Figure A5. Inverse thermal models depicting “Good fit” solutions in purple, “acceptable” solutions in green, the best fit solution in black and the weighted mean in blue. Model **A** depicts a variation of sample SLP_D-5 that utilizes both apatite and zircon. Model **B** and **C** are variations for sample SLP_D-6 that utilizes both apatite/zircon and zircon only respectively.

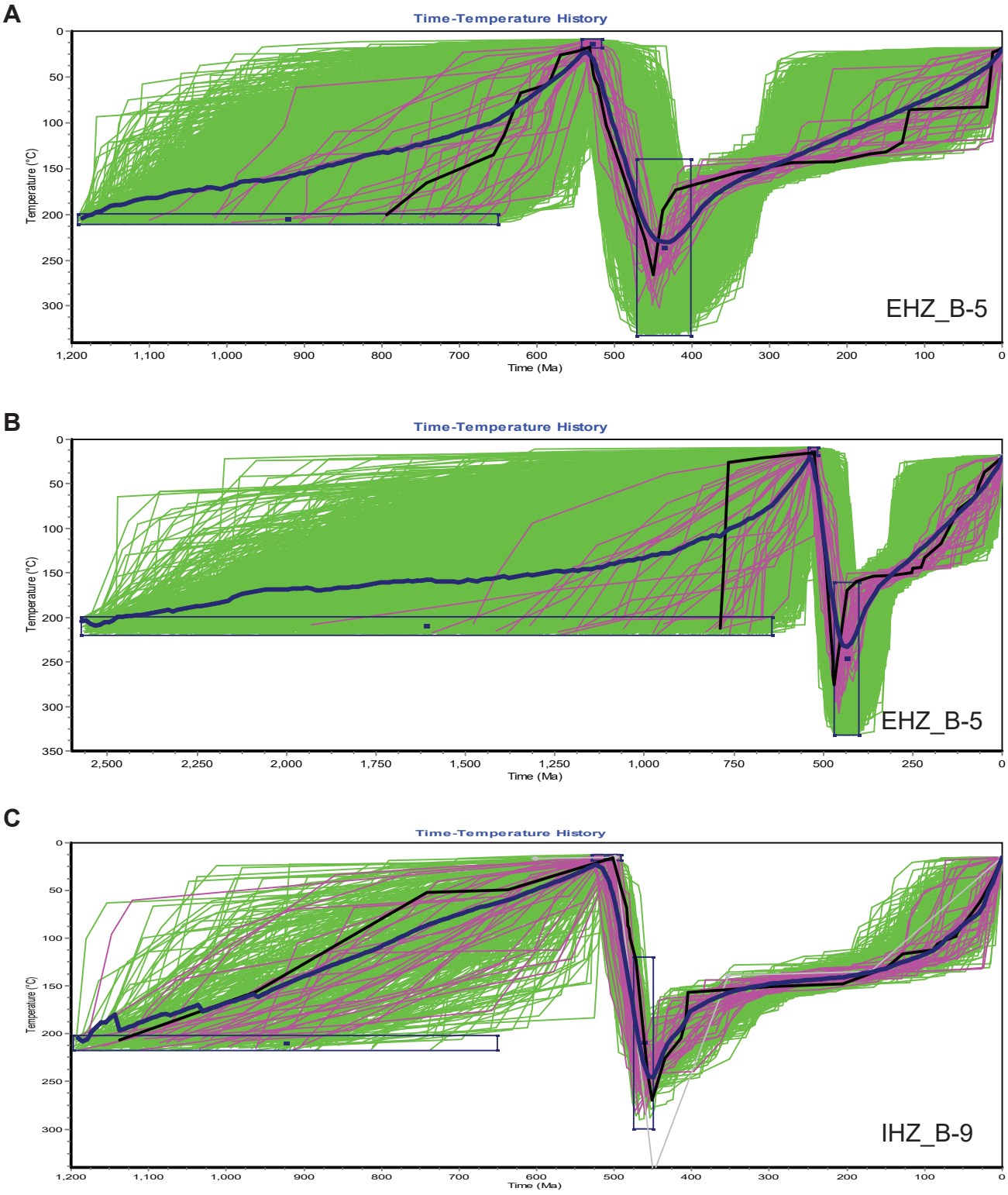

Figure A6. Inverse thermal models depicting "Good fit" solutions in purple, "acceptable" solutions in green, the best fit solution in black and the weighted mean in blue. Model **A**, for sample EHZ_B-5, is the same as that discussed in the main report except that it illustrates the entire pre-depositional history. Model **B** is a variation for sample EHZ_B-5 that utilizes a larger pre-depositional constraint that extends back to 1200 Ma. Model **C** for sample IHZ_B-9, is the same as that discussed in the main report except that it illustrates the entire pre-depositional history.

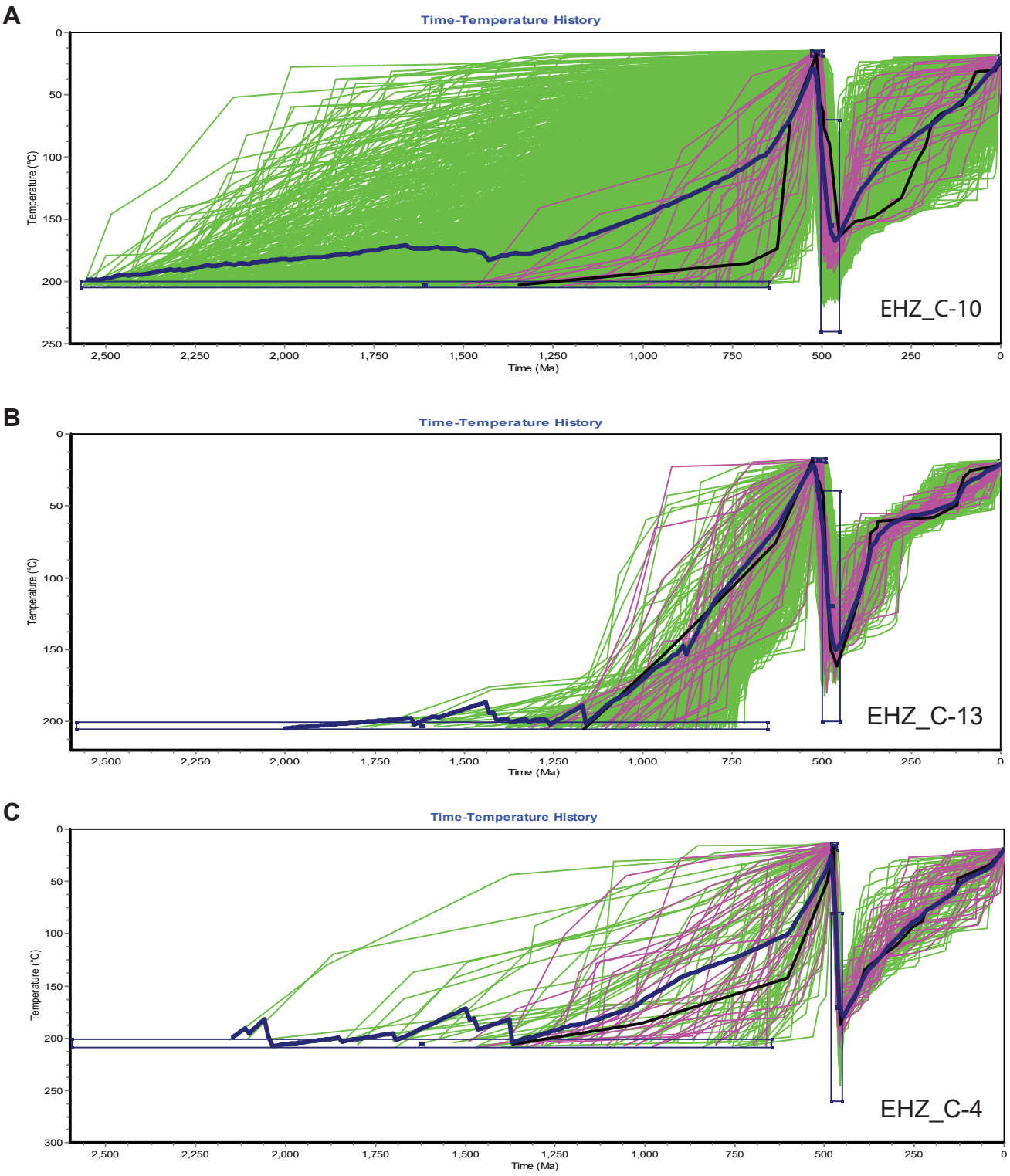

Figure A7. Inverse thermal models depicting "Good fit" solutions in purple, "acceptable" solutions in green, the best fit solution in black and the weighted mean in blue. Model **A** is for sample EHZ_C-10. Model **B**, for sample EHZ_C-13, is the same as that discussed in the main report except that it illustrates the entire pre-depositional history. Model **C** is for sample EHZ_C-4.

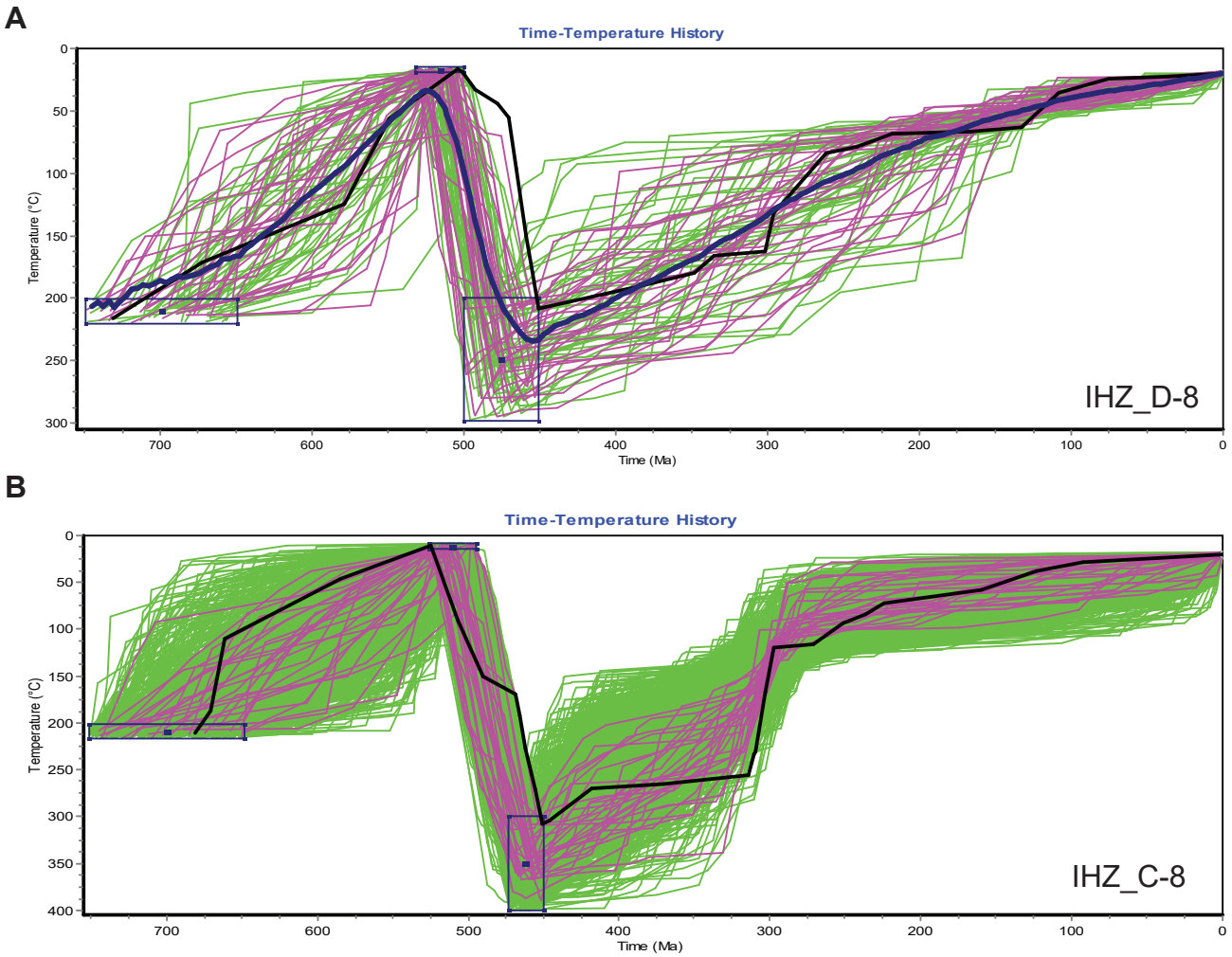

Figure A8. Inverse thermal models depicting “Good fit” solutions in purple, “acceptable” solutions in green, the best fit solution in black and the weighted mean in blue. Model **A** is for sample IHZ_D-8 and model **B** is for sample IHZ_C-8.

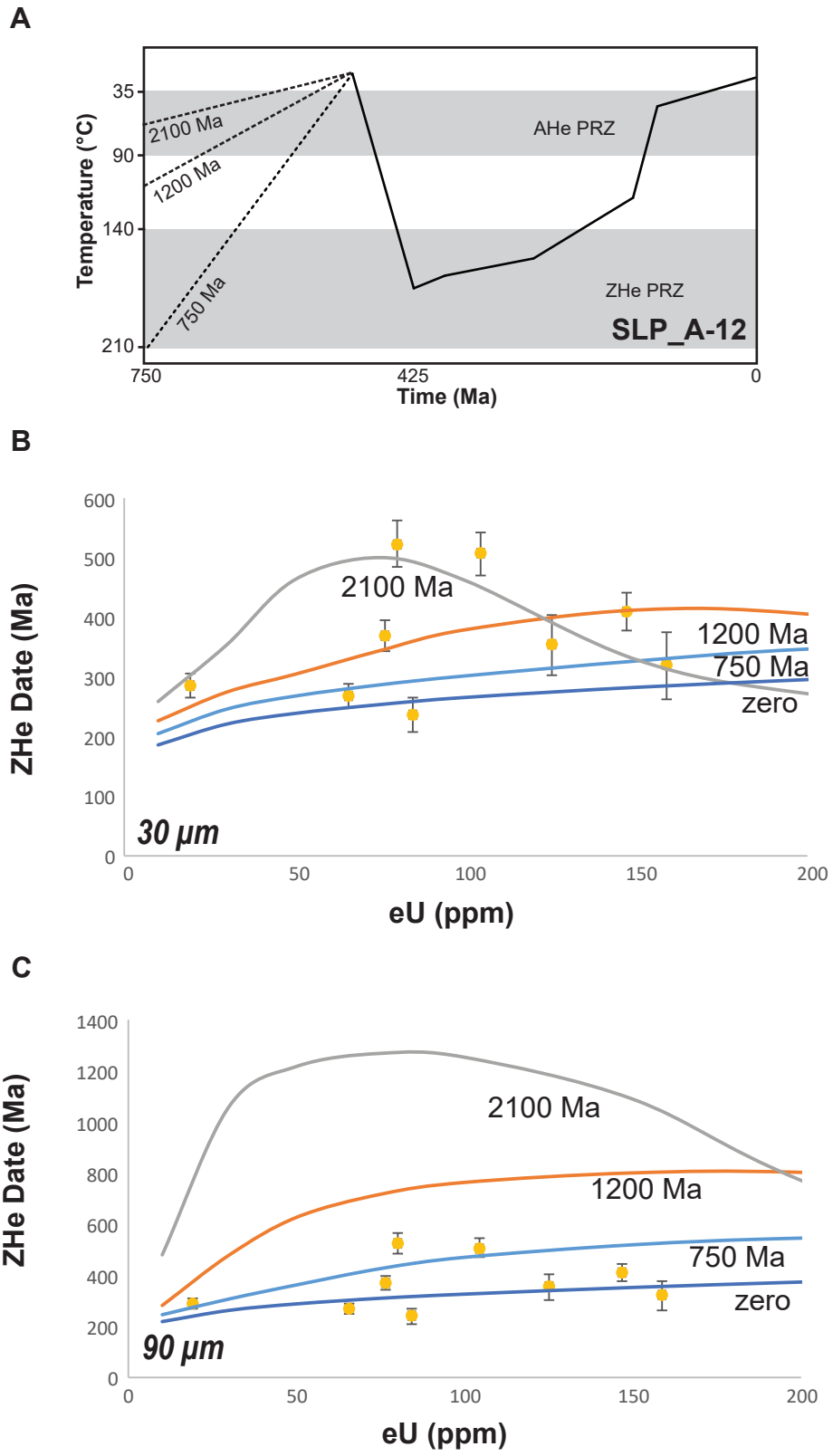

Figure A9. (**A**) Forward model from HeFTy for sample SLP_A-12 with three different pre-depositional histories. (**B,C**) Inheritance curves, created with varying grain size (30 µm and 90 µm respectively), based on the forward models in (**A**). The contrast in results between **B** and **C** illustrates how this large range in grain size can have a significant effect on modeling outcomes.

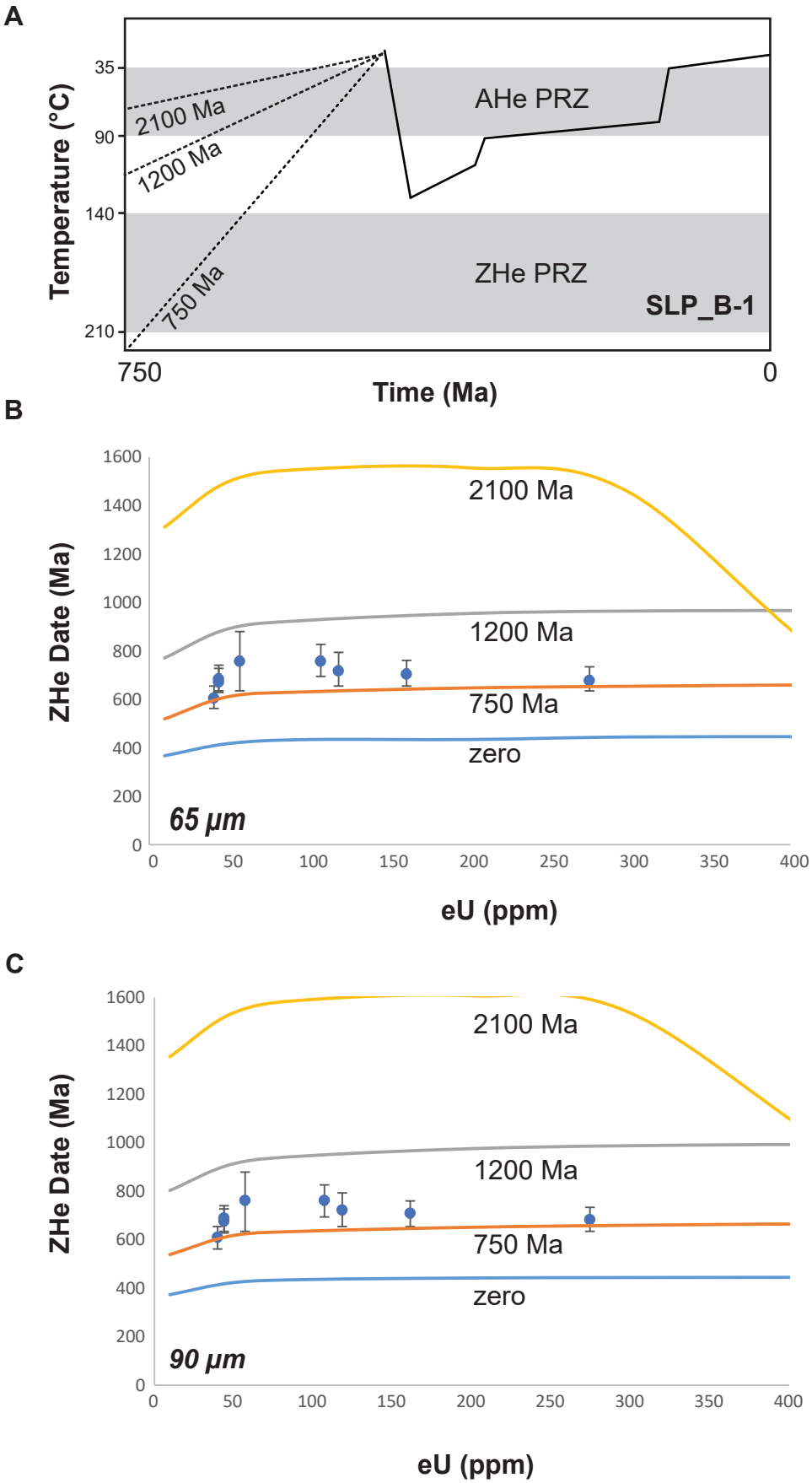

Figure A10. (**A**) Forward model from HeFTy for sample SLP_B-1 with three different pre-depositional histories. (**B,C**) Inheritance curves, created with a range in grain size that encompasses the entire spread for the sample (65 µm and 90 µm respectively), based on the forward models in (**A**). The similarities in results between **B** and **C** illustrates how this range in grain size, when associated with their respective forward models, did not have a significant effect on modeling outcomes.

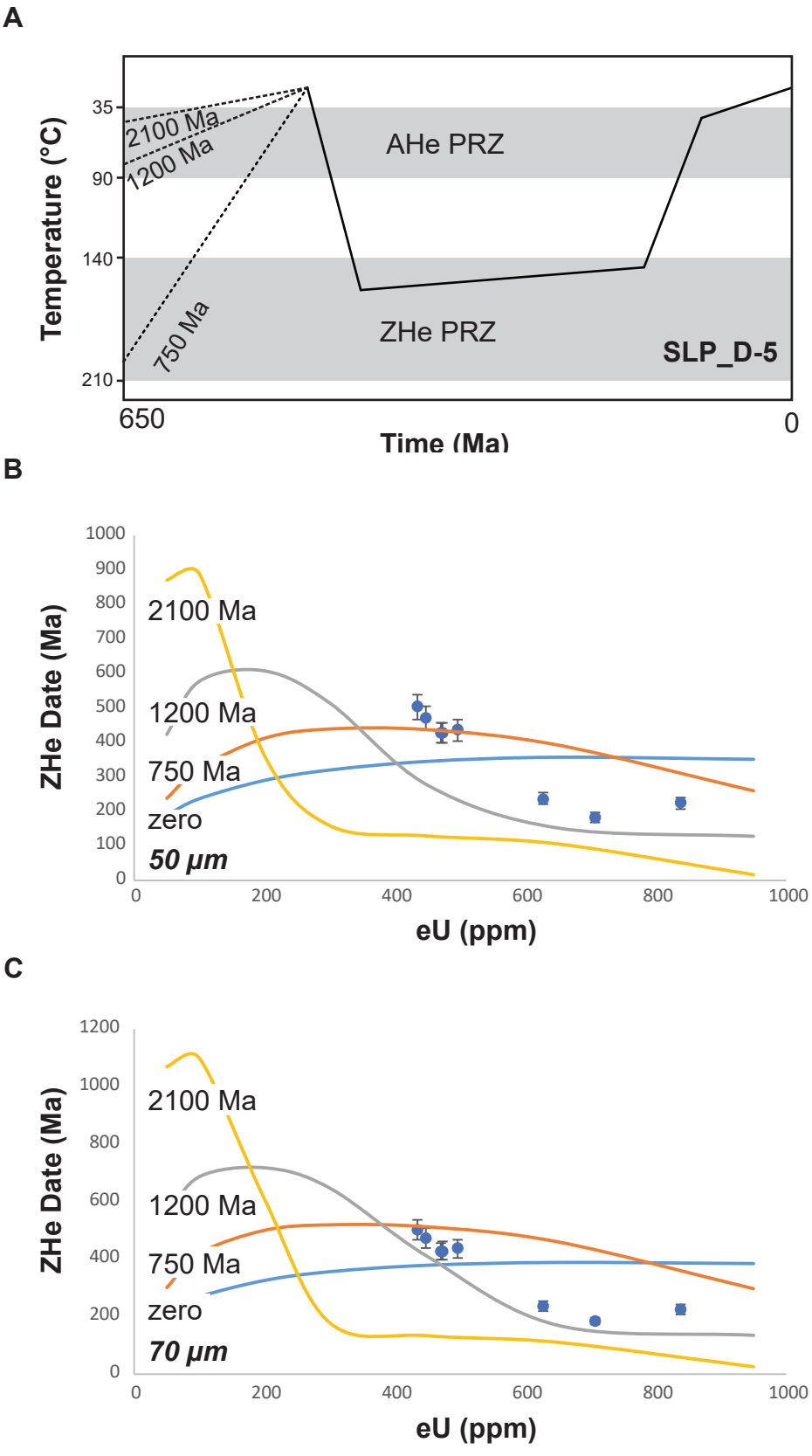

Figure A11. (**A**) Forward model from HeFTy for sample SLP_D-5 with three different pre-depositional histories. (**B,C**) Inheritance curves, created with varying grain size (50 µm and 70 µm respectively), based on the forward models in (**A**). The similarities in results between **B** and **C** illustrates how this range in grain size did not have a significant effect on modeling outcomes.

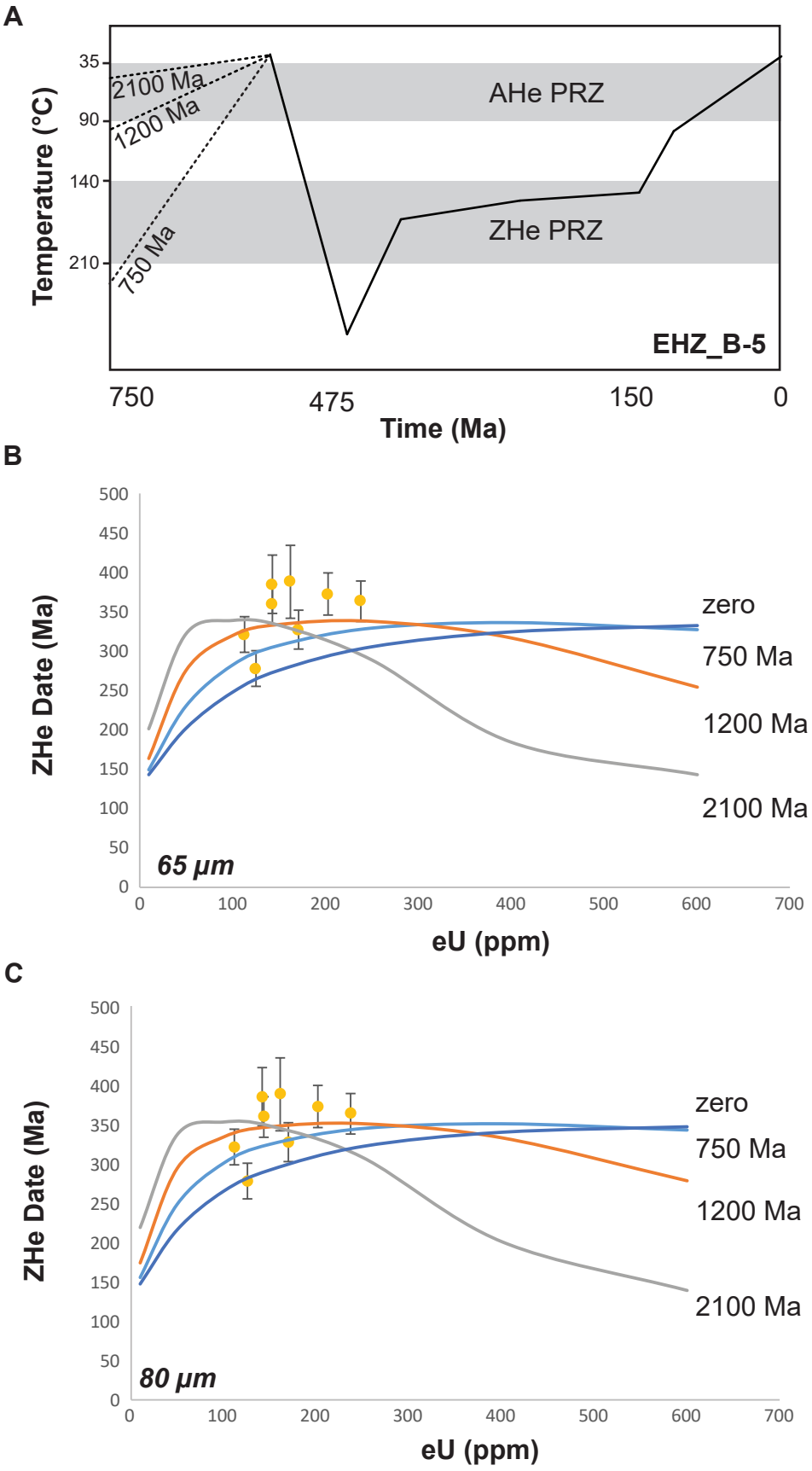

Figure A12. (**A**) Forward model from HeFTy for sample EHZ_B-5 with three different pre-depositional histories. (**B,C**) Inheritance curves, created with varying grain size (65 µm and 80 µm respectively), based on the forward models in (**A**). The similarities in results between **B** and **C** illustrates how this range in grain size did not have a significant effect on modeling outcomes.

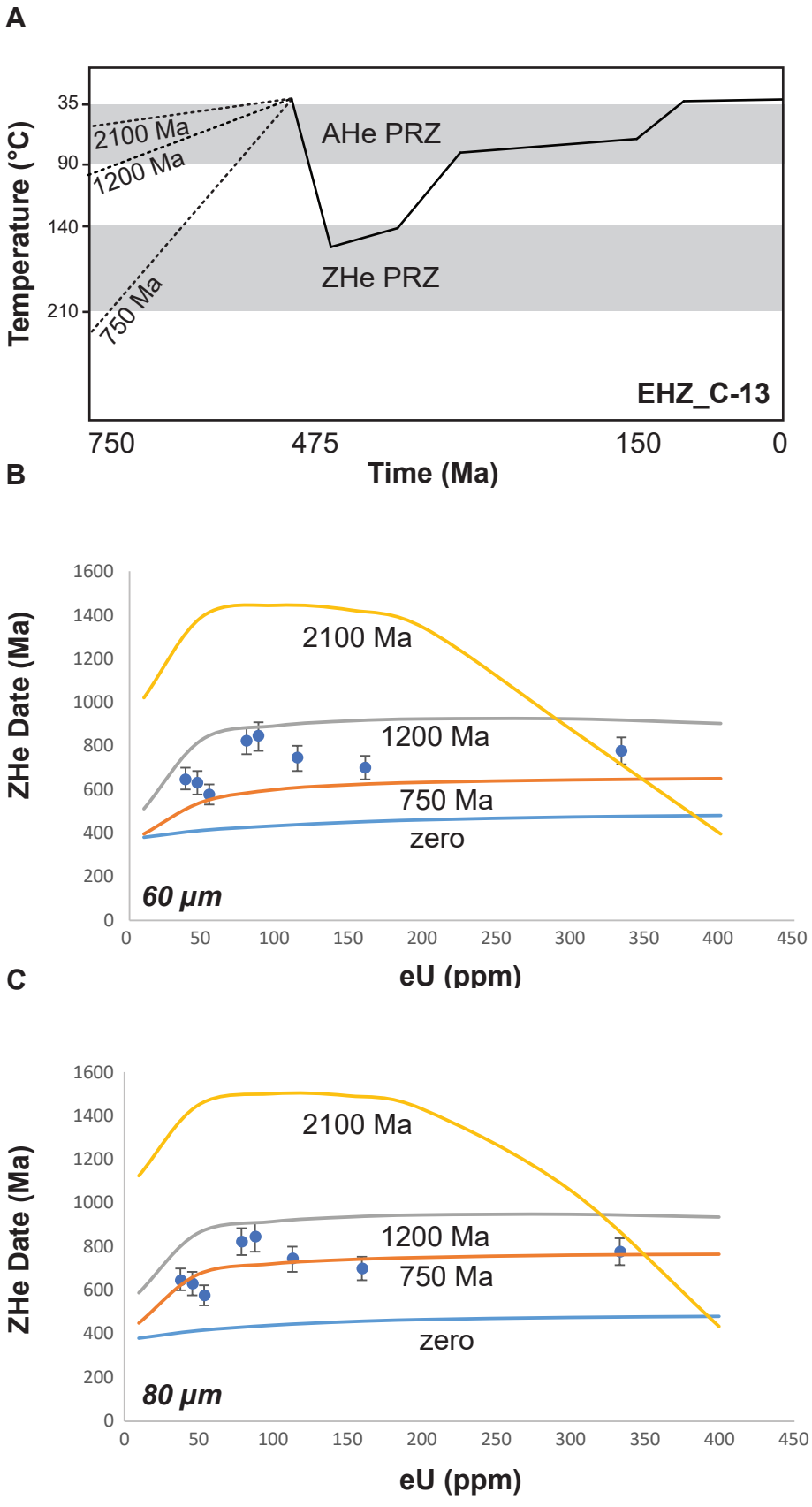

Figure A13. (**A**) Forward model from HeFTy for sample EHZ_C-13 with three different pre-depositional histories. (**B,C**) Inheritance curves, created with varying grain size (60 µm and 80 µm respectively), based on the forward models in (**A**). The similarities in results between **B** and **C** illustrates how this range in grain size did not have a significant effect on modeling outcomes.

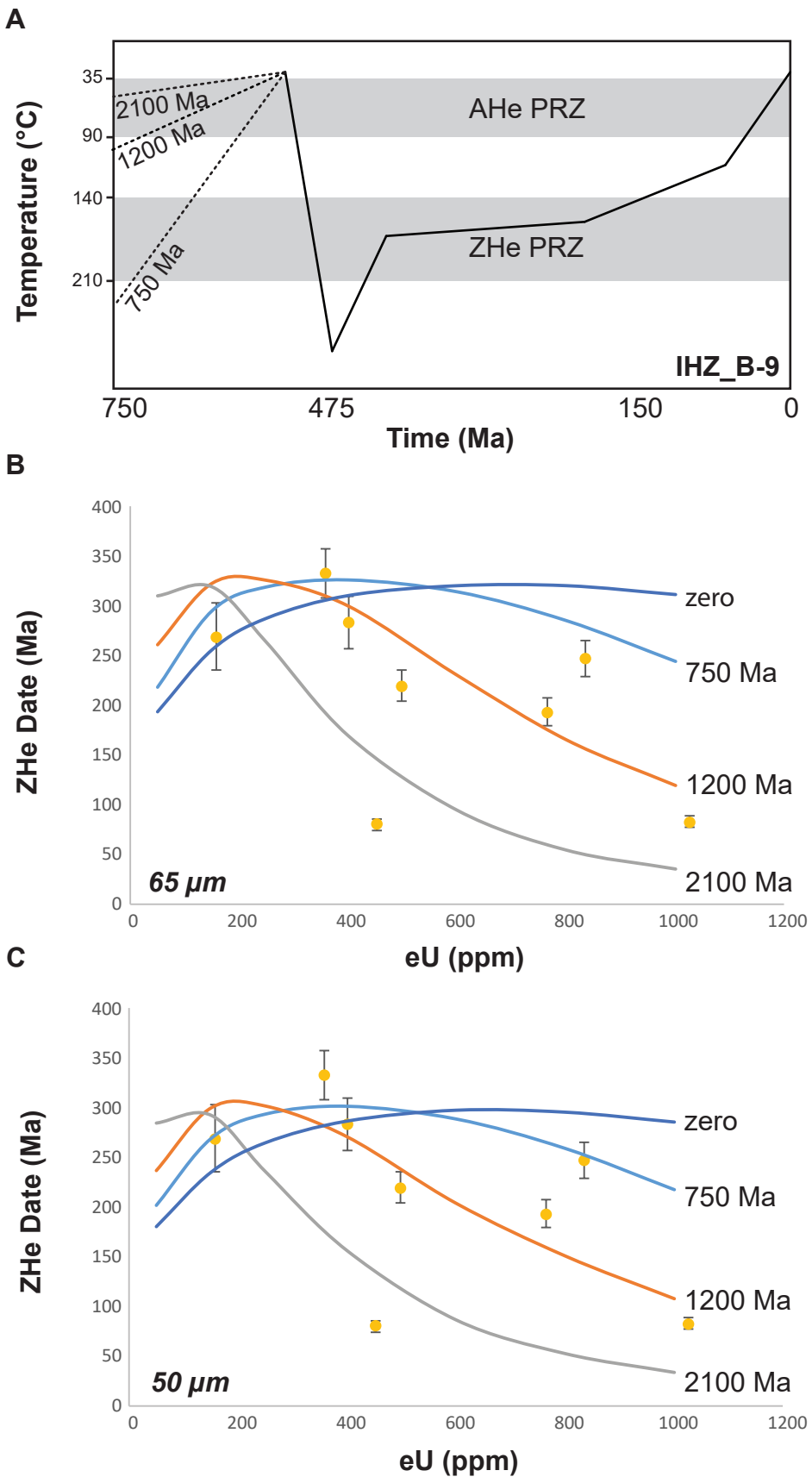

Figure A14. (**A**) Forward model from HeFTy for sample IHZ_B-9 with three different pre-depositional histories. (**B,C**) Inheritance curves, created with varying grain size (65 µm and 50 µm respectively), based on the forward models in (**A**). The similarities in results between **B** and **C** illustrates how this range in grain size did not have a significant effect on modeling outcomes.